



**UNIVERSITY OF NAIROBI**

**NUCLEAR FORENSICS ANALYSIS OF FISSION PRODUCTS BY MEANS OF  
CHEMOMETRIC LASER INDUCED BREAKDOWN SPECTROSCOPY**

By

**ONKANGI, JOSHUA NYAIRO**

B.Sc. (Physics, Egerton)

S56/71524/2014

Thesis submitted in partial fulfillment of the requirements for the award of the Degree of Masters  
of Science (M.Sc.) in Nuclear Science, University of Nairobi.

© November, 2018

## DECLARATION

I declare that this thesis is my original work and has not been submitted elsewhere for examination, the award of a degree or publication. Where other people's work or my own work has been used, this has properly been acknowledged and referenced in accordance with the University of Nairobi's requirements.

Onkangi, Joshua Nyairo  
S56/71524/2014  
Institute of Nuclear Science & Technology  
University of Nairobi.

Signature: ..... Date: .....

This thesis has been submitted for examination with our approval as University supervisors:

	Signature	Date
Dr. Angeyo H. Kalambuka Department of Physics, University of Nairobi. P.O Box 30197-00100, Nairobi Kenya. <a href="mailto:hkalambuka@uonbi.ac.ke">hkalambuka@uonbi.ac.ke</a>	.....	.....

Prof. Michael J. Gatari Institute of Nuclear Science & Technology, University of Nairobi. P.O Box 30197-00100, Nairobi Kenya. <a href="mailto:mgatari@uonbi.ac.ke">mgatari@uonbi.ac.ke</a>	.....	.....
---	-------	-------

## DEDICATION

*“That’s the thing about the collapse of civilization, Blake. It never happens according to plan – there’s no slaving horde of zombies. No actinic flash of thermonuclear war. No Earth-shuddering asteroid. The end comes in unforeseen ways; the stock market collapses, and then the banks, and then there is no food in the supermarkets, or the communications system goes down completely and inevitably, and previously amiable co-workers find themselves wrestling over the last remaining cookie that someone brought in before all the madness began.”*

– Mark A. Rayner –

*To my dear wife Consolata, my charming little daughters; Trinity and Curie, my modest parents Mama Naomi and the comical ‘philosopher’ Onkangi; whose tranquil sustenance, impels me incessantly.*

## ACKNOWLEDGMENTS

First and foremost, I wish to thank the Almighty God for providing me the forte and a craving desire to seek the knowledge embodied in this work. I must admit that my own efforts could be insufficient to have produced such work and therefore I wish to shine a spotlight on a few individuals who contributed immensely towards this success.

I am highly indebted to Dr. Angeyo H. Kalambuka of the Physics department of the University of Nairobi for proposing this research area. Through his scholarly ability, he familiarized me with the area of chemometrics as well as Laser-Induced Breakdown Spectroscopy as applied to nuclear forensics which indeed, was the best and most fascinating area of study. I also wish to recognize the late Mr. Maina David (DM) (Director, INS&T until his demise on 10/07/18) for his intellectual supervision (I wish he lived long enough to realize the fruits of his hard work). I am very grateful to Prof. Michael Gatari for fitting into the roles of DM and facilitating the completion of this thesis.

My heartfelt appreciation to Mr. Wambua, Ministry of Mining and Geology and Mr. Keter of the Radiation Protection Board for being resourceful in providing the uranium compounds and some required reference standards. In addition, Mr. Wambua generously provided fusion agent (lithium metaborate and LIT) without any attached cost that ensured success in this research. I also acknowledge Dr. Oduor of Chemistry Department, University of Nairobi for providing crucibles for glass fusion. Indeed, Dr. Oduor's support was a breakthrough at a time when I needed it most.

I wish to thank the Kenya Nuclear Electricity Board (KNEB) for offering me a scholarship and National Commission for Science Technology and Innovation (NACOSTI) for the partial support. I equally acknowledge The World Academy of Sciences for Advancement of Science in Developing Countries (TWAS) in Italy for funding my research work and providing a monthly stipend and conference facilitation. Indeed, I wish to affirm that without such mammoth support I could not have gotten the harmony to conduct research.

I could indeed be unfair if I failed to acknowledge the great support accorded to me by; Mr. Bartilol, Mr. Omucheni, Dr. Ian, Mr. Mangala, Ms. Bobby Bhatt, my comrades Mr. Moses Juma & Ms. Joy Namachanja for the motivation that enabled me to solve puzzles. Also, this work is a composition of constant litanies from my dear wife Consolata. My jubilant little daughters; Trinity Moraa and Felicity Curie with their Mona Lisa smiles kept me optimistic even when research challenges were at their heist. Finally, my loving parents, my brothers (Getakwa and Mong'are), my sisters (Nyamokami and Rose), rekindled my energy every moment I visited them in their meek background which was a persistent reminder of the unsolved puzzles awaiting. I suspect that, without their constant prayers, I could not have made it this far.

## ABSTRACT

In the wake of the current global nuclear renaissance, the threat of terrorism involving nuclear materials is real. The lethality involving detonated improvised nuclear devices (IND) “dirty bombs” or even radiological dispersal devices (RDD) is high as compared to any other form of terrorism. Such detonation events need to be timely detected and contained. As such, there is a need for a direct, rapid, non-invasive, remote and *in situ* state-of-the-art analytical techniques that can detect and characterize intercepted nuclear and radioactive materials (NRM) to apprise attribution. Nuclear forensics involves analysis of intercepted nuclear materials to provide sufficient evidence for attribution. Current nuclear forensics techniques are destructive, time-consuming, invasive and laborious besides requiring a sizeable sample size of NRM. As such, they are of limited utility in direct rapid nuclear security analytics and attribution. Laser-Induced Breakdown Spectroscopy (LIBS), when combined with chemometrics, has the potential to be developed towards overcoming these limitations.

The goal of this work was to develop a chemometric enabled LIBS methodology for direct, rapid and non-invasive nuclear forensics detection, quantitative analysis and attribution of fission products (FP) in the vitrified glass, nuclear powders and high-level liquid wastes (HLLW) in support of nuclear security. In this regard, selected FP (Rb, Sr, Y, Zr) were spiked in a uranium augmented (0-5 % natural grade) matrix (composed of;  $\text{SiO}_2$ ,  $\text{Na}_2\text{CO}_3$ ,  $\text{Al}_2\text{O}_2$ , and  $\text{CaCO}_3$ ) in typical levels at which they occur in high-level nuclear wastes. The resulting sample was prepared as fused glass to simulate nuclear glass, mixed with cellulose and pressed into pellets to mimic high-level nuclear powders as may be encountered in detonation events and a third batch prepared to mimic HLLW resulting from nuclear fuel reprocessing.

Drop coating deposition (DCD) of HLLW on perspex was found to produce the best signal to noise ratio (SNR) of 57.895 for Rb I 780.011 nm of 9 ppm. Multivariate calibration strategy for quantitative analysis of Rb, Sr, Y, and Zr was achieved by utilizing artificial neural network (ANN). Various ANN algorithms were tested with feed forward back propagation algorithm, providing ( $R^2 > 95\%$ ) calibration accuracy. The relative error of prediction (REP) of  $< 10\%$  was realized for each model. Validation of HLLW models was achieved using synthetic inductively coupled plasma (ICP) and atomic absorption spectroscopy standard solutions respectively and river clay PTXRFIAEA09 SRM with  $< 10\%$  deviation from certified values.

Detection limits for each of the spiked elements in different samples types were: fused glass LoD  $\leq$  200 ppm, powders pellets LoD  $\leq$  71 ppm and HLW liquids LoD  $\leq$  8 ppm. Simulate high-level nuclear waste fluids typical of a nuclear forensic scene (detonation or accidental spillage of HLW liquids or unlawful release of FP to the environment) were treated together with base matrix standards to achieve PCA clustering that differentiates the nuclear wastes and non-nuclear wastes based on trace FP.

Support Vector Machine (SVM) was utilized in developing qualitative clustering hyperplanes based on the presence of FP (Rb, Sr, Y, Zr) in samples. We report  $> 85\%$  accuracy in discrimination of FP in terms of trace concentrations and their corresponding spectral response signatures. These SVM findings are an important component of nuclear forensic attribution as samples containing FP in particular concentrations are separated by the developed hyperplanes and hence furnish useful nuclear forensic interpretations. The novelty of the developed analytical methodology lies in small samples involved ( $2\ \mu\text{l}$  for liquid samples with computed SNR of 57.895) and ( $\varnothing\ 3\ \text{mm}$  for solid fragments) to furnish nuclear forensic signatures. Hence, chemometric-LIBS provides a robust tool which can be integrated into a suitable software-user interface of a handheld LIBS for rapid analysis of NRM in the context of nuclear forensics.

## TABLE OF CONTENTS

DECLARATION .....	i
DEDICATION .....	ii
ACKNOWLEDGMENTS .....	iii
ABSTRACT.....	iv
LIST OF ABBREVIATIONS AND ACRONYMS .....	ix
LIST OF TABLES .....	xi
LIST OF FIGURES .....	xii
CHAPTER I.....	1
INTRODUCTION.....	1
1.1 Background .....	1
1.2 The Composition of Nuclear Waste .....	4
1.3 Quality Control/Quality Assurance Characterization of FP.....	5
1.4 Overview of Laser-Induced Breakdown Spectroscopy (LIBS) .....	6
1.5 Hypothetical Nuclear Forensic Scenarios .....	7
1.6 Problem Statement .....	8
1.7 Objectives.....	8
1.7.1 Main Objective.....	8
1.7.2 Specific Objectives .....	8
1.8 Justification and Significance of Study .....	9
1.9 Scope and Limitations of Study .....	10
1.10 Study Hypothesis.....	10
CHAPTER II.....	11
LITERATURE REVIEW .....	11
2.1 Overview .....	11
2.2 LIBS in Elemental Analysis of Materials .....	11
2.3 Isotopic and Molecular Analysis using LIBS .....	14
2.4 Analysis of Fusion Glass.....	15
2.5 Nuclear Fuel Reprocessing and Vitrification.....	17
2.6 Chemometric LIBS .....	19
2.6.1 Chemometrics in Other Applications.....	19

2.6.2	Chemometrics Methods in Nuclear Science .....	23
CHAPTER III	.....	25
THEORETICAL BACKGROUND	.....	25
3.1	Overview .....	25
3.2	Principles of LIBS .....	25
3.3	Multivariate Chemometric Calibration and Modeling .....	29
3.4	Artificial Neural Networks (ANN) .....	30
3.4.1	Feed Forward Back Propagation ANN Algorithm .....	33
3.4.2	Cascade Correlation Algorithm .....	34
3.5	Principal Component Analysis (PCA) .....	36
3.6	Support Vector Machines (SVM) .....	38
CHAPTER IV	.....	40
MATERIALS AND METHODS	.....	40
4.1	Overview .....	40
4.2	LIBS Instrumentation .....	40
4.3	Optimization of the LIBS System .....	42
4.4	Sample Preparation Procedures.....	42
4.4.1	Preparation Fused Glass Sample.....	46
4.4.2	Preparation of Pellet Samples .....	50
4.4.3	Preparation of Simulate Liquid Samples .....	52
4.4.4	Synthetic Standard Preparations .....	54
4.5	Evaluation of Limits of Detection (LoD).....	55
4.6	Spectral Data Pre-processing Techniques .....	56
4.7	Principal Component Analysis of Simulate HLNW .....	57
4.8	Artificial Neural Networks (ANN) of HLNW .....	57
4.9	Support Vector Machines of FP in Simulate HLNW.....	59
4.10	Safety Precautions .....	59
4.11	LIBS Line Selection Criteria.....	60
CHAPTER V	.....	64
RESULTS AND DISCUSSION	.....	64
5.1	Overview .....	64
5.2	LIBS Peak Selection and Qualitative analysis .....	64



5.3	Spectral Line Response with a Change in Concentration .....	67
5.4	LIBS Optimization Parameters .....	69
5.4.1	Optimization of LIBS for Fused Glass Analysis .....	69
5.4.2	Optimization of LIBS for Pellet Samples .....	69
5.4.3	Optimization Conditions for the Preparation of Liquid Samples .....	69
5.5	Univariate Calibration of FP in Simulate HLW .....	78
5.6	Multivariate Modelling for Quantitative Analysis of the FP in HLW .....	82
5.6.1	ANN Model for Quantitative Analysis of FP in HLW .....	82
5.6.2	ANN Models Validation Results for Nuclear Pellets and HLLW Simulates .....	95
5.7	Hypothetical Nuclear Forensic Scenario and Approach to Attribution .....	97
5.7.1	Principal Component Analysis of Simulate HLNW Samples .....	97
5.7.2	Support Vector Machine (SVM) Classification of Simulate Nuclear Wastes .....	102
5.7.3	Chemometric LIBS Methodology.....	111
CHAPTER VI.....		114
CONCLUSION, RECOMMENDATIONS AND PROSPECTS .....		114
6.1	Summary and Conclusions.....	114
6.2	Recommendations and Prospects .....	116
REFERENCES .....		117
APPENDICES .....		127
Appendix 1: Target Concentrations Spiking Scheme .....		127
Appendix 2: Artificial Neural Network Algorithm.....		128
Appendix 3: Support Vector Machine Algorithm (Binary Clustering) in R.....		130
Appendix 4: Principal Component Analysis Code in R.....		132
Appendix 5: ICP standard Solutions Validation Certificates.....		134

## LIST OF ABBREVIATIONS AND ACRONYMS

AMS	Accelerator Mass Spectroscopy
CCD	Charge Coupled Device
CRM	Certified Reference Material
CF-LIBS	Calibration Free Laser-Induced Breakdown Spectroscopy
DCDR	Drop Coating Deposition Raman
DCD-LIBS	Drop Coating Deposition Laser-Induced Breakdown Spectroscopy
FPS	Fission Products
HBRA	High Background Radiation Area
HLW	High-Level Nuclear Waste
HLLW	High Level Liquid Wastes
IAEA	International Atomic Energy Agency
ICA	Independent Component Analysis
ICRP	International Commission for Radiological Protection
ICP-AES	Inductively Coupled Plasma-Atomic Emission Spectrometry
ICP-MS	Inductively Coupled Plasma – Mass Spectroscopy
IEDs	Improvised Explosives Devices
IND	Improvised Nuclear Device
KNEB	Kenya Nuclear Electricity Board
LAMIS	Laser Ablation Molecular Isotopic Spectrometry
LEU	Lightly Enriched Uranium
LIBS	Laser-Induced Breakdown Spectroscopy
LoD	Limit of Detection
LPE	Laser Pulse Energy
MEU	Moderately Enriched Uranium
MVA	Multivariate Analysis
NF	Nuclear Forensics
NFC	Nuclear Fuel Cycle
NIR	Near Infra-Red
NWA	Non-Wetting Agent
PC	Principal Component

PCA	Principal Component Analysis
PCR	Principal Component Regression
PLS	Partial Least Squares
PLS-DA	Partial Least Squares-Discriminant Analysis
PHWR	Pressurized Heavy Water Reactor
RBK	Radial Basis Kernel
RDD	Radiological Dispersal Devices
REE	Rare Earth Elements
REP	Relative Error of Prediction
SVM	Support Vector Machines
SIMCA	Soft Independent Modeling of Class Analogy
TIMS	Thermal Ionization Mass Spectrometry
UOC	Uranium Ore Concentrate
UNSCEAR	United Nations Scientific Committee on Effects of Atomic Radiation
UV	Ultra Violet
Vis	Visible
Vis-NIR	Visible-Near Infra-Red

## LIST OF TABLES

Table 4.1: Specifications of spectrometers from Ocean Optics utilized in this study .....	41
Table 4.2: Other optimum parameters of the LIBS system used in this study .....	42
Table 4.3: Analytical grade reagents used as donors of the simulate fission products.....	43
Table 4.4: Composition of the glass forming support matrix .....	44
Table 4.5: Spectral lines observed in LIBS and utilized in the quantitative model development	63
Table 5.1: SNR and SNB for Rb II 779.985 nm line corresponding to 9 ppm of Rb in simulate liquid solution for varying volume of drop coat on Perspex .....	75
Table 5.2: Limit of detection for Rb, Sr, Zr and Y elements in fused glass, pellet, and DCD-LIBS samples .....	81
Table 5.3: Model prediction ability with a variation of ANN layers for <i>newff</i> algorithm.....	84
Table 5.4: Model prediction ability with a variation of the number of neurons for <i>newff</i> algorithm .....	84
Table 5.5: Prediction ability of the model with varied learning rate for <i>newff</i> algorithm .....	84
Table 5.6: Relative Error of Prediction (REP) for the feed forward back propagation ( <i>newff</i> ) and cascade correlation ( <i>newcf</i> ) models developed utilizing feature selected fused glass data.....	88
Table 5.7: Model performance based on the explained variance ( $R^2$ ), the Relative Error of Prediction (REP) and univariate LoD for fused glass, pelletized and liquid sample forms of the same analyte.....	95
Table 5.8 : HLLW Model validation results using certified standards.....	96
Table 5.9: Simulate nuclear pellet validation results using River Clay PTXRFIAEA09.....	96
Table 5.10: Confusion matrix of test data set ( $C = 1000, \gamma = 1,$ <i>RBK, 10 fold cross validation</i> ).....	104
Table 5.11: Confusion matrix of validation test data set at ( $C = 1000, \gamma = 1, RBK$ ) .....	106
Table 5.12: Confusion matrix for Y-Zr SVM classifier utilizing data from pellet samples at 10 fold cross validation ( $C = 1000, \gamma = 0.001, RBK$ ).....	107
Table 5.13: Confusion matrix for U-Zr SVM classifier utilizing data from pellet samples ( $C =$ $1000, \gamma = 0.001$ and <i>RBK</i> ) .....	108
Table 5.14: Ability of SVM model to cluster independent test pellet data at ( $C = 1000, \gamma =$ $0.1$ and <i>RBK</i> ) .....	110

## LIST OF FIGURES

Figure 1.1.1: The nuclear fuel cycle (After : Wilson (1996)).	3
Figure 2.5.1: Nuclear fuel reprocessing process (After: Murray and Holbert (2014)).	18
Figure 3.4.1: A sketch of a biological neuron (Source: Naguib and Sherbet (2001)).	31
Figure 3.4.2: Schematic of a simple ANN and its similarity to a biological neuron (After: Naguib and Sherbet (2001)).	32
Figure 3.4.3: Schematic diagram of feed forward back propagation utilizing LIBS spectral data (After: Andrade-Garda <i>et al.</i> (2009)).	34
Figure 3.4.4: Simple cascade correlation architecture (After: Schetinin (2003)).	35
Figure 4.2.1: Schematic diagram of LIBS (LIBS 2500 PLUS Operational Manual (2008)).	41
Figure 4.4.1: General fusion bead preparation procedure (After: Watanabe (2015)).	48
Figure 4.4.2: Procedure for preparation of fused glass, pellet and drop coating deposition forms of simulate high level samples.	51
Figure 4.8.1: ANN modeling approach.	58
Figure 4.11.1: Zoom in of LIBS spectrum of an HLW fused glass sample.	61
Figure 4.11.2: Typical line profile for YII 371.029 nm.	62
Figure 5.2.1: LIBS spectra of the salts (FP donors) (stacked for easy view).	65
Figure 5.2.2: Identified peaks of simulate HLW liquid FP coated on perspex substrate.	66
Figure 5.2.3: Selected observed emission lines of a pellet sample spiked with FP elements in fused glass and a blank fused glass matrix.	67
Figure 5.3.1: (A) Rb line at 780.011 nm and (B) Sr line at 460.733 nm and (C) Y ionic line at 371.029 nm responding with changes in the concentration of the respective analyte in different fused glass samples.	68
Figure 5.4.1: Spectral line intensity (YII 371.029 nm) response with energy variation.	70
Figure 5.4.2: Spectral line intensity response with distance of the optic fiber from the sample.	71
Figure 5.4.3: Spectral line intensity variation with the volume of drop deposition coating for the same sample.	73
Figure 5.4.4: Comparison between spectra acquired from fused glass and pellet samples.	76

Figure 5.4.5: Comparison of spectra acquired from fused glass, pressed powders and aliquot deposition coatings.....	77
Figure 5.5.1: Selected univariate graphs for fission products acquired from fused glass samples	79
Figure 5.5.2: Selected univariate regression plots for fission products in spectra acquired from pellet (powders) samples.....	80
Figure 5.5.3: Selected univariate calibration graphs for fission products in spectra acquired from the liquid sample.....	80
Figure 5.6.1: ANN multivariate regression plots for Sr utilizing newcf and newff algorithms respectively using fused glass samples data. ....	86
Figure 5.6.2: ANN multivariate regression plots for Rb comparing newcf and newff algorithm (newff) for the fused glass samples data.....	86
Figure 5.6.3: ANN multivariate regression plots for a) Y and b) Zr in fused glass. ....	89
Figure 5.6.4: ANN regression plots for (a) Y, (b) Sr using data acquired from pellet samples ...	91
Figure 5.6.5: ANN regression plot for Rb using data acquired from pellet samples.....	92
Figure 5.6.6: ANN regression plots for (a) Zr and (b) Sr for 2 $\mu$ l simulate HLNW liquid deposited on perspex substrate.....	93
Figure 5.6.7: ANN regression plots for (a) Y and (b) Rb for 2 $\mu$ l simulate HLNW liquid deposited on perspex substrate.....	94
Figure 5.7.1: PCA Scores plot for simulate high level liquid nuclear wastes. The samples SL and SLT contain FP spiked in trace quantitative levels while LB and LBT are reference blank samples matrix samples.....	99
Figure 5.7.2: PCA loadings plots for simulate high-level nuclear waste liquid samples .....	100
Figure 5.7.3: PC1 and PC3 scores plot for simulate high level liquid nuclear wastes.SL and SLT contain FP spiked at (0-1000 ppm) levels while LB and LBT are reference samples.....	101
Figure 5.7.4: 3D PCA scores plot for simulate HLLW. The samples SL and SLT contain FP spiked within 0-1000 ppm levels while LB and LBT are blank samples. ....	102
Figure 5.7.5: SVM plots utilizing selected zirconium and rubidium lines in fused glass with; a) linear kernel, b) RBK function.....	104
Figure 5.7.6: SVM plot of the feature selected fused glass samples training dataset ( $C = 1000$ , $\gamma = 1$ , <i>RBK</i> ).....	105

Figure 5.7.7: Y-Zr SVM classification plot for Pellet samples ( $C = 1000, \gamma = 0.001, RBK$ ).	107
Figure 5.7.8: SVM plot for for U-Zr SVM classifier utilizing data from pellet samples ( $C = 1000, \gamma = 0.001$ and RBK).	108
Figure 5.7.9: SVM clustering of FP utilizing simulated HLNW powders pressed into pellets with the best model ( $C = 1000, \gamma = 0.1$ and RBK).	110
Figure 5.7.10: Chemometric-LIBS nuclear forensic tool for analysis of FP in HLNW.	113

# CHAPTER I

## INTRODUCTION

### 1.1 Background

As of 31<sup>st</sup> December 2016, more than 3068 cases of illicit trafficking of nuclear or radioactive materials had been reported to the IAEA by member states participating in the Incident and Trafficking Database (ITDB) system (IAEA, 2017). This is just the tip of an iceberg inferring that the actual number of illicit smuggling is significantly higher (Mayer *et al.*, 2012). These cases have been rising gradually since the first interception of illicit smuggling of 1.5 Kg weapon-grade HEU (90%), Podolsk, Russia in 1992 (Moody *et al.*, 2014). Nuclear forensics (NF), a fairly new scientific discipline, emerged in the early 1990s to respond to such cases. NF refers to the analysis of materials of nuclear origin recovered either through interception of unused or radioactive debris from nuclear explosion scenes (May *et al.*, 2008). NF methodologies are used to characterize as well as to evaluate nuclear and radioactive materials (NRM) both in the front and the back-end of the nuclear fuel cycle (NFC). Terrorist groups more often seek NRM to pose threats in form of radiological dispersal devices (RDD) and improvised nuclear devices (IND). As such, NF probes intercepted NRM in order to provide sufficient evidence useful in nuclear attribution (Decker and Allison, 2011).

Nuclear attribution refers to the iterative process that provides clues useful in identifying the source of NRM used in illegal activities; determine the point of origin and routes of transit involving such materials, and also provide sufficient evidence necessary for prosecution of those responsible for illicit smuggling of NRM (Mayer *et al.*, 2012)). NF when conducted effectively, is in itself a restriction to the envisaged nuclear security threats as through nuclear material



characterization, acts of terrorism involving RDDs and INDs ('dirty bombs') can be deterred (Angeyo, 2018).

Technological changes that have taken root throughout the world call for sufficiency in energy which is always considered as the key driver of any nation's economy. Sources of energy such as wind, hydro and solar have a number of limitations including relatively higher dependency on natural aspects that vary over time (as compared to nuclear) hence they are greatly unpredictable. In addition, sources of energy such as coal are in the verge of being banned as they contribute to greenhouse gas emissions that adversely affect the planet (D'haeseleer, 1998; Sailor *et al.*, 2000) As such, nations have been embracing nuclear energy as it overcomes most of these limitations and is a reliable, safe and clean source of energy.

However, this global nuclear renaissance has a number of drawbacks which include lack of a long-term solution to the challenge of disposal of nuclear wastes. Operation of nuclear energy can follow an open or a closed fuel cycle (Baisden and Choppin, 2007) as shown in **Figure 1.1.1**.

Some nations like the US and Canada have chosen to work with an open fuel cycle in which the spent fuel and other nuclear wastes end up in permanent disposal facilities to eliminate the chances of the proliferation of weapon-grade plutonium which is a byproduct of reprocessing of spent fuel (Nash *et al.*, 2006). Some other nations operating nuclear power programs like UK and France prefer having the nuclear waste undergo reprocessing in order to reduce radio-toxicity as well as recover important fission products (FP) for various applications such as food preservation (Murray and Holbert, 2014), etc. Also, other useful nuclear fission products such as plutonium and depleted uranium are recovered for applications involving the formulation of mixed fuel oxides (MOX) which are utilized in hybrid reactors ('breeder reactors') (Şahin *et al.*, 1999; Yapıcı, 2003). During such processes, additional waste burden containing a number of

fission products, actinides, and trace metals are produced. Because of their negative impact on the environment, the release of these metals to the surroundings is detrimental (hydro-ecological) challenge. Therefore, there is a need for establishing operation of monitoring and surveillance programs geared towards control of the release of these fission products to the environment.

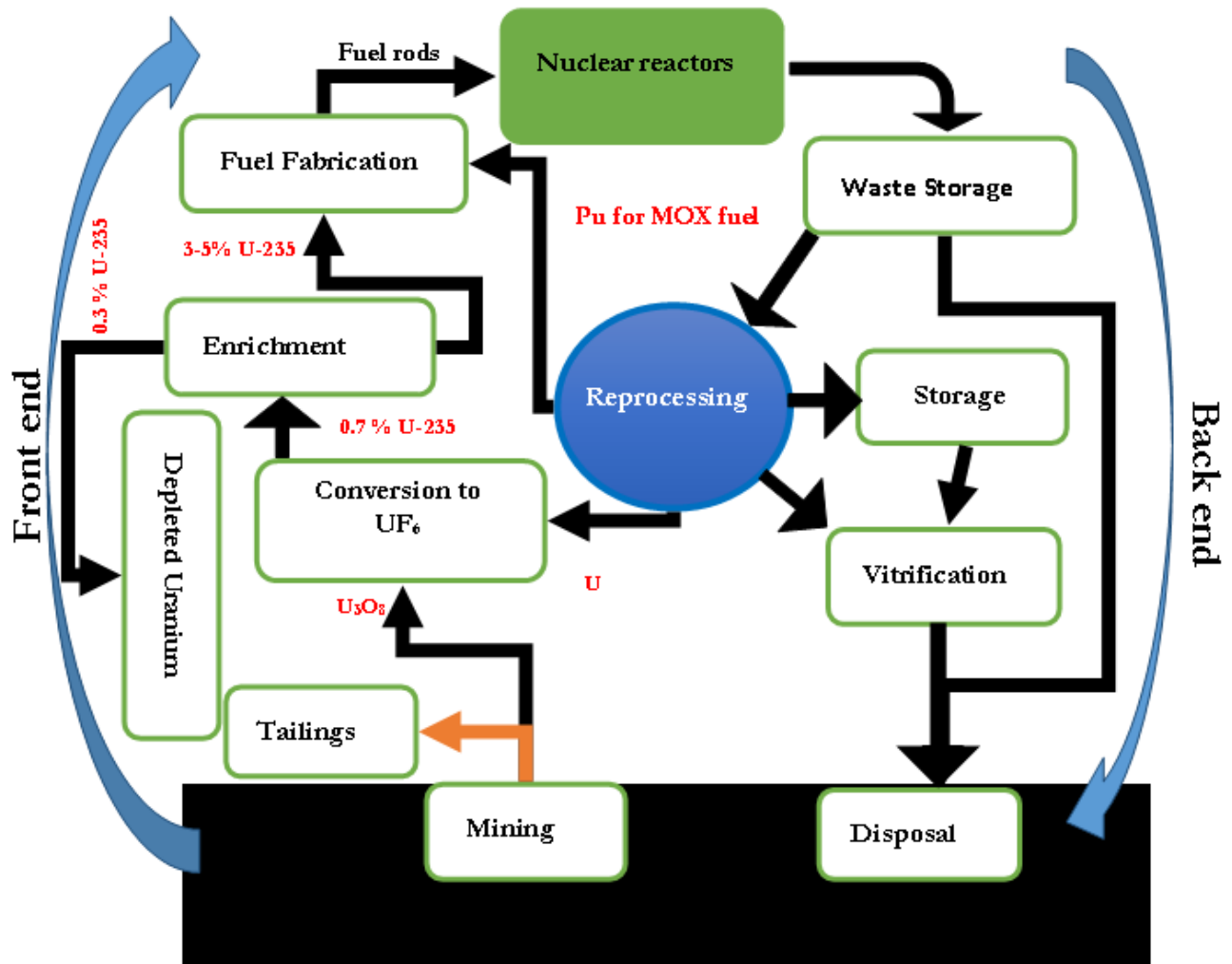
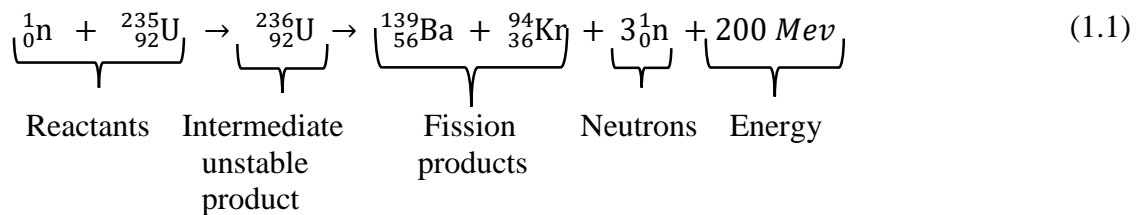


Figure 1.1.1: The nuclear fuel cycle (After : Wilson (1996)).

Consequently, amidst the wake of the current global nuclear renaissance, the threat of terrorism involving nuclear materials is real. The lethality involving detonated improvised nuclear devices (IND) “dirty bombs” or even radiological dispersal devices (RDD) is high as compared to any other form of terrorism. These nuclear materials need to be highly safeguarded and if diverted for non-peaceful purposes, there is a need for a NF tool for rapid detection of unused NRM or even nuclear attribution of detonation scenes to bring culprits into accountability and Law Enforcement.

## 1.2 The Composition of Nuclear Waste

In the reactor core,  $^{235}\text{U}$  undergoes nuclear reactions leading to generation and accumulation of nuclear fission products (FP). Equation 1.1 shows some fission products from uranium fission (Sally, 2014).



Some of the FP (e.g.  $^{149}\text{Sm}$  and  $^{135}\text{Xe}$ ) are poisons as they have very high neutron absorption cross sections and lead to a reduction of reactor reactivity (Stacey, 2018). In the long run, the accumulation of these fission products results in inefficiency in energy generation and therefore the fuel rods must be replaced to maintain the efficiency in generation of energy (Henderson, 2014). Spent fuel is highly radioactive and most nations running nuclear power plants have adopted a disposal facility to store the fuel in anticipation for an appropriate permanent solution.

Nuclear waste can be broadly classified as high-level waste (HLW) and low-level waste (LLW). High-level liquid waste (HLLW) is normally generated during the initial stages of reprocessing

of nuclear fuel (Xuegang *et al.*, 2012). In essence, HLLW is a composition of the nuclear fission products (e.g Mo, Tc, Nb, Ru, Cs, Y, Rb, Sr), some minor species from the actinide series and nitric acid which is used during extraction of FP (Donald *et al.*, 1997). This nitric acid used in the reprocessing is highly corrosive hence desired waste management procedures require that de-nitration be conducted. It is worth noting that metallic precipitates (Sr, Zr, Mo Ba, etc) are also generated during HLLW treatment as well as during de-nitrification process. Some of these precipitates are also important during the downstream portioning HLLW treatment process (Xuegang *et al.*, 2012). Immobilization of most of these fission products can be achieved by integrating the materials into vitrified (glass) form which provides a more compact form for long-term storage.

### **1.3 Quality Control/Quality Assurance Characterization of FP**

The goal of NF is to analyze suspected NRM to furnish information related to type, origin, production method for such material, the routes of transit and where possible, determine where the regulatory control was lost (L'Annunziata, 2012). In order to promptly respond to the questions raised in NF and achieve accurate attribution, the results must meet the required standards (Kristo, 2012). A laboratory analysis program, especially in NF, should be subjected to QA as it offers a means to deliver valid, traceable results and a capability to identify and correct anomalies consistent from reproducibility of results within a given technique (Leggitt *et al.*, 2009). Despite the rigorous procedures required to achieve full NF, QA facilitates the creation of a defensible and consistent input to the interpretation process in support of attribution assessments. As such, ISO accreditation is sought in NF laboratories in order to enable admissibility of scientific evidence for purposes of jurisdiction and holding the perpetrators

accountable. In this work, certified reference materials have been utilized in the development of the methodology for trace analysis of NF signatures of selected FP.

#### **1.4 Overview of Laser-Induced Breakdown Spectroscopy (LIBS)**

LIBS is an atomic emission spectroscopic technique that has the ability to perform elemental, isotopic and molecular analysis of a huge variety of samples irrespective of their physical state. In this technique, a short pulsed and focused high power laser is directed and made to cause a breakdown on the surface of the sample. The energy of the laser is used to ablate a minute fraction of the sample ( $\sim 1\mu g$ ) (Kasem and Harith, 2015 ; Hussain and Gondal, 2013) As a result, a dense microplasma characterized by high electron density ( $\sim 10^{18} \text{ cm}^{-3}$ ) and high plasma temperature ( $> 20\,000 \text{ K}$ ) is formed (Russo *et al.*, 1999). This high-density plasma expands at supersonic speeds and contains information about the ablated sample (Musazzi and Perini, 2014). The atoms and ions in the expanding plasma plume exist mostly in excited states assuming a stoichiometric ablation and as they transit to the stable states, they emit electromagnetic radiation that can be spectrally analyzed and interpreted to reveal the chemical composition of the target sample.

LIBS possess several advantages compared to other competing analytic techniques. These include; limited sample preparation, rapid real-time analysis, ability to perform *in situ* analysis and remote capability (suitable for radioactive samples), the unique advantage of achieving depth profiling of layered structures, the quasi-non-destructive (micro sample hence microanalysis) and also the unique portability advantage compared to other analytical methods fixed in a laboratory.

## 1.5 Hypothetical Nuclear Forensic Scenarios

In post-detonation nuclear forensics, the desire to attribute the material to its source, loss of regulatory control and even its composition and of holding criminals to accountability requires rapid state-of-the-art microanalytic protocols. Such detonation scenes are characterized by tiny samples as most of the constituents of the nuclear device get jumbled in a manner that is difficult to isolate. The dust particles and tiny glass debris that could contain NF signatures (uranium and nuclear fission products) are dominant. Therefore, getting sufficient sample size that can furnish NF signatures using the classical analytical techniques is a major challenge. The use of rapid LIBS based analytical methods overcomes this limitation as minute sample sizes (typically  $< 1 \mu\text{g}$ ) can furnish useful information.

Similarly, illicit trafficking of nuclear materials can take many forms. The materials can be stolen and trafficked in concealed forms which may involve mixing with powders, fusing in glass or even mixing with liquids and packaging for shipping. With the advanced microextraction techniques, one can extract the constituents at the other end. As such, there is a need to develop techniques that can detect NF signatures in such concealed forms to deter smuggling and proliferation of nuclear materials.

In performing analysis, detection of particular elements such as plutonium could link the material to a specific reactor hence a useful component of source apportionment. In addition, the concentrations of the detected elements (fission products) can offer information about the stage of the material in the nuclear fuel cycle.

## **1.6 Problem Statement**

Current nuclear forensics techniques are mostly destructive, time-consuming, invasive and laborious besides requiring a sizeable sample size of NRM. As such, they are of limited utility in rapid nuclear security analytics and attribution. Chemometric LIBS has the potential to be developed towards overcoming these limitations as it can simultaneously reveal the isotopic, molecular and elemental composition of NRM besides achieving attribution.

## **1.7 Objectives**

### **1.7.1 Main Objective**

The goal of this work was to develop a chemometrics enabled LIBS methodology for rapid and minimally-invasive detection, quantitative analysis and attribution of fission products in simulate vitrified glass, nuclear powders and HLLW based on their concentrations and characteristic patterns in support of nuclear security.

### **1.7.2 Specific Objectives**

The specific objectives are:

- i. To utilize standard reference materials (SRM) and LIBS in the air and atmospheric pressure to develop calibration models to detect and quantify trace Rb, Sr, Zr and Y in U augmented simulate nuclear fused glass, pressed powder pellets and liquid nuclear waste utilizing multivariate chemometrics (ANN).
- ii. To determine and compare the limit of detection (LoD) of each FP in each of the matrices (fused glass, pressed pellets and liquid samples).
- iii. To utilize the chemometric models developed in (i) to quantify fission products in synthetic standards for nuclear forensics applications.
- iv. To exploit the diversity of the information from (i-iii) to perform quasi-nuclear forensic

attribution (source apportionment, level of enrichment of the material and the stage of material in the nuclear fuel cycle) utilizing exploratory multivariate chemometrics (PCA and SVM).

### **1.8 Justification and Significance of Study**

Vision 2030 is Kenya's long-term development blueprint. It identifies nuclear power as a clean, safe and reliable energy source that can contribute 19 % of the national energy mix. However, the operation of a nuclear power plant (NPP) is always associated with NRM that is required in the nuclear fuel cycle. Lack of adequate security for such NRM as well as to high-level radioactive wastes would directly imply high chances of nuclear proliferation. If materials suspected to be NRM are seized, there is a need for a direct rapid, minimally-invasive nuclear forensic analysis tool that can accurately identify the nature, the source and attribution of the material.

NRM have been seized in various parts of the world over the last two decades. This means that the possibility of use of NRM in ‘dirty bombs’ and IND has also risen over time, even when the exact time of the attack is unknown. The consequences of a detonated IND in a populated region are great due to the negative impact of ionizing radiation and unpredicted future effects. As such, a rapid NF detection system such as chemometric LIBS is required.

LIBS has been shown to be one of the most promising analytical technique for rapid analysis in nuclear forensics. Other analytical techniques such as the ‘swipe sample kits’ followed by digestion and analysis using ICP-MS used by IAEA in the detection of plutonium, thorium or uranium provide accurate results; however, the process is time-consuming and tedious. Therefore, the development of a methodology that attempts to overcome the inconveniences



encountered in spectral analytical techniques in nuclear forensics is novel and can contribute towards ensuring non-proliferation of NRM in the context of nuclear security.

In addition, a national nuclear forensic laboratory is essential in order to better respond to nuclear terrorism crimes involving the use of RDD, IED, and IND. Findings from this research will be useful in generating data for potential establishment of a National Nuclear Forensics Library (NNFL) and models to quantify fission products which can assist regulatory authorities to characterize NRM towards combating illegal trafficking of NRM, etc. Moreover, as KNEB embarks on ensuring the reliability of electricity through NPP, research geared towards non-proliferation is the need of the hour. Also, the study will enable Radiation Protection Board of Kenya (RPB), the national and global security agencies, the IAEA, UNSCEAR and ICRP in the formulation of recommended strategies of fighting malicious possession and trafficking of NRM.

### **1.9 Scope and Limitations of Study**

Nuclear waste resulting from reprocessing of spent fuel is a composition of many fission products and actinides. Handling spent fuel is hazardous, hence simulates are employed to approximate the composition. In this study, four fission products; Rb, Sr, Zr, and Y spiked in a U augmented matrix were used to develop the methodology. These FPs and U were spiked in typical ranges they occur in HLW.

### **1.10 Study Hypothesis**

It is possible to quantify trace FP in HLW through nuclear forensics to inform attribution. Detection of trace FP in HLW is influenced by the matrix of the sample and the nature of the substrate used. It is possible to accurately simulate HLW resulting from reprocessing of spent fuel through representative selected FP.

## **CHAPTER II**

### **LITERATURE REVIEW**

#### **2.1 Overview**

This chapter reviews the literature on LIBS, chemometric spectroscopy and their utility in nuclear forensic analysis. The chapter identifies the progress as well as critiques the application of LIBS in elemental analysis of various materials in different forms. Other applications of LIBS which include achieving isotopic and molecular spectroscopy are presented. In addition, the growth of chemometrics which is a natural complement to atomic emission spectroscopy to achieve modeling and calibration is also presented.

#### **2.2 LIBS in Elemental Analysis of Materials**

The applicability of LIBS to perform elemental analysis has been demonstrated in various fields such as; pharmaceuticals, pottery, soil analysis etc., from explosives to non-explosives (Judge *et al.*, 2013; De Lucia *et al.*, 2008; Gottfried *et al.*, 2009). *In-situ* fingerprinting of radioactive surrogates (namely;  $^{60}\text{Co}$ ,  $^{88}\text{Sr}$ ,  $^{130}\text{Ba}$ ,  $^{133}\text{Cs}$ ,  $^{193}\text{Ir}$ , and  $^{238}\text{U}$ ) on materials found in urban areas (aluminum that is common in traffic signs, building bricks, pavement, concrete and glass on bus shelters) by LIBS has also been demonstrated (Gaona *et al.*, 2014). The research supports the ability of LIBS for remote analysis (samples 30 m away) in nuclear forensic scenarios for monitoring radiological threats and ionizing radiation sources. These findings reveal that the detection of the analytes depends significantly on the surface analyzed. However, employing multivariate techniques can be a potential solution irrespective of the nature of the surface analyzed. Therefore, as smuggling of NRM provides probable avenues to possible nuclear terrorism, there is a need for an analytical technique that is suitable for on-site, real-time, rapid

and sensitive analysis and that offers possibilities to realize simultaneous elemental, the isotopic and molecular composition of NRM.

Multi-elemental analysis of various mineral melt oxide samples at various elemental concentrations was achieved by means of ND:YAG laser based LIBS within a spectral range of 200-780 nm (Laville *et al.*, 2007). Notably, 19 samples were used for calibration of major elements (Fe, Al, Mg, Ca, Ti, and Si). Second order polynomial multi-linear regression was used to develop the calibration model. From this study, results were found to be in agreement with those obtained by means of X-Ray Fluorescence (XRF) spectroscopy. However, the approach employed in this work is univariate which has limitations including, non-uniform spectral intensity response with concentration especially when trace elemental concentration is involved. Therefore, the utility of chemometrics approach with such data has the potential to overcome such limitations.

Kim *et al.* (2012) performed quantitative analysis of U in uranium ore concentrates (UOC) by means of LIBS in order to develop measurement techniques applicable in high temperatures or high radioactivity environments such as in the nuclear reactor. In this work, uranium was selected because it is the element commonly available in spent reactor fuel. Raw uranium ore powders were mixed with natural uranium oxide powders to attain uranium ore samples with uranium at different concentrations. By means of a pulsed Q-switched Nd:YAG laser operating at 532 nm laser excitation wavelength, a neutral atomic emission peak at 356.659 nm gave a limit of detection (LoD) of ~158 ppm uranium in the ore matrix. The concentration of uranium in the ore samples was consistently determined within the limits of experimental uncertainty compared to ICP-AES measurements. However, there is a need to develop methods capable of

lowering the detection limits so as to achieve trace elemental impurities in NRM in order to respond to illicit smuggling of NRM and address NF situations.

Martin *et al.* (2012) explored the applicability of LIBS in nuclear material analysis and *in-situ* nuclear applications. The technique was applied on strontium (Sr) and cesium (Cs) which are common products of nuclear fission process. The study was achieved by means of a Nd:YAG laser at a fundamental wavelength of 1064 nm, doubled in frequency to 532 nm with an energy of 50 mJ per pulse. Comparative study of Sr and Ce at various concentration in calcium carbonate and black carbon matrix was achieved. Notably, Ce is a difficult element to excite by LIBS compared to Sr and therefore, these matrices were used in order to investigate the effect of the nature of the matrix on detection efficiency of Ce and Sr. This study shows the inherent potential of LIBS in *in-situ* applications such as detection of fission products in a nuclear reactor environment.

Loudyi *et al.* (2009) applied a combination of LIBS and Laser-Induced Fluorescence (LIF) to investigate the limit of detection (LoD) of trace metallic impurities (Pb and Fe) in water. Using 100 laser shots, the LoDs for Pb and Fe were found to be 39 ppm and 65 ppm respectively. The findings demonstrate the systematic ability of LIBS in the analysis of liquid matter. Despite the quenching problem commonly associated with LIBS, the findings of this study demonstrate that LIBS is a versatile analytical method. As such, this research supports the hypothesis that tiny liquid (say dew drops on surfaces) sampled from a detonation scene can be directly analyzed to furnish useful information about nuclear forensics signatures of fission products to apprise attribution.

### 2.3 Isotopic and Molecular Analysis using LIBS

Isotopic analysis of materials using LIBS faces a major challenge that is attributed to small isotope shifts due to Stark line broadening and Doppler's effect on the LIBS spectra resulting in loss of information (Noll, 2012 ; Mao *et al.*, 2011). However, over the past few years, advances have been made towards ensuring improved results in the use of LIBS in isotopic measurements. The feasibility of LIBS in the isotopic analysis was demonstrated by Russo *et al.* (2011) wherein, detection of isotopes of hydrogen, boron, carbon, and oxygen were illustrated using Laser ablation isotopic spectroscopy (LAMIS). Similarly, direct analysis of uranium isotope ratios by means of nanosecond laser ablation (LA) in combination with multi-collector inductively coupled plasma mass spectrometer (ICP-MS) have been reported (Kappel *et al.*, 2012). Molecular spectroscopy in ambient air and atmospheric pressure using LIBS is also affected by relatively small isotope splitting in atomic species (Mao *et al.*, 2011). This is influenced by the vibrational and rotational states of the molecule. The use of plasma sources with low electron densities such as inductively coupled plasmas (ICP), and performing laser ablations with the sample in a vacuum or in a noble gas environment have been proven to overcome this limitation. However, considering field portability of such systems and when measurements have to be made in air and atmospheric pressure conditions, chemometric-LIBS becomes more convenient.

The usefulness of uranium in nuclear energy and forensics remains high and study of such IS shifts is one of the measures towards mitigation of possible trafficking. LIBS has been used to determine isotopic shifts (IS) for uranium contained in complex matrices. This study addressed the detection limits for a variety of uranium lines as compared to the non-uranium lines with special emphasis accorded to the spectral interference. Results suggested that IS determination require high spectral resolution (Choi *et al.*, 2013).

Chemometric LIBS has been demonstrated to be a suitable approach for determining isotope ratios of  $^{235}\text{U} / ^{238}\text{U}$  and  $^1\text{H} / ^3\text{H}$  using low-resolution LIBS in the air and atmospheric pressure (Doucet *et al.*, 2011). Enriched uranium solutions were deposited on ceramic holder for LIBS measurements. The prepared samples were interrogated using 300 laser shots. PLS1 regression was used to construct a model that permitted prediction of isotopic ratios under conditions in which the univariate approach was not attainable without the use of ultra-high resolution spectrometer. This research illustrates the usefulness of isotopic analysis using a portable LIBS in NF. Also, this work suggests the robustness of chemometric procedures used and the integration of these procedures into a software user-interface can enable a non-qualified person to use it for NF applications. Therefore, development of a methodology that can simultaneously provide trace elemental, isotopic and molecular impurities in NRM is desirable.

#### **2.4 Analysis of Fusion Glass**

The first atomic bomb blast test was done on 16<sup>th</sup> July 1945 at Alamogordo in New Mexico, USA. The material mixture that melted around the range of the device formed a green glassy material referred to as trinitite (Eby *et al.*, 2010). Within the trinitite glass beads obtained, the distribution of the radioactive components reflects the actual situation if a nuclear blast was to go off. Thus in any suspected nuclear detonation, the similarity between the materials collected from such an explosion with the already known characteristics of the trinitite test (accompanied with corresponding radiochemical interpretation) has potential to infer the type of detonated device, the explosive ability, and even its source. This forms a very important part of nuclear forensics and attribution.

In order to realize the properties of nuclear melt glass and hence to develop deterrence procedures for analysis of potential nuclear terrorism involving nuclear bombs, there is need to

understand the chemical, physical and even morphological properties of the remnants – so-called post-irradiation nuclear forensics. Synthetic glass melts developed by Molgaard *et al.* (2015) serve as useful NF tools that give insight into the actual nuclear security case. In this work, a close resemblance material was produced as a surrogate trinitite with similar properties useful in conceptualizing and analyzing a similar NF situation.

Fusion bead is a common sample preparation method in X-ray fluorescence (XRF) analysis. It is considered an effective sample preparation method for accurate analysis of soils, rocks and even other refractory samples. Advantages of the fusion bead method include the inherent ability to remove heterogeneity which is as a result of various grain sizes as well as other mineralogical effects (Yamada *et al.*, 1995). In addition, the fusion bead approach reduces the co-existing component effect by dilution and also offers the possibility of preparation of standard samples from synthetic oxides.

LIBS, like XRF, suffers from matrix related effects which limit its ability to produce accurate trace element quantitative analytical results (Musazzi and Perini, 2014). Sample integration into a glass form has been found to reduce mineralogical effects. Notably, the fused glass approach does not solve the chemical matrix issues encountered in LIBS; but it provides a rather stable physical matrix which eliminates the inconsistencies in the absorption of the laser energy, improved calibration models and also, reduces the saturation commonly observed on strong peaks due to sample dilution (Pease, 2013). In addition, in typical post-detonation NF scenarios glass is an unavoidable form in which glass debris is recovered for NF analysis.

Pease (2013) used LIBS to investigate the possibility of fused glass sample preparations as opposed to pressed pellet powders in calibration models. A total of twenty-two samples were prepared both in fused glass form and pelletized form using eight major oxide elements. Fused

glass offered a more physical matrix that provided much more reliable spectral line responses as well as spot-to-spot repeatability compared to the pressed powders. Furthermore, there was appreciable discrimination of different elements when the fused glass data was statistically treated as opposed to the traditional pressed powders.

Limited research has been directed into detection of fission products in glass form using LIBS. The integration of these fission products and other high-level liquid wastes into a more compact solid phase is a necessity in nuclear waste management practices. Jung *et al.* (2011) have however demonstrated the ability of LIBS in performing analysis of actinides embedded in a glass matrix. U and Eu were chosen as surrogates for high-level nuclear wastes. In this research, the findings are presented in the context of the feasibility of LIBS measurements of trace elements in glass matrices.

## **2.5 Nuclear Fuel Reprocessing and Vitrification**

Reprocessing of used nuclear reactor fuel refers to the chemical or physical treatment of the used fuel in order to salvage the useful uranium, weapons-grade plutonium and other useful fission products. **Figure 2.5.1** illustrates the procedure that is adopted during this process. Notably, spent fuel rods are received and chopped into pieces to recover the fuel pellets. Dissolution of the constituents of the pellets is achieved using nitric acid to recover uranium and other fission products extracts (Dey and Bansal, 2006).

Solvent extraction is achieved with a mixture of tributyl phosphate (TBP) and kerosene or dedocane which are made to flow in a direction opposite to the flow of organic materials (Murray and Holbert, 2014). As a result, an aqueous solution containing uranium, plutonium and an array of other fission products such as  $^{239}\text{Ne}$ ,  $^{85}\text{Kr}$ ,  $^{90}\text{Sr}$ ,  $^{137}\text{Ce}$ , etc., is retrieved which is further separated and purified to attain U and Pu oxides.



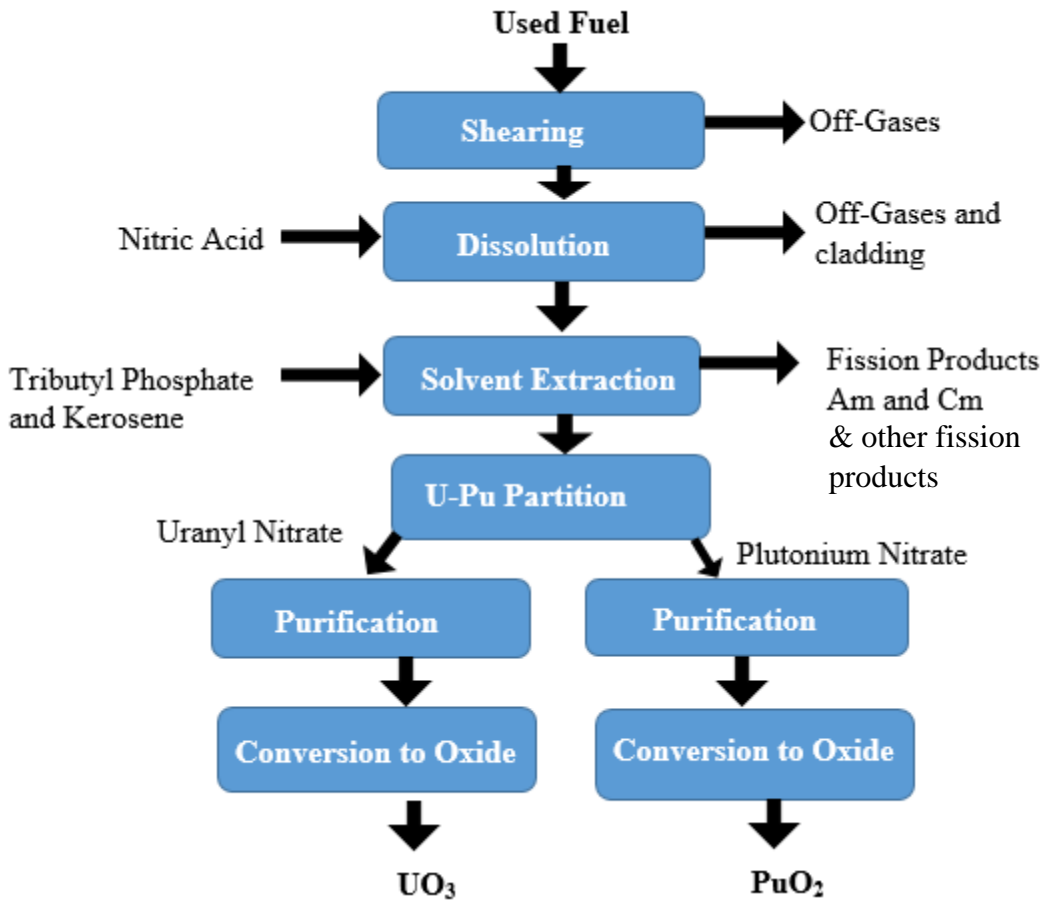


**Figure 2.5.1:** Nuclear fuel reprocessing process (After: Murray and Holbert (2014)).

It is worthwhile noting that, all these procedures i.e., digestion, dilution and even dissolution create additional radioactive wastes burden which requires specific procedures for storage as well as handling. Some of these FPs are toxic if they find their way to the hydrogeological system (Henderson, 2014). As such, these FPs are immobilized in glass in a process called vitrification. These vitrified form of the wastes is still radiotoxic and like any other high-level nuclear wastes, they must be safeguarded to eliminate the possibility of proliferation for malicious activities involving use in IED by terrorist groups. In this work, a chemometric-LIBS methodology for detection of selected fission products in simulated vitrified, powdered and liquid samples was developed for high-level nuclear wastes.

## 2.6 Chemometric LIBS

According to International Chemometrics Society, chemometrics is defined as “the science of relating the measurements made on a chemical system or process to the state of the system via application of mathematical or statistical methods” (Hibbert *et al.*, 2009). These methods involve the automated detection of useful patterns in a set of data (Shalev-Shwartz and Ben-David, 2014).

Chemometrics utilizes statistical and mathematical methods to design or select optimum procedures and experiments as well as to provide maximum information by analyzing chemical data (Yang *et al.*, 2010). Although spectra from LIBS can be perceived as elemental fingerprints of a substance, the spectra are usually very complex because, thousands of data points are collected in a matter of a second (Labbé *et al.*, 2008). As such, the practical utility of LIBS gets limited due to the complex spectra; that provides an interpretation challenge. Especially, when tiny amounts of samples are to be analyzed and maximum information is desired from the data, chemometric techniques can be employed to extract and model useful information from the LIBS spectra since solid-state detector acquired spectral data is by its nature multivariate (Angeyo, 2013; Labbé *et al.*, 2008).

### 2.6.1 Chemometrics in Other Applications

Chemometric techniques have been widely applied in different fields and have proved to be powerful tools. In biology and medical applications, SVM has been widely utilized in both disease diagnostics and prognostics (Salas-Gonzalez *et al.*, 2010 ; Xue *et al.*, 2004; Williams *et al.*, 2004; Takeuchi and Collier, 2005).

In an attempt to discriminate among different shards of pottery using LIBS, Erdem *et al.* (2008) applied principal component analysis (PCA) in correlating the spectral data with the origin of

pottery sherds from Ayanis, Dilkaya and Karagunduz excavations in Turkey. These sherds date back to the early and middle Iron Age. PCA results indicated that there was a close correlation between the composition of clay sherds obtained from Karagunduz and Dilkaya. As such, LIBS coupled with PCA offered an efficient tool for pottery characterization in the context origin assessment hence a similar combination has the potential for use in the characterization of high-level nuclear wastes in the context of NF attribution.

A combination of least squares support vector machine (LS-SVM) and LIBS has been shown to provide a sensitive analytical tool for analysis of pharmaceutical samples to detect counterfeits (Dingari *et al.*, 2012a). The authors affirm the utility of SVM in the classification of samples especially the insusceptibility to outliers compared to other linear least squares methods.

LIBS coupled with chemometrics has been shown to provide simultaneous quantitative and qualitative prediction of the molecular composition of pharmaceutical formulations (Doucet *et al.*, 2008). Chemometrics techniques were employed to establish the active pharmaceutical ingredients (API) and excipients. PCA and supervised SIMCA were used to exploit the multivariate nature of LIBS data obtained from pharmaceutical tablets in an attempt to discriminate among the drugs (Myakalwar *et al.*, 2011). The findings reveal that apart from the presence of elements such as C, H, N and O which are considered active pharmaceutical components, other inorganic atoms (Fe, Mn and Ca) were also present. The findings emphasize the importance of such PCA tablet discrimination methodology as it plays a crucial role in rapid on-line process monitoring, the accuracy of quality control and assurance process in the pharmacological industry.

LIBS in combination with chemometric techniques has been utilized in performing quantitative and explorative analysis in soil and rock samples acquired from High Background Radiation

Areas (HBRA) (Mukhono, 2012). The goal of the study was to establish both atomic and molecular signatures that have utility in characterizing HBRA and evaluating the impact of HBRA geothermic discharges on the immediate environment. Chemometric techniques (PCA, PLS, ANN, and SIMCA) provided good quantitative calibration and modeling of spectra obtained using LIBS in relation to the concentrations of the analytes of interest namely; Cu, Ti, As, Pb and Cr.

Duchêne *et al.* (2010) focused on the utility of LIBS combined with chemometrics to perform archaeological metal characterization, pigment, and stone identification in cultural heritage applications. In particular, 30 commercial pigments traditionally used in murals were directly analyzed using LIBS technique to detect the characteristic chemical constituents. The acquired spectral data were used together with two different chemometric models namely; soft independent modeling of class analogy (SIMCA) for pigment identification and partial least squares discriminant analysis (PLS-DA) for characterization. The use of multivariate analysis approach led to a remarkable improvement of pigments identification despite the background noise. This implies that chemometric methods are handy in the analysis regardless of the background noise.

Sirven *et al.* (2006) measured the concentration of chromium in soil samples. Calibration curve method was compared with two multivariate chemometric calibration techniques namely PLS and ANN. The precision, accuracy, of prediction and the LoD for the three techniques were compared. ANN technique was shown to correctly model the non-linearity due to self-absorption and provided the most acceptable results of order 10% compared to PLS. PCA was used to classify spectra from different soil samples.

A novel analytical methodology for the classification of soils in Brazil was achieved by means of LIBS with chemometric techniques (Pontes *et al.*, 2009). Linear discriminant analysis (LDA) was employed based on the reduced subset spectral variable to build a classification model. A total of 149 Brazilian soil samples were grouped into three major classes namely Latossolo, Nitossolo, and Argissolo. Three techniques were used for variable selection namely; successive projection algorithm (SPA), genetic algorithm (GA) and stepwise formulation. Wavelet data compression approach was utilized in reducing the computational workload, especially in variable selection. Consequently, a classification rate of 90 % was achieved within the validation set whereas for cross validation set, an average classification rate of 72 % was achieved using a combination SPA-LDA. The wavelet transforms compression procedure was found to provide a 100-fold reduction in computational workload without any noticeable effect on the classification accuracy of the models (Pontes *et al.*, 2009).

Multivariate calibration of LIBS for *in situ* monitoring of the composition of Pu feed in plutonium lanthanide borosilicate (PuLaBS) glass has been shown to improve results compared to univariate calibration (Tripathi *et al.*, 2009). Multivariate calibration on the LIBS data was deemed useful in predicting the concentration of Ce, Cr, Fe Mo and Ni in the plutonium oxide surrogate residue. Through univariate calibration, the coefficient of determination was found to be 0.87 with a root mean squared error (RMSE) of 7.46%. By means of PCR and PLS, a multivariate calibration model, the coefficient of determination was found to be 0.97 and RMSE of 2.93 %. Therefore, multivariate calibration models for Ce performs better compared to the univariate approach.

## 2.6.2 Chemometrics Methods in Nuclear Science

Chemometric techniques have been used in nuclear science in a wide range of applications. These techniques also have potential in NF in achieving origin assessment and composition of nuclear materials based on sample properties. Jones *et al.* (2014) demonstrated the feasibility of pattern recognition to determine the reactor type of a given spent fuel using isotopic and elemental investigations. PCA was employed in dimensionality reduction as well as in the removal of outliers (to preserve 99 % of the useful information). The Parzen window classifier (a probabilistic neural network) technique was used to achieve classification of reactor type data (generated through FISPIN depletion package) and achieve classification of different reactor fuels. However, the authors noted that the approach was based on FISPIN generated data and therefore had a limitation when applied to real samples. As this work does not rely on computer-generated data, the analysis of FP in HLW could better closely match the expected results in a typical nuclear forensics case.

Sirven *et al.* (2009) demonstrated a technique in which LIBS coupled with chemometrics was used to successfully discriminate between yellow cake (powdered uranium ore concentrate) from the different geographical origins on the basis of 502.752 nm uranium emission line free from spectral interference. LIBS spectra for eleven samples obtained from different locations were used together with PCA and SIMCA models. It was found that the SIMCA model provided a 100 % correct identification for all classes. In another study, PCA clustered soil and rock samples acquired from different geological origins into distinct groups which infer potential of LIBS in geochemical fingerprinting of uranium sources. Notably, the rare earth elements (REE) were identified to contribute greatly to the clustering observed (Bhatt *et al.*, 2015; Bhatt *et al.*, 2018).

Similarly, PCA has demonstrated attribution of geolocation of UOC samples through iterative PLS-DA (Robel *et al.*, 2009).

PCA and FDA have been utilized in the visualization of various uranium-bearing compounds with a particular interest in nuclear forensics. In their work, different uranium compounds namely; “ $(\text{NH}_4)_2\text{U}_2\text{O}_7$ ,  $\text{Na}_2\text{U}_2\text{O}_7$ ,  $\text{UO}_2\text{CO}_3 \cdot 2(\text{NH}_4)_2\text{CO}_3$ ,  $\text{UO}_2(\text{OH})_2$ ,  $\text{UO}_2$ ,  $\text{UO}_3$ ,  $\text{UO}_4$ ,  $\text{U}_3\text{O}_8$  and  $\text{UF}_4$ ” (Ho *et al.*, 2015) were analyzed using Raman spectroscopy. The clustering of these samples into distinct groups was in support of the hypothesis that different uranium-bearing compound exhibit different properties such that any suspected UOC sample can easily be identified as a UOC or not. These results are useful especially in the front end of the nuclear fuel cycle because the study does not involve fission products. However, considering that there is a need for nuclear safety especially when radioactive FP from the back end of the nuclear fuel cycle are involved, this thesis applies a similar concept to discriminate samples with FP from those without, utilizing PCA and SVM.

In this thesis, we have demonstrated that a combination of SVM, PCA, and ANN offers a robust methodology for nuclear forensic applications. The methodology enables accurate discrimination of uranium and FP in vitrified samples, pressed pellets and HLLW samples which offers useful information in quasi-nuclear forensic attribution.

## CHAPTER III

### THEORETICAL BACKGROUND

#### 3.1 Overview

In this chapter, the basic principles of qualitative and quantitative LIBS are presented. The theory behind multivariate techniques namely ANN, PCA, and SVM are discussed and linked with nuclear forensics applications. Different neural network architectures used in ANN are discussed. Multivariate chemometric calibration and exploratory modeling principles are also discussed.

#### 3.2 Principles of LIBS

Elemental analysis is very important in many fields. There are many analytical techniques that can be employed to facilitate analysis of materials for elemental content to appreciable detection levels. Where accuracy and precision are highly desirable like in a nuclear forensic analysis, the need for direct rapid, non-invasive technique that can enable analysis of limited sample sizes is desirable. LIBS has developed over time to be a useful technique that has immense ability to realize such an analysis.

LIBS is thus a versatile atomic emission spectroscopic technique for elemental analysis. In this technique, a highly focused pulsed laser beam is used to ablate very small (microgram) amount of sample to create a high-temperature microplasma. The specific characteristics of plasmas include; the degree of ionization, plasma temperature and the electron density (Cremers *et al.*, 2006). If the ratio of the electrons to other species in the plasma is less than 10 %, then the plasma is weakly ionized. Conversely, very highly ionized plasmas consist of high electron



densities. For instance, electron number density in ICP is approximately  $10^{15} \text{ cm}^{-3}$  compared to  $10^{17} \text{ cm}^{-3}$  in ablation plasmas used in LIBS (Mao *et al.*, 2011).

In LIBS, the properties of the plasma used in achieving breakdown ought to be known since these plasma features contribute towards the nature of the line profiles (Stavropoulos *et al.*, 2004; Cremers *et al.*, 2006). The plasma is considered optically thin when there is negligible self-absorption or scattering of the laser radiation such that the photons emitted by the constituent elements escape the plasma core freely. The intensity of radiation emitted  $I(\lambda)$  is given by (Cremers *et al.*, 2006):

$$I(\lambda) = \left[ \frac{\varepsilon(\lambda)}{\alpha(\lambda)} \right] \{1 - e^{-\alpha(\lambda)L}\} \quad (3.1)$$

Where;  $\varepsilon(\lambda)$  is the emissivity,  $\alpha(\lambda)$  the linear absorption coefficient and  $L$  is the plasma length observed along the line of sight. It is important to note that when  $\alpha$  is very small, the equation defines the condition for an optically thin plasma which is given by:

$$I(\lambda) = \left[ \frac{\varepsilon(\lambda)}{\alpha(\lambda)} \right] [\alpha(\lambda)L] \sim \varepsilon(\lambda)L \quad (3.2)$$

The optical thickness of the plasma can be evaluated by observing a well-known spectral line for the presence of an absorption feature. Usually, the line will appear to possess a dip at the centroid frequency. This observed feature creates a problem of converting the resulting intensities into concentrations which is a major challenge in calibration free LIBS (CF-LIBS) technique (Cremers *et al.*, 2006). Notably, in CF-LIBS an assumption of the existence of a local thermodynamic equilibrium (LTE) is made. The relative intensities of the spectral lines are used

to construct a family of Boltzmann plots for all the components of the plasma. The intercept of the lines gives the concentration of the constituents. However, the major challenge encountered in CF-LIBS is to account for the contribution of each of the constituents within the plasma in addition to the fact that plasma can exist in different temperatures.

The Saha-Boltzmann equations provide the average electron density ( $N_e$ ) within the spectroscopic time window. The number of ions in first ionization state is determined by (Barbini *et al.*, 2000):

$$N_e = \frac{N_a}{N_i} \cdot \frac{U_i(T)}{U_a(T)} \cdot B \cdot (KT)^{\frac{3}{2}} \cdot e^{\left(\frac{-E_{\infty}}{KT}\right)} \quad (3.3)$$

Where, B is a constant,  $U_a(T)$  and  $U_i(T)$  are partition functions of the atomic and ionic state respectively,  $N_a$  and  $N_i$  are the population density of atoms and ions respectively within the spectroscopic window, T is the plasma temperature, K is the Boltzmann constant and  $E_{\infty}$  is the ionization energy.

The instantaneous temperature at the surface of the sample can reach up to 30,000 °C (Russo *et al.*, 1999). At this high temperature, the ablated material of the sample dissociates directly into excited ionic and atomic species (Rinke-kneapler and Sigman, 2014; Judge *et al.*, 2013). The microplasma expands rapidly outwards at supersonic speeds and cools at which time, the excited ions and atoms emit characteristic radiation as they de-excite to the lower energy states (Loudyi *et al.*, 2009). This optical emission (which contains information about elemental composition) of the ablated material is collected by means of an optic fiber and focused onto a spectrometer (Choi *et al.*, 2013; Loudyi *et al.*, 2009). By means of a suitable detector, the emission is

spectrally resolved to enable the identification and measurement of the spectral emission peaks, which are characteristic of the elemental composition of the sample under investigation.

The distribution of speeds of the excited particles and even the relative population of energy levels following plasma formation can well be explained using the concept of near local thermodynamic equilibrium (nLTE). This concept acknowledges the fact that equilibration occurs only in small regions of space (e.g. the core of the microplasma), however, it is dynamic from one particular region to another (Musazzi and Perini, 2014). Hence, if the experiment supports the possibility of the existence of an LTE, then the distribution of velocities of the quantities follows the Maxwell velocity distribution function:

$$f_M = \left( \frac{m}{2\pi kT} \right)^{3/2} e^{-\frac{mv^2}{2kT}} \quad (3.4)$$

In which,  $m$  and  $v$  are the mass and the velocity of the electron respectively. Thus the population of the energy levels assuming atomic or molecular species given by the Boltzmann distribution with the ground state as a reference point is given as:

$$\frac{N_j}{N_o} = \frac{g_j}{Z} e^{-\frac{E_j}{kT}} \quad (3.5)$$

Therefore, for relative populations the binding relationship is given as:

$$\frac{N_j}{N_i} = \frac{g_j}{g_i} e^{-\frac{E_j - E_i}{kT}} \quad (3.6)$$

Here,  $i$  and  $j$  are energy levels,  $N_o$  is the total population of the species,  $N_{i,j}$  are the populations of the energy levels and  $Z$  is the partition function which is the statistical weight of the reference state (ground state). Thus, the spectral line has intensity (radiant energy per unit volume) is given as:

$$I = \frac{h\nu g A N}{4\pi} = \frac{hc N_o g A}{4\pi \lambda Z} e^{-\frac{E}{kT}} \quad (3.7)$$

With  $\nu$  as the frequency of the line,  $A$  is the transition probability (Einstein coefficient) and  $N$  the absolute number density of species. The concentrations of a particular element of interest can be obtained by performing a comparison between the unknown line intensity and that of a known reference sample which possess approximately similar thermal properties (Stavropoulos *et al.*, 2004).

LIBS also offers the possibility of performing depth-profiling of layered structures and surface coatings (Noll, 2012). As the laser drills into the material, spectroscopic measurements can be performed providing the elemental composition of the material as a function of the depth into the layered structure.

### 3.3 Multivariate Chemometric Calibration and Modeling

Adoption of chemometric techniques in laser spectroscopy serves to overcome some of the limitations encountered during analysis of samples especially in instances where rapid nuclear forensics is desired. Multivariate analysis methods have the potential of minimizing the complexity of data, extracting the most relevant features in the data as well as developing

calibration strategies in trace quantitative measurements which classical LIBS or even calibration free LIBS cannot achieve (Labbé *et al.*, 2008).

### **3.4 Artificial Neural Networks (ANN)**

An ANN as a chemometric tool is derived from the principles of operation of a biological neuron. It is a special biological tool that processes information. A typical biological neuron is shown in **Figure 3.4.1**. Its main components include the cell body (soma) that contains plasma with molecular equipment necessary for forming materials required by the neuron (Jain *et al.*, 1996). The dendrites (receivers) receive impulses from axons of other neurons through the synaptic gap and the resulting signal generated by the soma cell is transmitted along the axon (transmitter) to the dendrites of other neurons. The point of contact between the axon of one neuron and a dendrite of another neuron is called the synapse. The synaptic joint is an elementary functional unit that contains neurotransmitters. These neurotransmitters diffuse across the synaptic gap to inhibit or enhance an impulse to the receptor neuron to emit electrical signals. The cell body mainly serves the purpose of summing up the incoming signals and determine whether they exceed a given threshold value. In case the summation of the incoming signals exceed the threshold value, the cell body sends a signal to other neurons to effect a response in the muscles involved (Fausett, 1994).

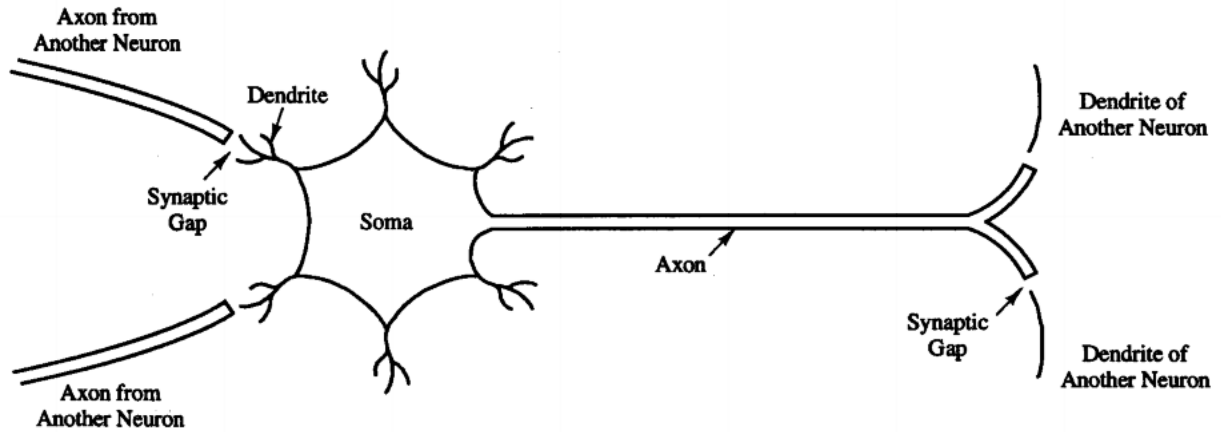


**Figure 3.4.1:** A sketch of a biological neuron (Source: Naguib and Sherbet (2001)).

In this regard, the components of an ANN are akin to the biological neuron in a variety of ways. The transfer function, the inputs, the output and the weights mimic the soma cell, dendrites, axon, and synapse respectively. The learning process which refers to the problem of updating the neural network to perform specified tasks with a high level of confidence is likened to the efficiency of impulse transfer across the synapse. **Figure 3.4.2** shows the components of an ANN and its similarity to a biological neuron.

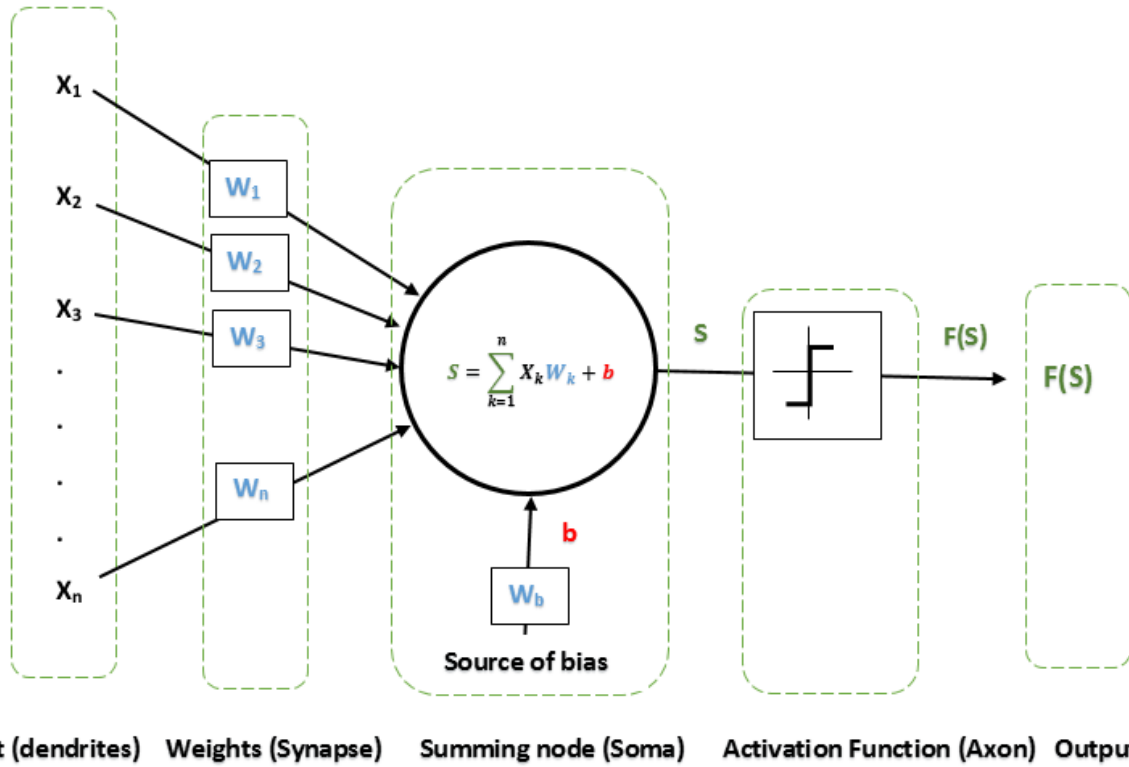


**Figure 3.4.2:** Schematic of a simple ANN and its similarity to a biological neuron (After: Naguib and Sherbet (2001)).

Therefore, ANN is a nonlinear computational tool capable of modeling complex functions such as spectral data from LIBS. ANN is useful in non-linear ordination and visualization of data models (Angeyo, 2013). In order to achieve a robust artificial neural network, the network has to be trained using a set of reference spectra or concentration data which represents part of what is to be analyzed; for example a set of known emission intensities corresponding to a known concentration of particular target elements. In training the network, sets of weights and bias through a system of neurons are developed in order to reduce the errors in the desired output. Prediction ability of the network is then achieved by a validation set of data that has not been initially shown to the network.

#### **3.4.1 Feed Forward Back Propagation ANN Algorithm**

The backpropagation algorithm is the most popular ANN. A simple approach followed by this algorithm is as given in **Figure 3.4.3**. This type of algorithm can be characterized by four main parts which involve; the feedforward nature of computation, a gradual backpropagation to the output layers, a continuous back-propagation to the hidden layers of the network and a gradual update of the weights of the network (Cilimkovic, 2015).



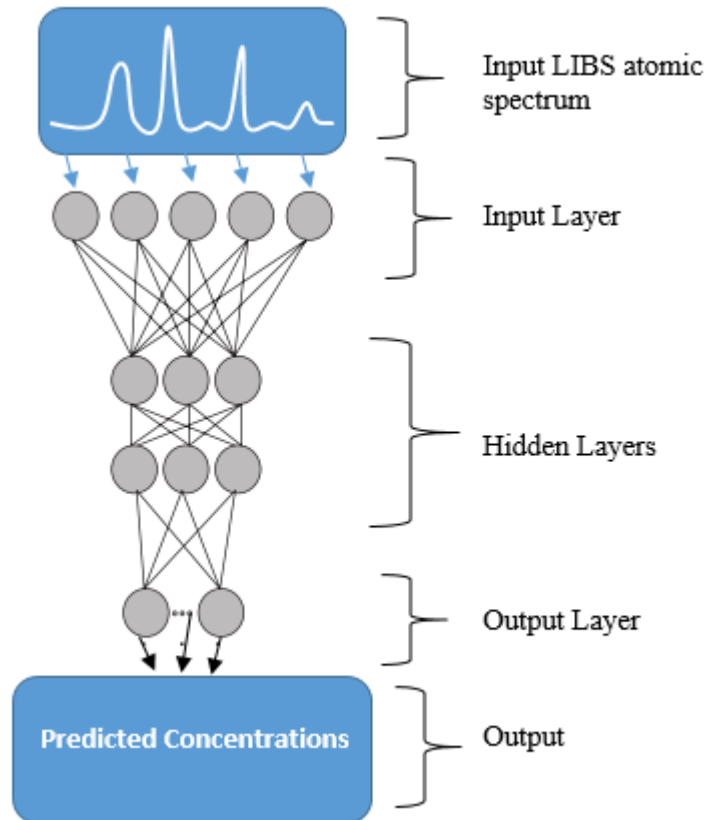


**Figure 3.4.3:** Schematic diagram of feed forward back propagation utilizing LIBS spectral data (After: Andrade-Garda *et al.* (2009)).

### 3.4.2 Cascade Correlation Algorithm

Cascade-correlation is an ANN architecture that begins out as a network without a pre-defined topology (Schetinin, 2003). **Figure 3.4.4** shows a simple schematic of the process followed when utilizing the cascade correlation algorithm. It can be considered as a multilayer architecture because normally it begins out as a network without any hidden neurons, throughout the training process new neurons are added one by one. When a new neuron is added its input side weights are frozen as a result, each of the hidden neuron added becomes part of the network that influences the creation of other neurons as well as affecting the output (Fahlman and Lebiere,

1990). Because of the intrinsic ability to adjust the weights and neurons by itself, the cascade correlation architecture defines its own topology and size hence it learns more rapidly and retains much of the structures despite changes in the training set.

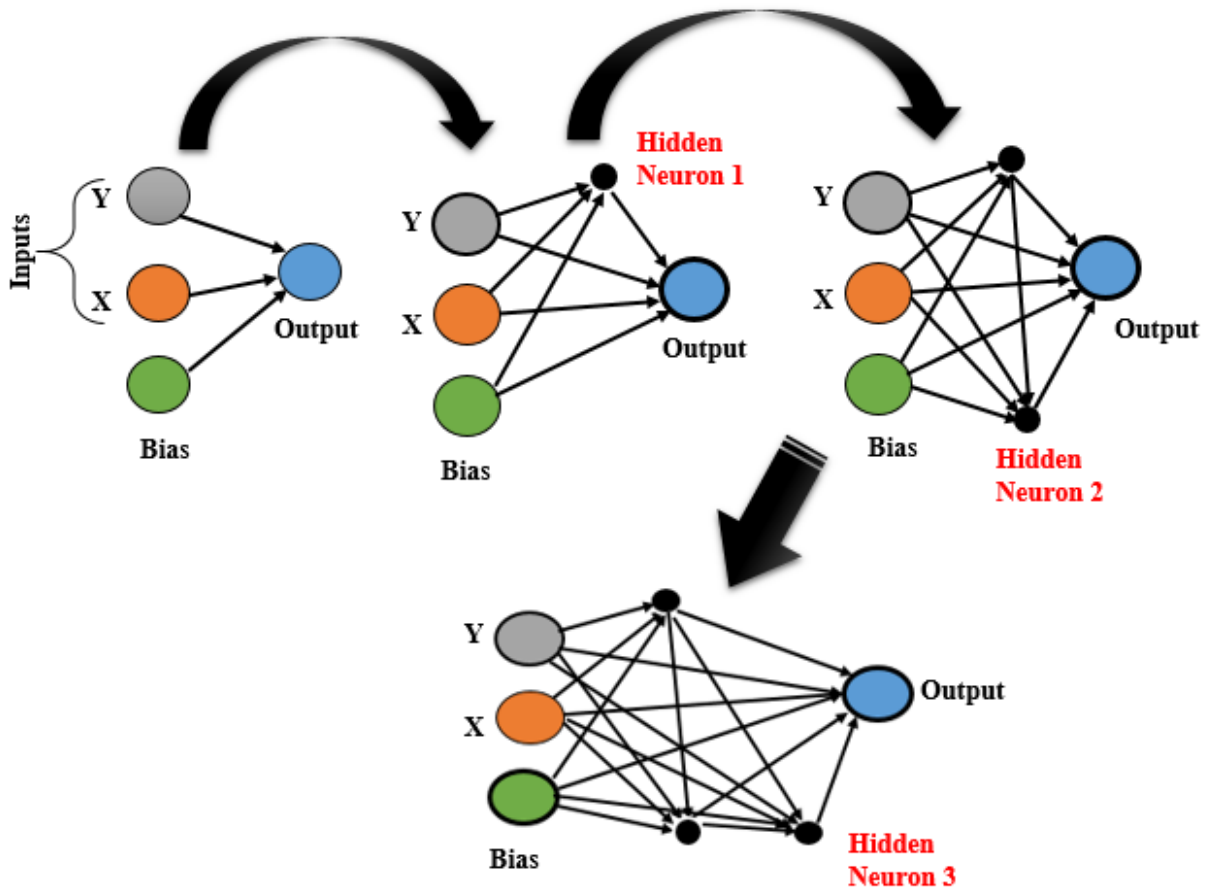


**Figure 3.4.4:** Simple cascade correlation architecture (After: Schetinin (2003)).

The cascade architecture algorithm looks for the termination of the learning process which is evaluated through analysis of the error obtained as compared to the target error.

### 3.5 Principal Component Analysis (PCA)

Principal component analysis is an unsupervised technique for exploratory data analysis. As opposed to supervised learning that provides a set of features  $(X_1, \dots, X_p)$  measured on a given number of variables  $(n)$  with corresponding expected outcome  $Y$ , unsupervised learning lacks the associated response variable  $Y$  and therefore its goal is to explore the data with the aim of discovering interesting outcome about the measurements. PCA provides avenues to summarize high dimensional data into a lower dimensional data set with a smaller number of variables (principal components) which, to a higher percentage, summarize the variability in the actual data set. In general, if  $\mathbf{X}$  is a matrix of  $n \times p$  dimensions then there are  $(n - 1, p)$  distinct principal components. However, it is a common practice to take into consideration the smallest number of PCs which is the aim of unsupervised learning. The criteria for selecting the number of PC to work with largely depends on the individual decision, the nature and type of the data involved. The *scree plot* which shows the proportion of variance explained by each of the PCs is often used to select the number of PCs through eyeballing the *scree plot* to identify the elbow point where the proportion of explained variance drops off. In addition, PCA aids in visualizing the nature of the data and even the associated variables.

PCA operates following the concept of the high dimensional dataset having smaller components. Assuming a set of features  $X_1, X_2, \dots, X_p$  then according to James *et al.* (2013), the first principal component is the summation of the linear combination of the features that possesses the largest variance

$$Z_1 = \phi_{11}X_1 + \phi_{21}X_2 + \dots + \phi_{p1}X_p \quad (3.8)$$

Note that, the data is normalized so that  $\sum_j^p \phi_{j1}^2 = 1$  and the elements  $\phi_{11}, \dots, \phi_{p1}$  are the loadings of the first principal component.

The principal component loading vector is given by:

$$\phi_1 = (\phi_{11} \phi_{21} \dots \phi_{p1})^T \quad (3.9)$$

A linear combination of measurements of the sample takes the form given by:

$$z_{i1} = \phi_{11}x_{i1} + \phi_{21}x_{i2} + \dots + \phi_{p1}x_{ip} \quad (3.10)$$

The first principal component solves the optimization problem given by equation 3.11 whose solution can be obtained by eigen decomposition approach.

$$\text{Maximize}_{\phi_{11}, \dots, \phi_{p1}} \left\{ \frac{1}{n} \sum_{i=1}^n \left( \sum_{j=1}^p \phi_{j1} x_{ij} \right)^2 \right\} \text{ subject to } \sum_{j=1}^p \phi_{j1}^2 = 1 \quad (3.11)$$

It is worth noting that the object that is maximized in the equation above represents the sample variance of n values of  $z_{i1}$ . Also  $z_{11}, \dots, z_{n1}$  are called the scores of the first principle component.

The second principal components represent a linear combination of the measurements that have maximal variance out of all linear combinations that have no correlation with the first principal component.

The scores of the second PC is given by:

$$z_{i2} = \phi_{11}x_{i2} + \phi_{22}x_{i2} + \dots + \phi_{p2}x_{ip} \quad (3.12)$$

Where,  $\phi_2$  is the second PC loading vector. The fact that the first PC is uncorrelated with the second PC is equivalent to constraining the individual loading vectors to be orthogonal to each other.

### 3.6 Support Vector Machines (SVM)

Support vector machine (SVM) is a maximal margin classifier that is used in discriminating between given groups of data using *hyperplanes*. A *hyperplane* is defined depending on the dimension of the data. In two dimensional space, a *hyperplane* is simply a line or a flat one-dimensional subspace that offers maximum margin between two sets of data. In three dimensional space, a *hyperplane* can be perceived as a surface or a two-dimensional subsurface that separates the groups (Varmuza and Filzmoser, 2016). Therefore without loss of generality, in  $p$  dimensional space, the *hyperplane* corresponding to such space is given by  $p - 1$ . Notably, in two dimensions the equation of a separating hyperplane is given

$$\beta_0 + \beta_1X_1 + \beta_2X_2 = 0 \quad (3.13)$$

Here  $\beta_0, \beta_1$  and  $\beta_2$  are parameters and if there is a value of  $X = (X_1, X_2)^T$  for which equation holds true, then the point can be located on the hyperplane. Conversely, if  $X$  does not satisfy the above equation

$$\beta_0 + \beta_1X_1 + \beta_2X_2 > 0 \quad (3.14)$$

On the other hand,  $X$  can also take the form

$$\beta_0 + \beta_1 X_1 + \beta_2 X_2 < 0 \quad (3.15)$$

In which case, the value lies on the other side of the equation.

Therefore for a p dimensional space, the equation of the hyperplane takes the form

$$\beta_0 + \beta_1 X_1 + \beta_2 X_2 + \dots + \beta X_p = 0 \quad (3.16)$$

Hence equally, a value of  $X = (X_1, X_2, \dots, X_p)^T$  for which the equation above is satisfied, then the point can be located on the hyperplane. Generally, “a hyperplane divides a p-dimensional space into two halves and one can easily determine which side of the hyperplane a point lies by simply calculating the sign of the left hand side” (James *et al.*, 2013).

If any data can be separated by a hyperplane, then there is an infinite number of *hyperplanes* that can be determined. The maximal marginal *hyperplane* is the criterion for selecting the most optimal *hyperplane*. This is because a classifier that has a maximum margin on the training data will equally have a large margin on data that has not been shown to the classifier. The data points in any dimensional space that determine and support maximum margin of hyperplane are called support vectors. The maximal margin classifier provides the best means of data classification if a hyperplane exists. Naturally, spectral data such as LIBS data is non-separable in most cases and instead of maximal margin classifier, support vector classifier is used. This classifier is also known as the soft margin classifier as it violates the need to have every observation in the data on the desired side of the separating *hyperplane*.

## CHAPTER IV

### MATERIALS AND METHODS

#### 4.1 Overview

This chapter presents the methodology that was used in achieving the objectives of this work. The LIBS system used to perform the analysis is presented together with the operating conditions. The methodology that led to the production of fused glass samples is presented. For a similar concentration of fission products, pellet samples were also prepared to closely match nuclear waste powders. In addition, samples of a similar set of the fission products were prepared as liquids to mimic high-level nuclear wastes. Spectral pre-processing techniques employed in this work to achieve a robust modeling are briefly described.

#### 4.2 LIBS Instrumentation

Ablation and excitation of the sample was achieved by means of a Q-switched pulsed Nd:YAG laser operating at a fundamental wavelength of 1064 nm. Emission from the microplasma was collected by means of the optical fiber (fused silica, 0.22 mm numerical aperture, and 101 mm focal length). **Figure 4.2.1** shows the schematic diagram of LIBS.

The detection system consists of seven high resolution (HR) spectrometers from Ocean Optics covering 200-980 nm range whose specifications are provided in **Table 4.1**. These spectrometers are composed of 2048 pixel linear silicon CCD array with an optical resolution of 0.065 nm (LIBS 2500 PLUS Operational Manual, 2008). Notably, this system of spectrometers acquires data through the OOILIBS software with the ability to identify spectral lines, compare the corresponding wavelength with the existing database of atomic or molecular emission wavelengths and delivers distinct peaks of the elements present in the sample. Other optimum parameters of the LIBS system are summarized in **Table 4.2**.

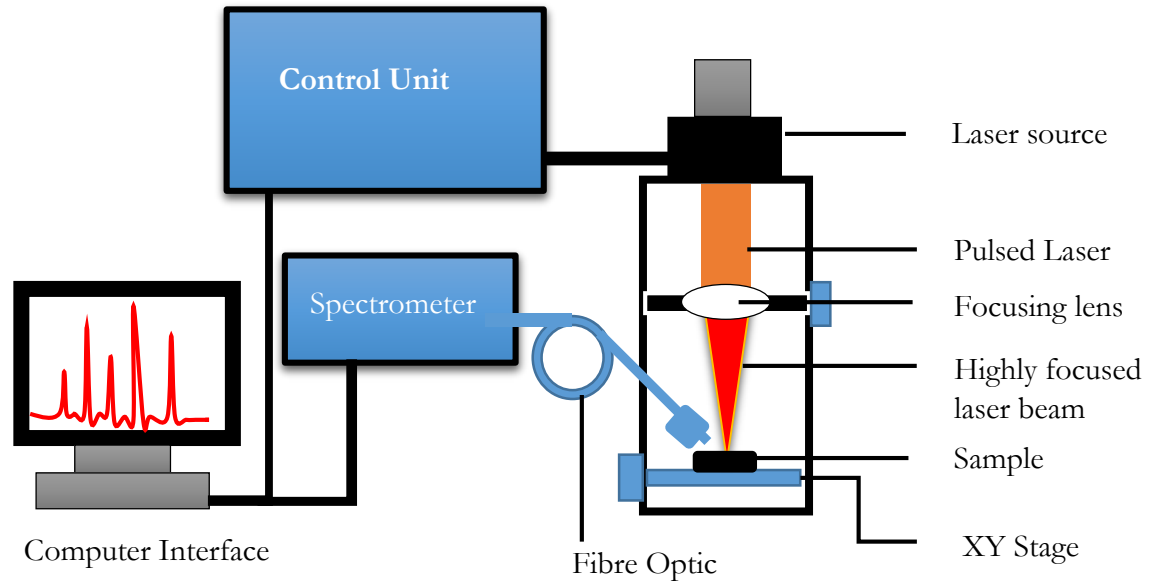


**Figure 4.2.1:** Schematic diagram of LIBS (LIBS 2500 PLUS Operational Manual (2008)).

**Table 4.1:** Specifications of spectrometers from Ocean Optics utilized in this study

	<b>Model</b>	<b>Region</b>	<b>Gratings (lines/mm)</b>	<b>Wavelength Range (nm)</b>
<b>1</b>	HR+C0463	UV	2400	200-305
<b>2</b>	HR+C0464	UV	2400	295-400
<b>3</b>	HR+C0465	Vis	1800	390-525
<b>4</b>	HR+C0466	Vis	1800	520-635
<b>5</b>	HR+C0467	Vis-NIR	1800	625-735
<b>6</b>	HR+C0468	NIR	1800	725-820
<b>7</b>	HR+C0469	NIR	1800	800-980



**Table 4.2:** Other optimum parameters of the LIBS system used in this study

---

<b>LIBS 2500 PLUS, Q-Switched Nd:YAG Laser (Ocean Optics)</b>	
<b>1. Laser wavelength</b>	1064 nm
<b>2. Pulse width</b>	10 ns
<b>3. Pulse repetition frequency</b>	10 Hz
<b>4. Maximum energy</b>	50 mJ
<b>5. Q-switch delay</b>	150 $\mu$ s
<b>6. Integration time</b>	0.42 $\mu$ s

---

### **4.3 Optimization of the LIBS System**

Optimization of the LIBS was achieved using uranium pellet standard together with LIBS spectral reference database (Ralchenko *et al.*, 2006) to ensure the best signal-to-noise ratio (SNR) of selected well-defined peaks. The Q-switch delay time ( $t_d$ ), the distance between the optical fiber to the sample, the choice of the energy of the laser, the inter-pulse delay, and the number of laser ablations was investigated as a function of intensity in order to ensure optimal spectral output.

### **4.4 Sample Preparation Procedures**

The analytical grade chemical compounds used in this work to mimic the fission products are as listed in **Table 4.3**. These salts are analytical grade chemicals with 99.9% purity defined by the accompanying certificates.

The compounds listed in **Table 4.4** were utilized as a glass-forming matrix on which the FPs were spiked at varying concentrations. This approach was undertaken to mimic the borosilicate glass commonly used in the immobilization of fission products. Notably, pure silicon dioxide (silica) normally melts at temperatures greater than 1600 °C. The furnace available at the University of Nairobi could support a maximum temperature of 1400 °C . However, when low atomic number oxides and carbonates are added, an ‘aggressive’ mixture is formed in which the melting point of silicon oxide is greatly reduced. This approach was undertaken in producing simulate fused glass beads due to lack of high-temperature furnace.

**Table 4.3:** Analytical grade reagents used as donors of the simulate fission products

<b>Name of the Compound</b>	<b>Chemical Formula</b>	<b>Formula Mass (g/mol)</b>	<b>Target species</b>	<b>Manufacturer</b>
1. Rubidium chloride	RbCl	120.921	Rb	Aldrich chemical Company, Inc, USA
2. Strontium chloride	SrCl <sub>2</sub> .6H <sub>2</sub> O	266.610	Sr	Aldrich chemical Company, Inc, USA
3. Tellurium dioxide	TeO <sub>2</sub>	159.600	Te	Darmstadt, Germany
4. Yttrium nitrate	Y(NO <sub>3</sub> ) <sub>2</sub> .5H <sub>2</sub> O	364.993	Y	Sigma-Aldrich, Darmstadt, Germany
5. Zirconium (IV) oxide	ZrO	123.218	Zr	Aldrich chemical Company, Inc USA
6. Uranium trioxide	UO <sub>3</sub>	286.026	U	BDH Chemicals, Poole, England
7. Uranyl nitrate	UO <sub>2</sub> .(NO <sub>2</sub> ) <sub>2</sub> .6H <sub>2</sub> O	502.129	U	BDH Chemicals, Poole, England

**Table 4.4:** Composition of the glass forming support matrix

Compound	Chemical Formula	Formula Mass (g/mol)
1. Silicon (IV) oxide	SiO <sub>2</sub>	60.083
2. Calcium carbonate	CaCO <sub>3</sub>	100.087
3. Sodium carbonate	Na <sub>2</sub> CO <sub>3</sub>	105.989
4. Aluminum oxide	Al <sub>2</sub> O <sub>2</sub>	101.960
5. Lithium metaborate (Fusion agent)	LiBO <sub>2</sub> .2H <sub>2</sub> O	85.780

Among the compounds in **Table 4.3**, yttrium nitrate, rubidium chloride and strontium chloride were highly hygroscopic forming crystalline crumps when left in the air. Weighing of these compounds was a major challenge due to the hygroscopic behavior and also considering that minute masses were involved. The compounds were therefore quickly weighed into a crucible and quickly ground to reduce exposure time in the air. The compounds were then ground to fine powder to reduce particle sizes.

Randomized concentrations within the typical range (i.e 10 to 1000 ppm) for each element were generated using the RANDBETWEEN function in Microsoft Excel. Each of the resulting samples represented a 0 – 5 % augmented natural uranium (grade) as a representative of the post-irradiation fuel simulate. Utilizing the randomized concentrations, the respective masses required to get any chosen target concentrations were calculated using the serial dilution formula given in equation 4.1 (Ali and Raouf, 2011).

$$C_1V_1 = C_2V_2 \quad (4.1)$$

Where  $C_1$  and  $C_2$  are initial and final concentration respectively, and  $V_1$  and  $V_2$  are the initial and final volumes respectively. By means of weighing balance (AT60 Delta Range METTLER TOLEDO), the masses of the individual FP and U were weighed for each of the samples. The composition of uranium in each of the samples was set between 1000 ppm and 50000 ppm typical to its occurrence in spent fuel, while that of the other FP was retained between 0 and 1000 ppm except for zirconium whose occurrence in radioactive wastes can have concentration values up to 4000 ppm (Bevilacqua *et al.*, 1987; Audero *et al.*, 1995). Zirconium concentration is higher compared to other FP because it is applied as the main cladding of nuclear fuel pellets and sintered at high temperature.

Reactor technology and the corresponding reactor types have been discussed in Bodansky (2007). For example, pressurized heavy water reactor (PHWR) utilizes heavy water as a coolant as well as a moderator (McIntyre, 1975). The unique feature of this reactor is that it uses natural uranium as the fuel. From the objectives of this work, it is thus easier to simulate spent fuel from PHWR as the uranium composition is that of yellow cake. ORIGEN FP depletion package is used to estimate fission products in spent fuel. In this work, the FP reference figures which represent the concentration of fission products in HLLW arising from the reprocessing of PHWR with a burnup of 7000 MW d/t U with a concentration of 250 l HLLW/t U and a cooling period of 20 years. The FP compositions have been evaluated based on the abundance of these fission products and the actinide family by means of the ORIGEN computer code as reported in (Bell, 1973).

The compounds giving the glass matrix were also weighed one by one for each of the samples and mixed thoroughly as described in the paragraph below. The total composition of uranium

plus the fission products and the glass forming matrix compounds in **Table 4.4** were maintained at 1g for each of the 30 samples prepared.

Homogeneity in solid-solid dilution is a major challenge in analytical chemistry involving such samples. To maximize sample homogenization, the sample was put in a set up with a mixer and a drill machine rotating at 2800 rev/min for 5 minutes while shaking vigorously. Each of the samples was then coded S1, S2, S3 ...etc. These samples were divided into three groups. The first group was fused with lithium metaborate to form 30 fused glass samples as described in section 4.4.1. The second group of the samples was used to simulate high-level nuclear waste powders as described in section 4.5.1. Lastly, to simulate high level liquid nuclear waste part of the sample was used as described in section 4.5.3.

#### **4.4.1 Preparation Fused Glass Sample**

After preparing stock samples for 30 varying concentrations of each of the fission products, the mixture was again thoroughly mixed to maximize homogeneity. 0.043 g of a sample was carefully weighed and placed in clean containers. 0.215 g of lithium metaborate was carefully weighed and mixed with the sample. The resultant mixture was placed in a Pt-Au crucible (top outer diameter 20 mm, bottom diameter 12 mm, height 5 mm, capacity 2.5 mL) and introduced into the furnace as shown in **Figure 4.4.1**. The total weight of the crucible before fusion was measured and recorded. Fusion and casting of the fused glass were done in the same crucible. The above procedure was repeated for the remaining 29 samples with varying concentrations of U and the associated fission products. The flux to sample ratio was maintained at 5:1 for all of the samples.

Non-wetting-agents (NWA) behave as surfactants that lower the probability of the glass melt sticking onto the surface of the platinum molds. In glass fusion, alkaline halides are commonly

used as NWA. These releasing agents are added in small quantities usually a few milligrams. One major disadvantage of NWA is their tendency of remaining within the fused bead (Watanabe, 2015) hence analysis of elements that exhibit spectral interference with the alkaline halides is a potential challenge. The NWA is normally added before fusion or during fusion depending on the type of fusion machines used. Too much of the NWA results in high surface tension which may cause the fusion bead to assume a spherical or crescent shape (Watanabe, 2015). Notably, the sufficiency of the NWA depends mainly on the surface conditions of the mold, the dilution ratio, as well as the type and nature of the sample involved.

In this work, potassium bromide was used as a NWA in which case 241 mg of the KBr salt was dissolved in distilled water forming a stock solution of 10 ml of 2.41 % (w/v). Using a micropipette 200  $\mu$ l was added to the constituents of the Pt crucible to act as a releasing agent during fusion hence prevent the fused glass from sticking to the walls of the crucible. Finally, the total mass ( $M_i$ ) of the contents of the crucible before fusion was recorded.

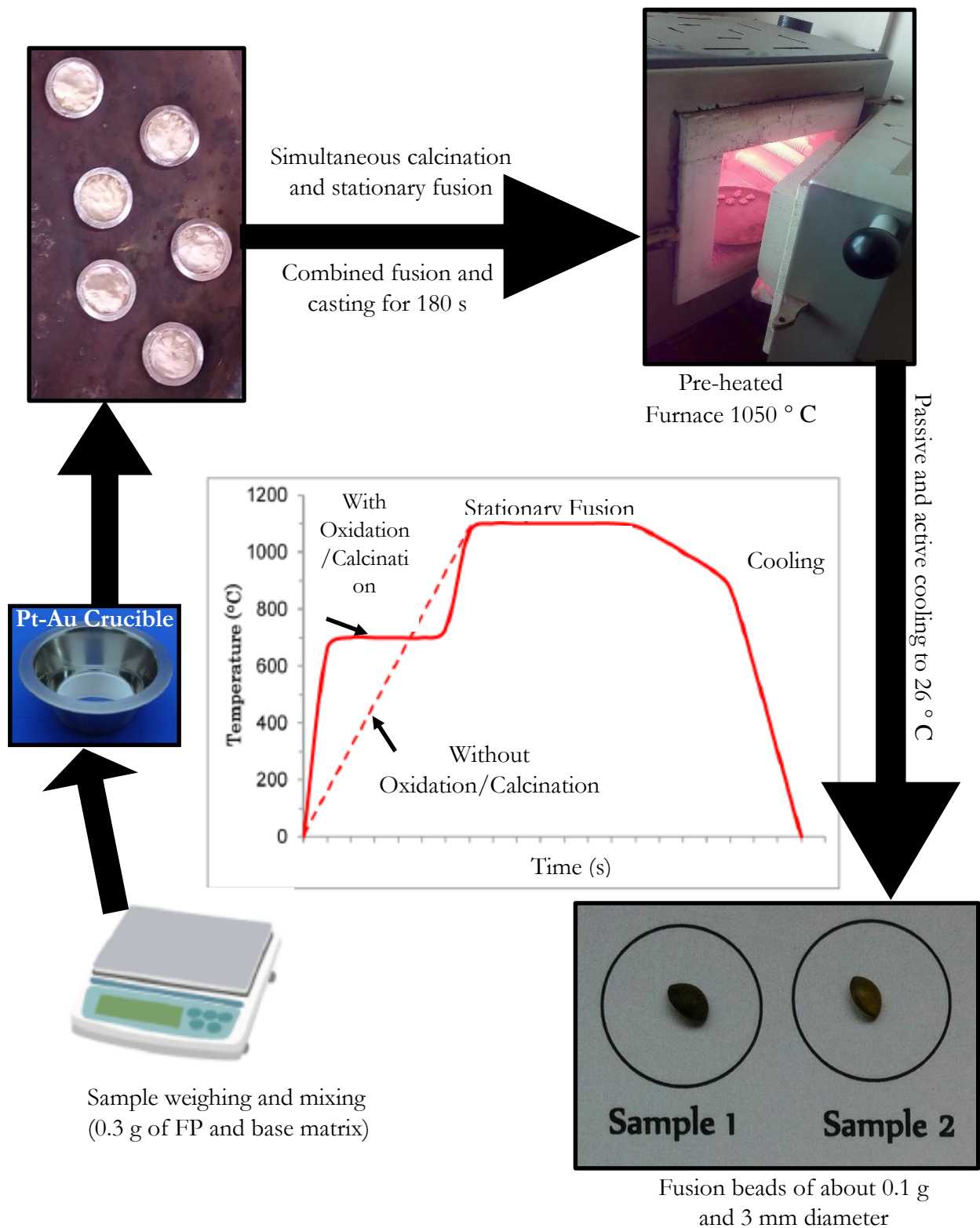


**Figure 4.4.1:** General fusion bead preparation procedure (After: Watanabe (2015)).

#### 4.4.1.1 Nuclear Glass Fusion Process

A Nabertherm furnace that supports a maximum temperature of 1400 °C was employed in the production of the fusion beads. The furnace was preheated to 1050 °C. The sample mixture in Pt-Au crucibles with NWA, arranged on an alumina plate, were introduced slowly into the high-temperature furnace as shown in **Figure 4.4.1** and a stopwatch was started. The total fusion time was 180 seconds. The surface temperature at each of the melt was determined using a laser-based handheld pyrometer. All the samples were allowed to cool slowly for five minutes by slowly taking the crucible out of the furnace. This was done to minimize fracturing of the resulting beads as a result of sudden temperature changes as well as to avoid recrystallization in case of very slow cooling rate (Fausett, 1994; Watanabe, 2015). Finally, the crucibles were removed out of the furnace and allowed to cool under ambient air to a final room temperature (26°C).

It was also noted that during fusion, the sample rose above the crucible and some spill around each crucible. This, coupled with the loss of weight due to the escape of the gaseous components namely; CO<sub>2</sub>, NO<sub>3</sub> and NO<sub>2</sub>, and Loss of Ignition (LOI) contributed immensely towards analytical inaccuracy especially on the final masses of the fused beads (Homma *et al.*, 2012; Rousseau, 2001).

The mass of the glass ( $M_f$ ) beads obtained and recorded. The fused beads were placed in small petri dishes and carefully labelled. The ratio between the final mass ( $M_f$ ), and the initial mass ( $M_i$ ) was evaluated and represented the total mass recovery. Hence, the average mass recovery was found to be 32.20 % for all the glass beads. Nevertheless, because the components of each sample was thoroughly mixed prior to fusion and during fusion, the sample dissolved in the melt; so it was assumed that even in an event of spillage, there could be minimal errors in subsequent analysis.



#### **4.4.2 Preparation of Pellet Samples**

Trafficking nuclear and radioactive materials in concealed form for use in ‘dirty bombs’ is a potential terrorist act. One of the possible concealed conditions may involve packaging nuclear materials with powders like cellulose at one end and performing extractions at the other end. As such a methodology that involves rapid and noninvasive detection of this fission products in trace quantities in powdered substances is desirable to deter possible trafficking. In this work, cellulose was used as a reference powder (concealed form in which nuclear materials can be trafficked) in addition to acting as an organic binder.

**Figure 4.4.2** shows the procedure that was used in preparing the pelletized samples. Notably, 0.1 g of the sample and 0.5 g of cellulose powder were weighed and thoroughly mixed for 10 minutes. Using a manual pellet press machine (LPM-15T) with a die of 2.5 cm diameter, 10 tons pressure was applied on the powder mixture to produce a pellet of 0.3 g. The pellet was kept in a clean petri dish awaiting further analysis.

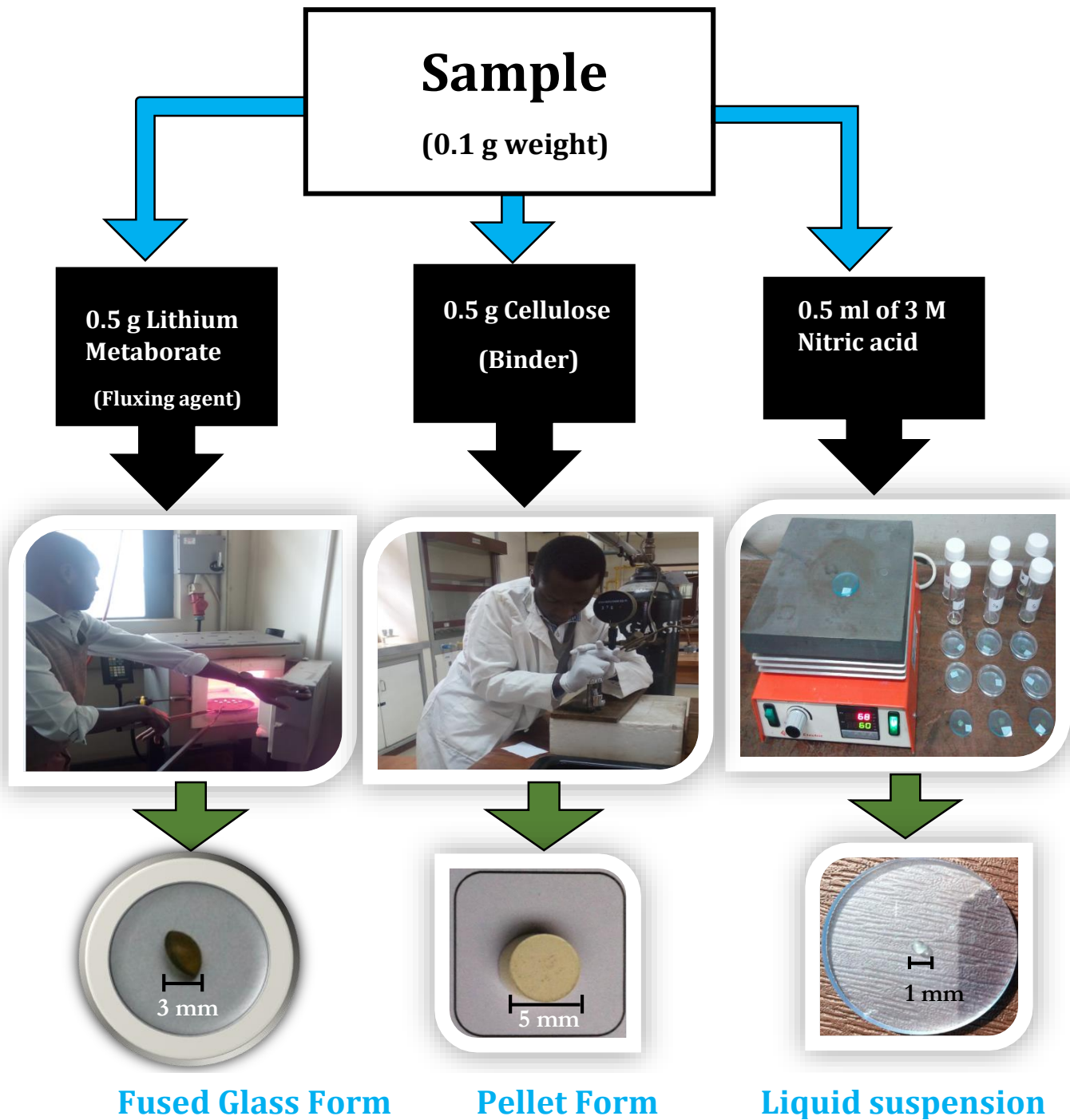


**Figure 4.4.2:** Procedure for preparation of fused glass, pellet and drop coating deposition forms of simulate high level samples.

### 4.4.3 Preparation of Simulate Liquid Samples

Spent fuel is chemically or physically treated in order to salvage plutonium, uranium and other fission products. Reprocessing of nuclear fuel requires dissolution in nitric acid and subsequent partitioning of actinides and other FP downstream (Murray and Holbert, 2014). As a result, high level liquid nuclear wastes are generated. A potential malicious terrorism act may involve HLW solutions trafficked in concealed conditions such as mixing with nitric acid or other solutions. FP from such HLW may be extracted and give rise to clandestine programs involving utility of such materials for IND and IED. Particles from a detonation scene more often settle on plant leaves and other surfaces and swipe samples can be taken to determine the characteristic of the detonated device. Dew drops forming on such plant leaves can dissolve such particles. In this research, we developed a laboratory simulate of the HLW solution form. We propose a methodology of sampling microliter samples that may contain some of the particles to offer an alternative supplementary information.

The nitric acid in the slurry resulting from reprocessing of spent fuel is normally of about 3M (Audero *et al.*, 1995; (Benedict *et al.*, 1982) The molarity of the concentrated nitric acid was evaluated from the certificate provided by the manufacturer using the following formulation

$$Molarity = \frac{\% \text{ Assay} \times \text{Density}}{\text{Molecular Mass}} \times 10 \quad (4.2)$$

The density of nitric acid is  $1420 \text{ Kg m}^{-3}$ , the molecular mass calculated to be  $63.01 \text{ g/mol}$  and the assay was 69 %. Therefore the effective molarity of the nitric acid was found to be 15.54 M.

Using the volume proportion in equation 4.1,

For  $V_2 = 20 \text{ ml}$ ,  $C_1 = 15.54 \text{ M}$ , and  $C_2 = 3 \text{ M}$

$$V_1 = \frac{3 \text{ M} \times 20 \text{ ml}}{15.54 \text{ M}}$$

$$V_1 = 3.9 \text{ ml}$$

Therefore, to make 3 M nitric acid, 3.9 ml of the concentrated acid was pipetted and added to 16.1 ml of water and the final solution was 20 ml.

The same samples were treated as shown in **Figure 4.4.2**. 0.1 g of the first sample was carefully weighed and placed in a container. 500  $\mu\text{l}$  of the prepared 3 M nitric acid was added into the sample and thoroughly shaken to dissolve and maximize homogeneity.

By means of a micropipette, varying aliquots of the resultant liquid sample were placed on perspex wafer between 2  $\mu\text{l}$  to 6  $\mu\text{l}$ . This procedure was undertaken to investigate the effect of the volume of the sample on the spectral line response of the analyte using LIBS. The wafer was then placed inside a petri dish and covered to minimize chances of contamination. The petri dish was then placed on a hot plate set at 50 °C temperature until a dry drop deposition coating was obtained.

Upon finding the optimum volume for such liquid deposition analysis, the procedure was repeated for all the remaining 30 samples and the LIBS data acquired from the samples was used to develop both univariate and multivariate quantitative calibration models that facilitate detection of fission products in simulated HLW solution, a technique called drop coating deposition LIBS (DCD-LIBS).

#### 4.4.4 Synthetic Standard Preparations

Synthetic standards were prepared from strontium and yttrium ICP standard whose certificates of analysis are given in Appendix 5. About 2 ml of strontium ICP standard of concentration 1000 ppm was pipetted into a 50 ml plastic bottle. 18 ml of 3M nitric acid was added to the solution and mixed to form a synthetic standard of 100 ppm. Triplicate synthetic standards were prepared to provide a comparative study of the prediction ability of the model. The procedure was repeated for Yttrium ICP standard. The concentration range for Zr while developing the ANN model was 0 – 4000 ppm compared to Y and Sr whose model range was 0 – 1000 ppm. Therefore, a relatively higher target concentration (500 ppm) was selected as the target concentration. The 2ml of zirconium atomic standard solution was also diluted with 2 ml of nitric acid to produce a solution of 500 ppm Zr concentration.

Analysis involved deposition of 2  $\mu$ l of each of the sample on perspex substrate and dried on a hot plate to produce a dry coat. Twenty spectra were acquired from the sample and averaged to obtain a representative spectra. Selected regions containing the peaks of FP (Sr, Y and Zr) were used in developed ANN models to test the predicted concentrations.

River clay standard reference material PTXRFIAEA09 was used in the validation of ANN models developed using powder (pellet) samples (IAEA, 2014). The river clay powder was pressed into two pellets (25 mm diameter and 0.4512 g mass). Twenty spectra were acquired from both sides of the pellet and averaged to obtain representative spectra. Selected regions were utilized with the ANN models developed to determine the prediction ability of the model.

#### 4.5 Evaluation of Limits of Detection (LoD)

For any given analytical technique, the limit of detection refers to the smallest concentration of the analyte that can be detected and proved to be present (Cremers *et al.*, 2006; Cremers and Radziemski, 2002 ; Van Grieken and Markowicz, 2001). Therefore, it is the lowest concentration that can be distinguished from an analytical blank. According to the International Union of Pure and Applied Chemistry (IUPAC), a spectrum from a given element is statistically significant when the signal is raised 3 standard deviations above the background reference (Long and Winefordner, 1983; Ripp, 1996). Hence;

$$\text{LoD} = \frac{3\sigma_b}{S} \quad (4.3)$$

Where  $\sigma_b$  is the standard deviation of the multiple samples of the blank and S is the sensitivity. LoD can be influenced by a number of parameters including; the delay time, fluctuations in the laser pulse energy as well as the characteristics of the sample being investigated. The relationship between the LIBS spectra and the concentrations of the analyte also known as sensitivity is given by the slope of the calibration curve.

Detection limits for each of the FPs in their respective matrices (fused glass, pellet and drop coats on perspex) were computed. Spectrally isolated and interference-free peaks were identified and used in the evaluation of the LoD. Usually, small variations in the intensity of the central peak frequency create non-linearity if the peak height at a particular frequency is chosen. Therefore, the area under the curve (intensity) for each peak of interest was considered as a more uniform representation of the emitted intensities. This methodology was achieved by selecting the range containing the peak for 10 different analyte concentrations and a non-linear curve fitting employing the Gaussian function with Levenberg Marquart iteration algorithm in

OriginPro 9.1.0 data analysis and graphing software. All the peaks were treated simultaneously and fitting was done until convergence was attained.

A scatter plot of the concentration against the corresponding peak area was utilized in univariate calibration. A line of best fit was drawn from which the slope of the line was extracted. Six blank samples (base matrix) were prepared and used to determine the standard deviation. The spectral region containing the specific lines was used to find the standard deviation of the blank minus the signal. The slope, the standard deviation obtained were used to calculate the LoD according to equation (4.3). The procedure was repeated for all the sample types (liquid, pellet and fused glass) and contrasted.

#### **4.6 Spectral Data Pre-processing Techniques**

Spectral data pre-processing techniques namely; PCA for outlier detection, baseline restoration, and normalization were applied on the data to de-noise the spectra, to reduce variability in the data and also to improve the accuracy and robustness of subsequent classification and analyses. A spectrum is considered normalized when the area under the curve for such a spectrum is evaluated to correct the spectra for the unknown path length. Standardization removes scatter effects from the individual spectra and puts all variables on the same scale such that, variables with high and low concentrations assume equal significance (Mark, 2001). Additionally, these spectral preprocessing techniques were useful in removing outliers and redundant information while retaining the most significant features of the spectra to be used during multivariate modeling.

#### **4.7 Principal Component Analysis of Simulate HLNW**

PCA was performed on nuclear waste liquid simulates spiked with trace fission products in order to discriminate nuclear liquids from those that are not, based on the presence of trace FP. The PCA was performed in R by selecting a partial section of the spectrum (340 nm to 395 nm) which contain most of the lines of the spiked elements. Variable scaling was performed and the resulting principal components were visualized in 2D and 3D score plots respectively.

#### **4.8 Artificial Neural Networks (ANN) of HLNW**

ANN was employed in regression modeling of the FP in the simulated nuclear wastes in glass (vitrified), high-level waste liquids, and powders. The schematic of the proposed ANN modeling approach employed in this work is given in **Figure 4.8.1**.



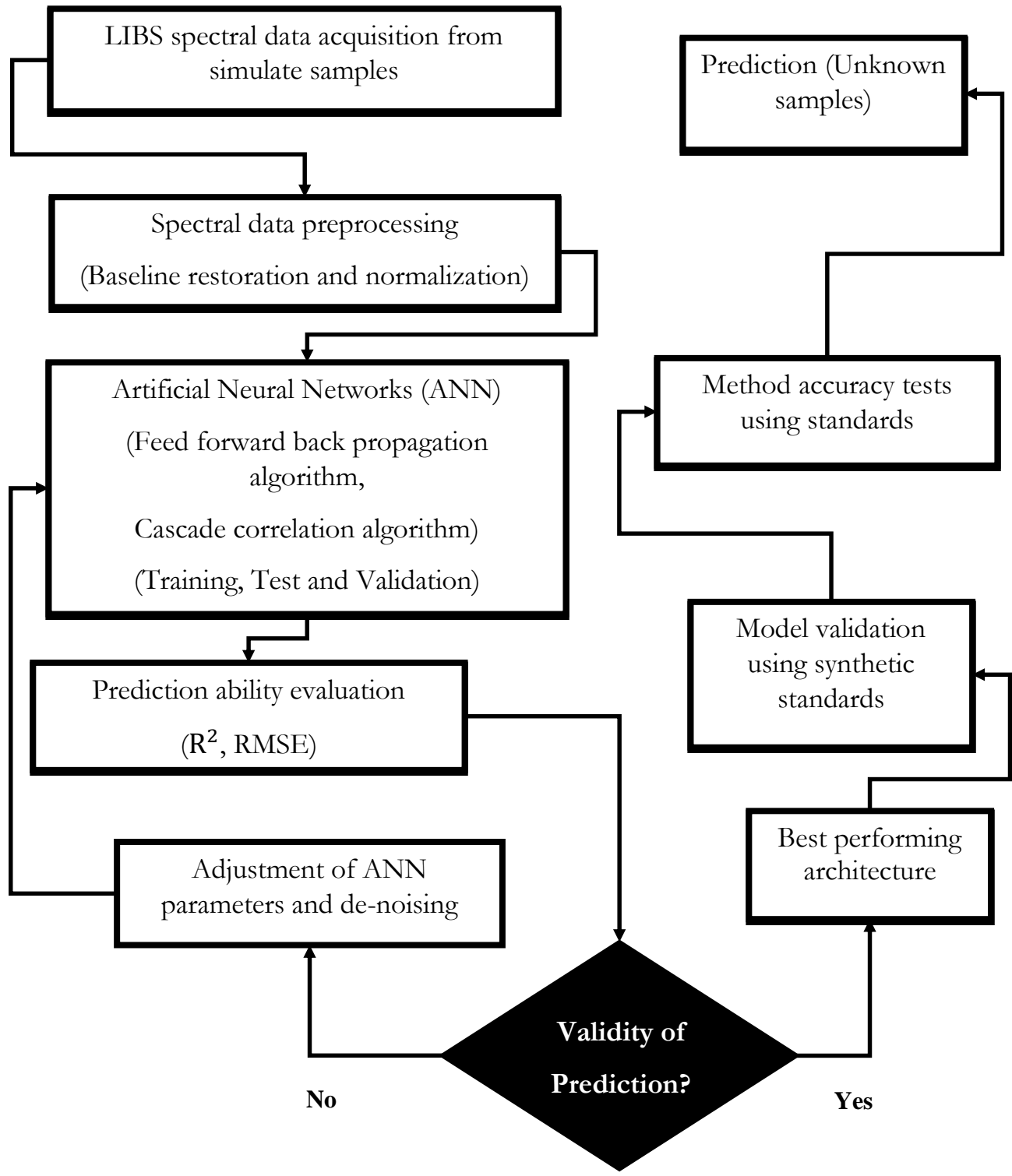


Figure 4.8.1: ANN modeling approach.

#### **4.9 Support Vector Machines of FP in Simulate HLNW**

In this work, support vector machines was used for discrimination of samples based on the presence and the concentration of FP. Quantitative features (sample concentration) and qualitative features (spectral peaks) of each of the FP can infer the stage of the material in the NFC. Notably, in high level wastes, the FP occur in typical concentrations (Audero *et al.*, 1995 ; Bevilacqua *et al.*, 1987). If FP together with U are measured in unknown material and are found to be within these typical ranges, then there is a high likelihood of associating such material to HLW. Considering one fission product in relation to the rest of the FP, SVM *hyperplanes* can be used to classify a new sample as to whether it contains the fission product or not. Using OriginPro 9.1.0, the area under the peak for selected interference-free peaks of each of the spiked fission products (Rb, Sr, Zr, Y) and U together with their spiked concentrations were prepared as a matrix. The FP (Rb, Sr, Zr, Y) and U columns in the matrix were utilized as a predictor and the SVM classification was performed based on these fission products. The procedure was repeated for the three sample types (fused glass, pellets, liquid coats on perspex). The model was tuned to obtain the best parameter combination that produced optimal *hyperplanes*. Notably, both linear and radial kernels were utilized. Samples that had not been shown to the model were then fed to the model to determine the clustering ability of the model. The classification of the samples into their correct groups is a useful component of NF attribution as it can be utilized in a rapid positioning of the material in NFC.

#### **4.10 Safety Precautions**

This work involves laboratory simulation of high-level nuclear wastes resulting from reprocessing of nuclear fuels. Some of the elements eg (U, Sr, etc.) utilized are radiotoxic hence the need for precautionary measures. Despite the fact that stable elements were utilized in the

simulation,  $^{238}\text{U}$  emits alpha particles of 4.2 MeV energy (Bleise *et al.*, 2003; Grenthe *et al.*, 2008). Also, the presence of small amounts of  $^{235}\text{U}$  decay with 4.4 MeV alpha particles and approximately 0.21 MeV gamma rays. For these reasons, exposure time was minimized while maximizing the distance from a subject from the samples during sample preparation. The survey meter was used to check the levels of ionizing radiation from the uranium salts and it was always below background. A protective face mask was always worn throughout the process of sample preparations. Sr also has a tendency of replacing calcium in bones and if the isotope is radioactive then it gradually releases radiation to the nearby muscles tissues. In addition, these elements are harmful if they find their way to the hydro-ecological system (Henderson, 2014). Radiacwash towels courtesy of the Radiation Protection Board (RPB) were used to clean the surfaces contaminated during the analysis.

#### **4.11 LIBS Line Selection Criteria**

Line selection criteria for quantitative model development was done based on the following spectral line properties;

- a) The lines identified were spectrally isolated and interference free. Peaks with a dip at the apex (suggesting self-absorption) were avoided.
- b) For each FP element, the ratio of the intensities of two adjacent visible lines was determined and compared to realize whether it corresponded with the ratio of the intensity of the same lines in atomic spectroscopy database. This was done to ascertain the authenticity of the lines.
- c) The net wavelength shifts from the LIBS reference database was also confirmed and maintained at  $\pm 0.2 \text{ nm}$ . However in some special cases, depending on the operation conditions of LIBS, a deviation greater than 0.2 nm was noted.

Tellurium (Te) lines were not visible and identifiable on the LIBS spectrum. Further analysis of Te could not be achieved hence it was excluded in the subsequent analysis.

Figure 4.11.1 shows a typical LIBS spectrum acquired from simulate HLW fused glass sample.

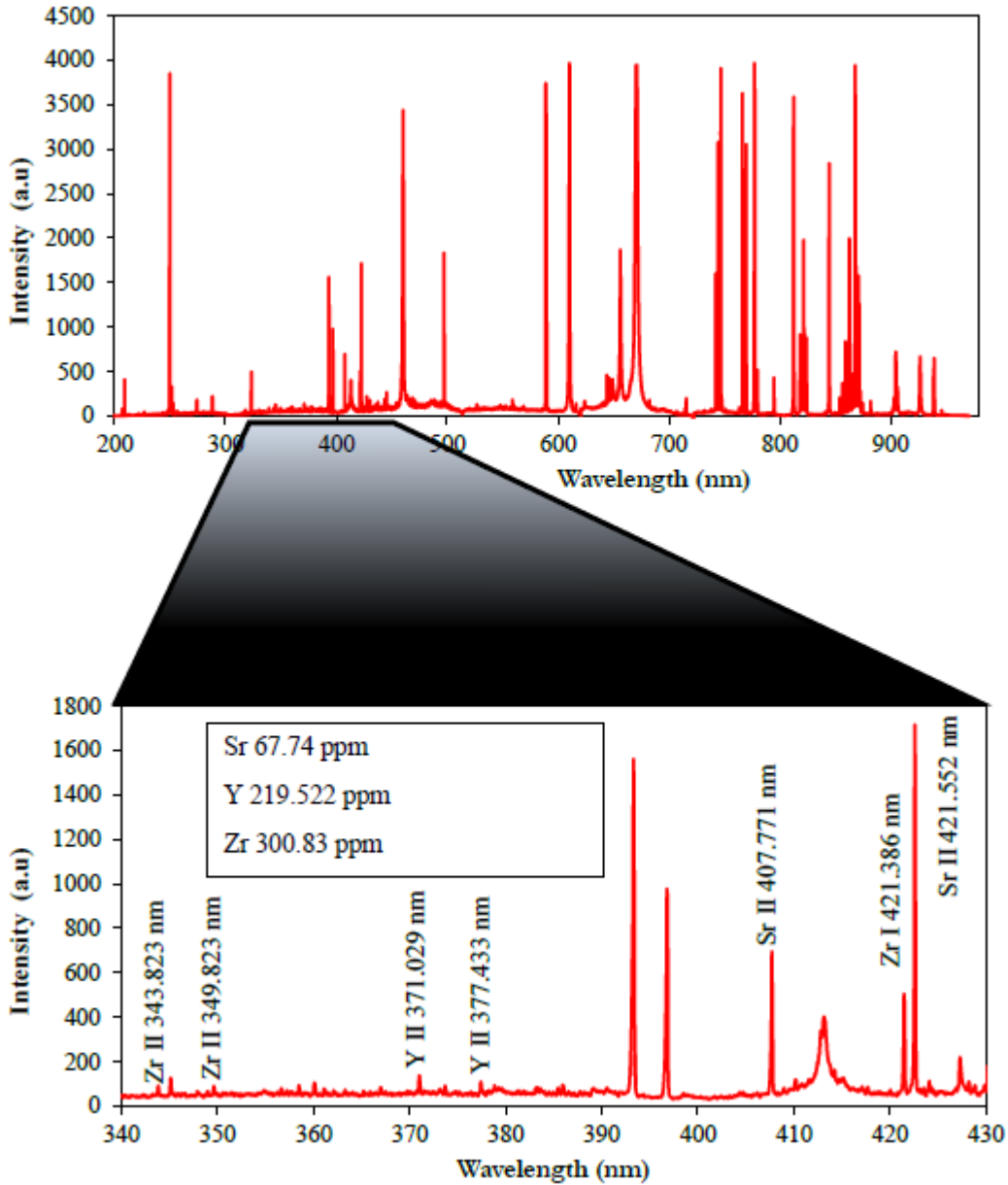
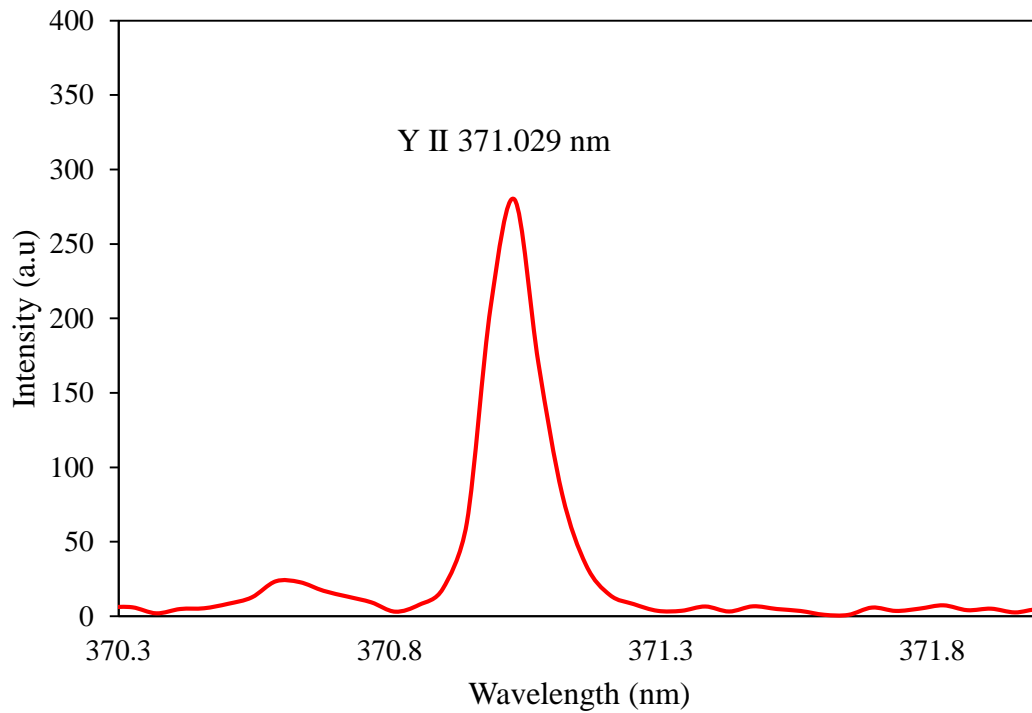


Figure 4.11.1: Zoom in of LIBS spectrum of an HLW fused glass sample.

**Figure 4.11.2** shows the further zoom in into **Figure 4.11.1** illustrating a typical spectrally isolated and interference-free lines chosen for model development. Such lines were employed in feature selection of the specific regions of interest for support vector machines, principal component analysis, and artificial neural network model development.



**Figure 4.11.2:** Typical line profile for YII 371.029 nm.

**Table 4.5** shows some of the lines that were chosen for quantitative model development. These lines were identified with the help of the OOILIBS spectral library as well as the atomic spectroscopy online database available on the NIST website (Ralchenko *et al.*, 2006).

**Table 4.5:** Spectral lines observed in LIBS and utilized in the quantitative model development

Element	Species	Wavelength (nm)
Yttrium	Y II	371.029
	Y II	377.433
	Y II	437.494
	Y II	360.073
	Y II	363.312
	Y II	488.368
	Y II	523.810
	Y II	324.227
Zirconium	Zr I	421.386
	Zr I	422.931
	Zr I	356.610
	Zr II	273.486
	Zr II	274.556
	Zr II	327.305
	Zr II	267.863
	Zr II	339.197
	Zr II	343.823
	Zr II	357.247
Strontium	Sr II	407.771
	Sr II	421.552
	Sr II	430.810
	Sr II	460.733
Rubidium	Rb I	780.011
	Rb I	794.760
	Rb II	424.440
	Rb II	645.833

## CHAPTER V

### RESULTS AND DISCUSSION

#### 5.1 Overview

This chapter presents the results and discussion for the utility of chemometric methods in LIBS analysis of simulate nuclear fission products in glass, pressed pellets of simulate HLW powders and simulate HLW liquids. Section 5.5 presents the results for univariate calibration of the FP in glass, pellets and liquids of simulate high-level nuclear wastes. Section 5.7 presents optimization results and the outcome of quantitative ANN models of the FP in the above matrices. The elemental analysis is presented under the qualitative analysis section. Results and discussion for a DCD-LIBS approach to the simulate HLW liquid are presented in section 5.9. The PCA conducted on simulate nuclear wastes to infer attribution is presented in section 5.10. Finally, SVM performed on the samples as presented in section 5.11 as a discriminatory attempt among the spiked fission products.

#### 5.2 LIBS Peak Selection and Qualitative analysis

In order to identify the peaks associated with each of the fission products (Y, Zr, Sr, U, Rb) pellets of analytical grade chemicals donors of each FP were analyzed using LIBS. The salts were pressed into a 2g pellet with 25 mm diameter using the pellet press machine (LPM-15T). A total of 10 spectra were taken from each of the pellets and averaged for a representative spectrum. The average spectra were then stacked with y-offsets in ORIGEN Lab graphing software. **Figure 5.2.1** shows the result obtained.

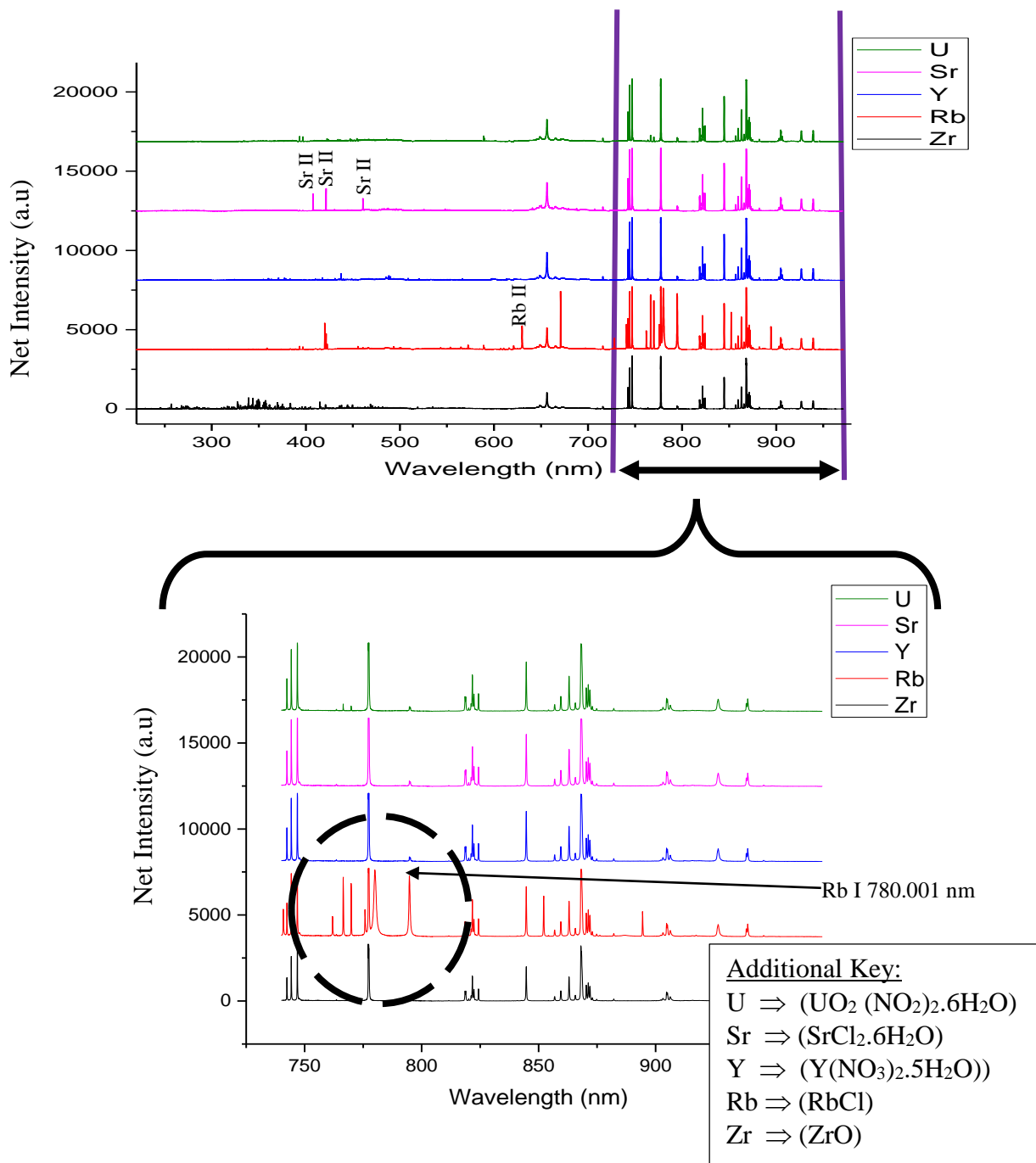


**Figure 5.2.1:** LIBS spectra of the salts (FP donors) (stacked for easy view).

Zooming around the region between 740 nm to 980 nm reveals that most of the lines are due to the contribution of the atmosphere around the sample because these peaks remain unaltered for all the compounds analyzed. However, within this region, there are a number of conspicuous/dominant Rb lines (780.011nm and 794.760 nm) which appear on the rubidium



chloride spectrum only as compared to other spectra. The database of atomic emissions identifies these lines as the most dominant lines of Rb (Ralchenko *et al.*, 2006). Hence these lines were adopted for model development. Following a similar approach, the lines given in **Table 4.5** were identified for each analyte and used for model development.

In qualitative analysis, the following lines were identified. These lines were reproducible for fused glass samples, pelletized samples, and the drop coating deposition LIBS samples. Figure 5.2.2 and Figure 5.2.3 shows some of the peaks identified from the spiked FP.

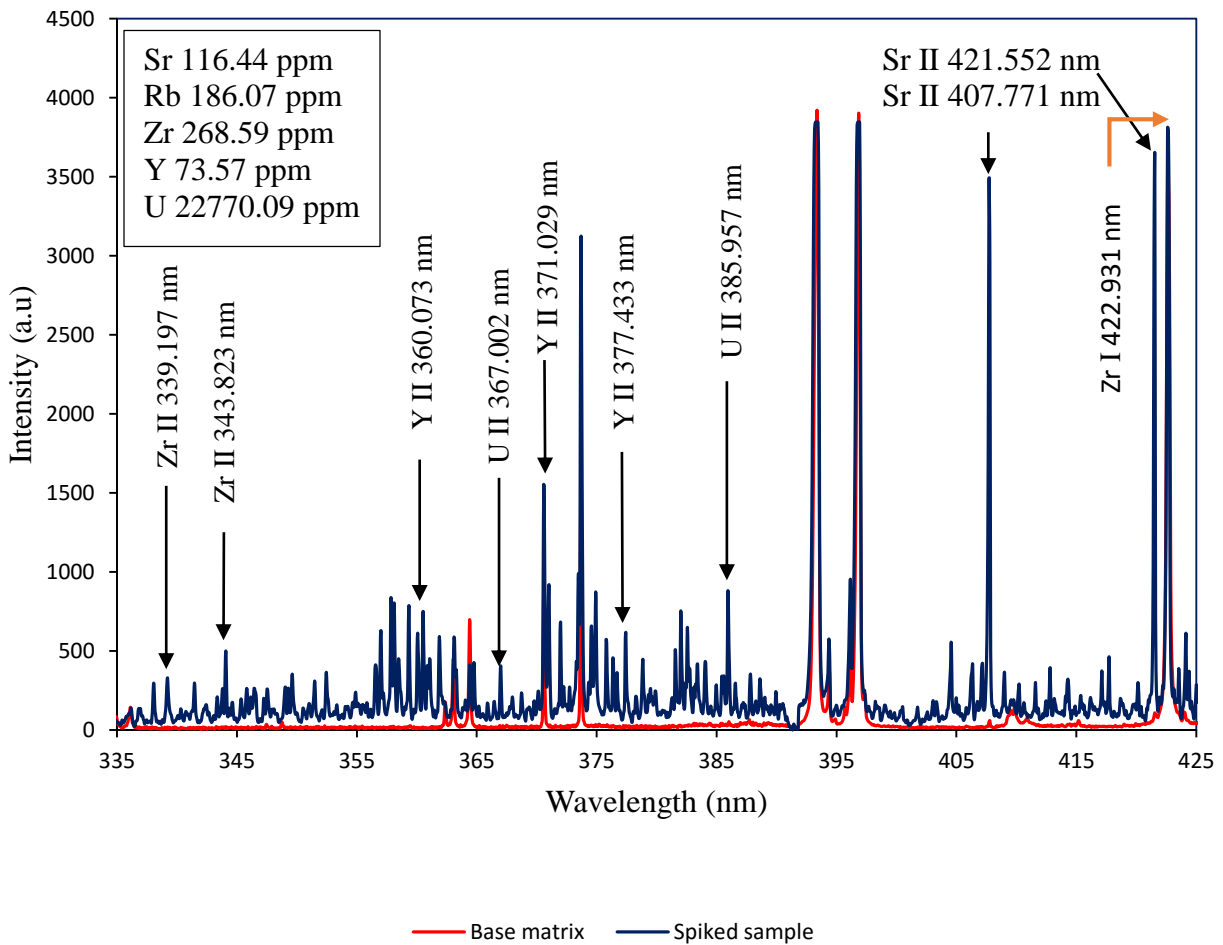


**Figure 5.2.2:** Identified peaks of simulate HLW liquid FP coated on perspex substrate.

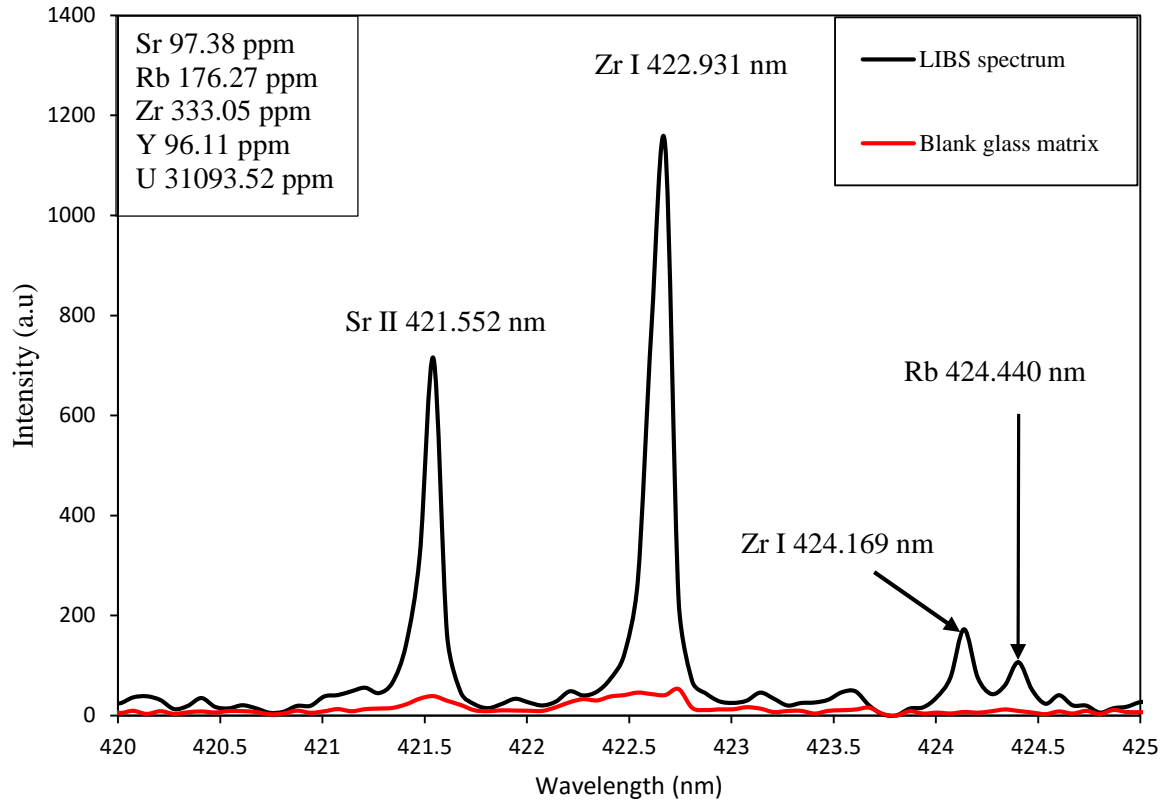


**Figure 5.2.3:** Selected observed emission lines of a pellet sample spiked with FP elements in fused glass and a blank fused glass matrix.

### 5.3 Spectral Line Response with a Change in Concentration

In laser spectroscopy, ideally, the intensity of a given line profile should be proportional to the concentration. This means that higher intensities should be noticeable for a higher concentration of the given species of interest. **Figure 5.3.1** illustrates some of the line profiles of chosen elements that were identified to rely on this principle.

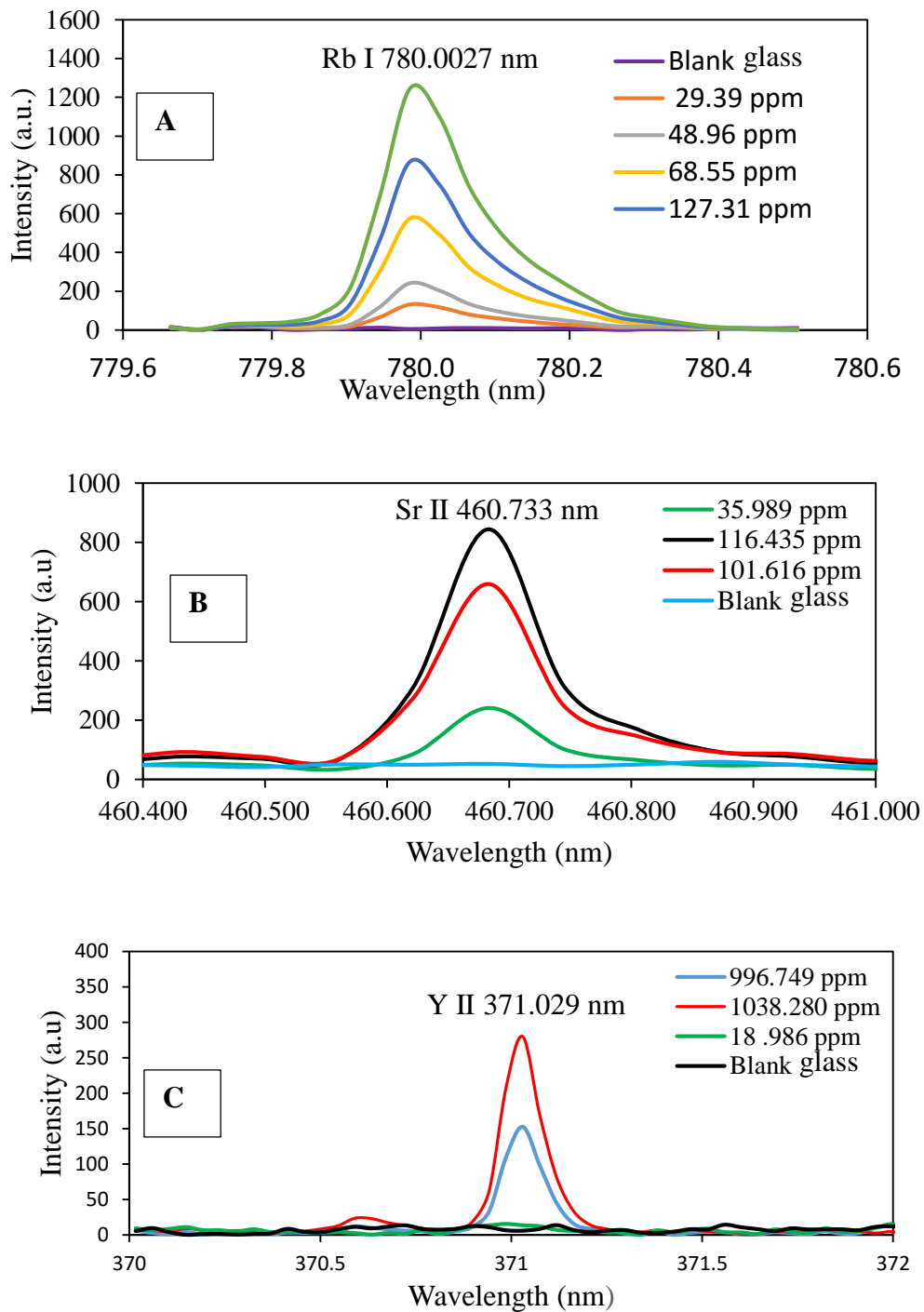


**Figure 5.3.1:** (A) Rb line at 780.011 nm and (B) Sr line at 460.733 nm and (C) Y ionic line at 371.029 nm responding with changes in the concentration of the respective analyte in different fused glass samples.

## **5.4 LIBS Optimization Parameters**

Prior to analysis, it is a common practice in atomic spectroscopy to optimize the conditions of the analytical instrument to maximize detection ability. In LIBS measurements the main factors influencing the intensity of spectral lines include the laser energy, the distance of the sample to lens distance, the number of laser shots and the Q-switch delay.

### **5.4.1 Optimization of LIBS for Fused Glass Analysis**

The appropriate laser energy that gave the best signal to noise ratio for a spectrally isolated and interference-free U II peak at 367.002 nm was found to be 45 mJ with a Q-switch delay of 150  $\mu$ s , an integration time of 0.42 s and an optical fibre to sample length of approximately 5.3 mm. These conditions were held constant throughout the analysis of the fused glass samples.

### **5.4.2 Optimization of LIBS for Pellet Samples**

The optimized parameters for analysis of pelletized samples was reported by (Mukhono, 2012) Since our work involved the use of cellulose as a binder and the work therein involved analysis of trace elements bound in cellulose, the conditions (laser pulse energy (LPE)) of 45 mJ, 0.42  $\mu$ s integration time, a delay time of 150  $\mu$ s and an optical fiber-to-lens length of 10 mm) were assumed to be applicable.

### **5.4.3 Optimization Conditions for the Preparation of Liquid Samples**

For liquid simulates, there was no methodology reported for optimized LIBS conditions. As such, the LPE and the distance of spectrometer from the plasma were investigated for the best performing combination.

### 5.4.3.1 Optimum LPE

It is important to optimize the laser energy before analysis of samples is done. The laser energy was varied from the minimum value 10 mJ to the feasible maximum 50 mJ with all other variables held constant. A Y line (YII 371.029 nm) that was spectrally isolated and free of overlapping was monitored with the changes in the laser energy. Through non-linear curve fitting, the area under each of the peaks was calculated. The area under the peak against each of the laser pulse energy is plotted as shown in **Figure 5.4.1**.

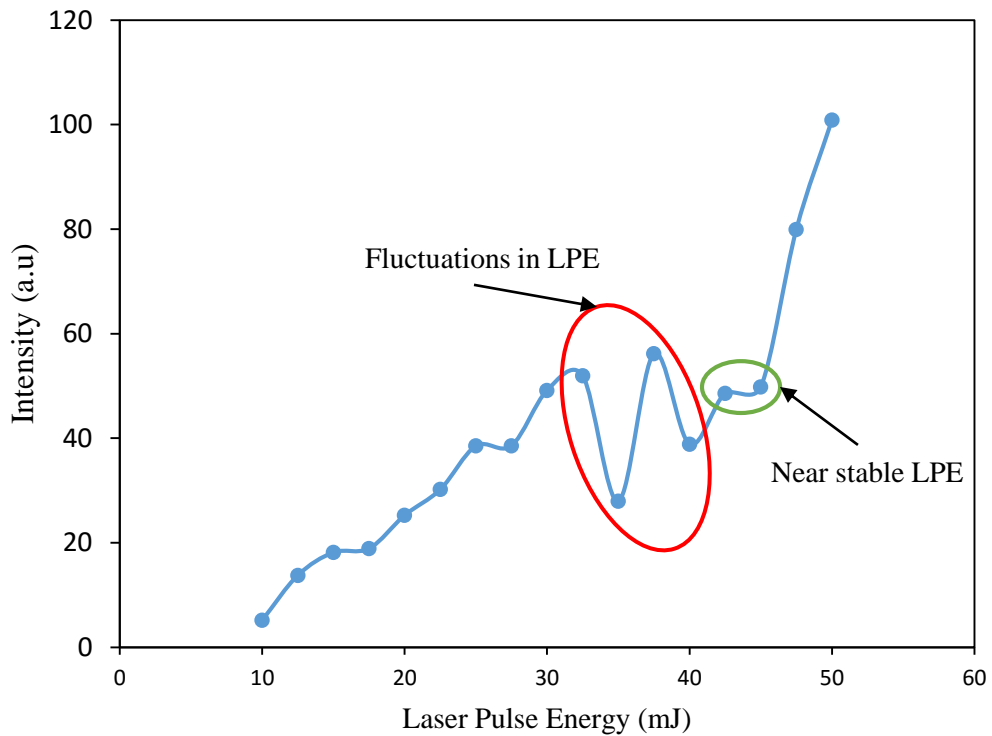


**Figure 5.4.1:** Spectral line intensity (YII 371.029 nm) response with energy variation.

The intensity of the emitted lines increases with the increase in laser energy up to 32.5 mJ. There is an irregular intensity response after 32.5 mJ which could be possibly due to fluctuations in the laser energy of the pulses. The response at 42.5 mJ was approximately equal to the response at

45 mJ implying approximate stability in the laser energy. Hence the energy 42.5 mJ was chosen as the most appropriate optimum energy.

### 5.4.3.2 The distance of the spectrometer from the plasma

The distance between the spectrometer and the position struck by the laser was varied. Fifty single shot spectra were acquired for various distances from the sample surface at 42.5 mJ energy, 0.42 s integration time, and 150  $\mu$ s Q-Switch delay. The average of each of the spectra for each of the lengths was computed and presented as a single spectrum. Through feature selection, three lines were chosen and their intensity response at their centroids were plotted against the distance of the spectrometer from the sample (plasma). **Figure 5.4.2** indicates that the optimum distance between the spectrometer and the laser spot where the plasma produces the highest peak response is around 5.3 mm.

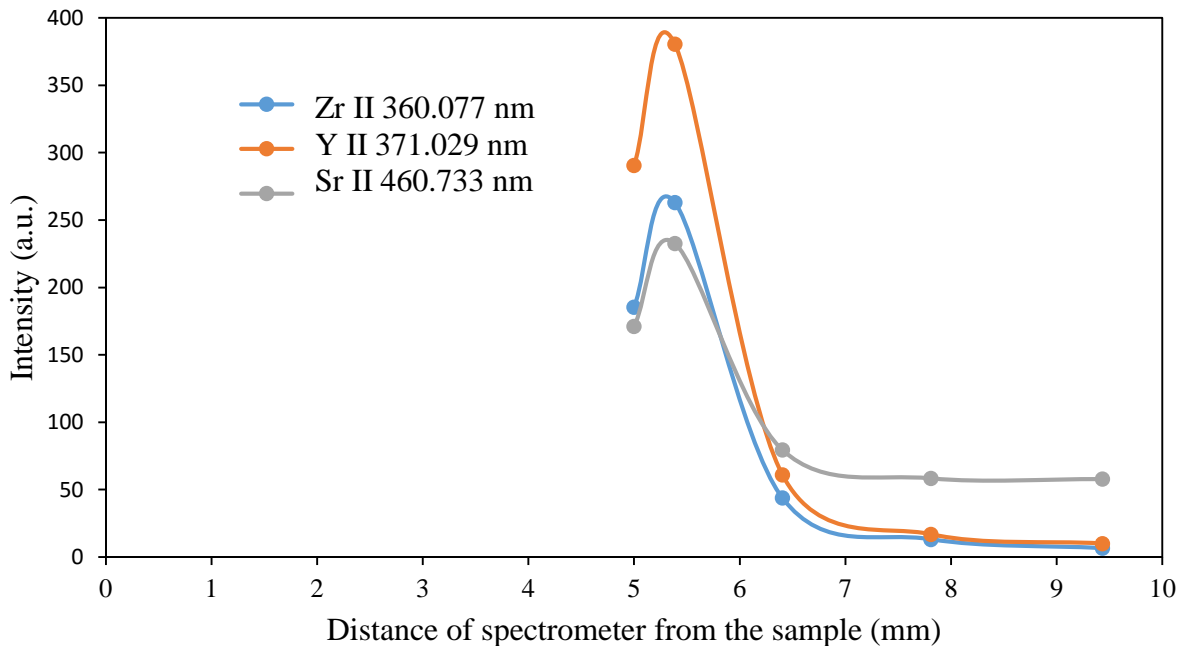


**Figure 5.4.2:** Spectral line intensity response with distance of the optic fiber from the sample.

Therefore the optimized conditions for analysis of the drop coating deposition LIBS samples were set to be 42.5 mJ laser pulse energy, 0.42 s integration time, 5.3 mm optic fiber lens the to sample distance and a Q switch delay of  $150\mu\text{s}$ . These conditions were preserved during the analysis of the 30 samples necessary for model development.

Drop coating deposition is not a common technique in LIBS. There is limited research that has been directed towards this topic especially with LIBS in perspective. However, drop coating deposition Raman (DCDR) has been widely used in achieving sample analysis including; analysis of protein mixtures (Filik and Stone, 2007), DCDR of liposomes (Kočiřová and Procházka, 2011) and even identification of variants in insulin by means of DCDR (Ortiz *et al.*, 2004). Since laser Raman and LIBS are laser-based techniques, drop coating deposition LIBS is also a potential analytic technique as illustrated in this work especially in the analysis of liquid samples. **Figure 5.4.3** illustrates the spectral response with different volume of the drop deposited on the perspex substrate.

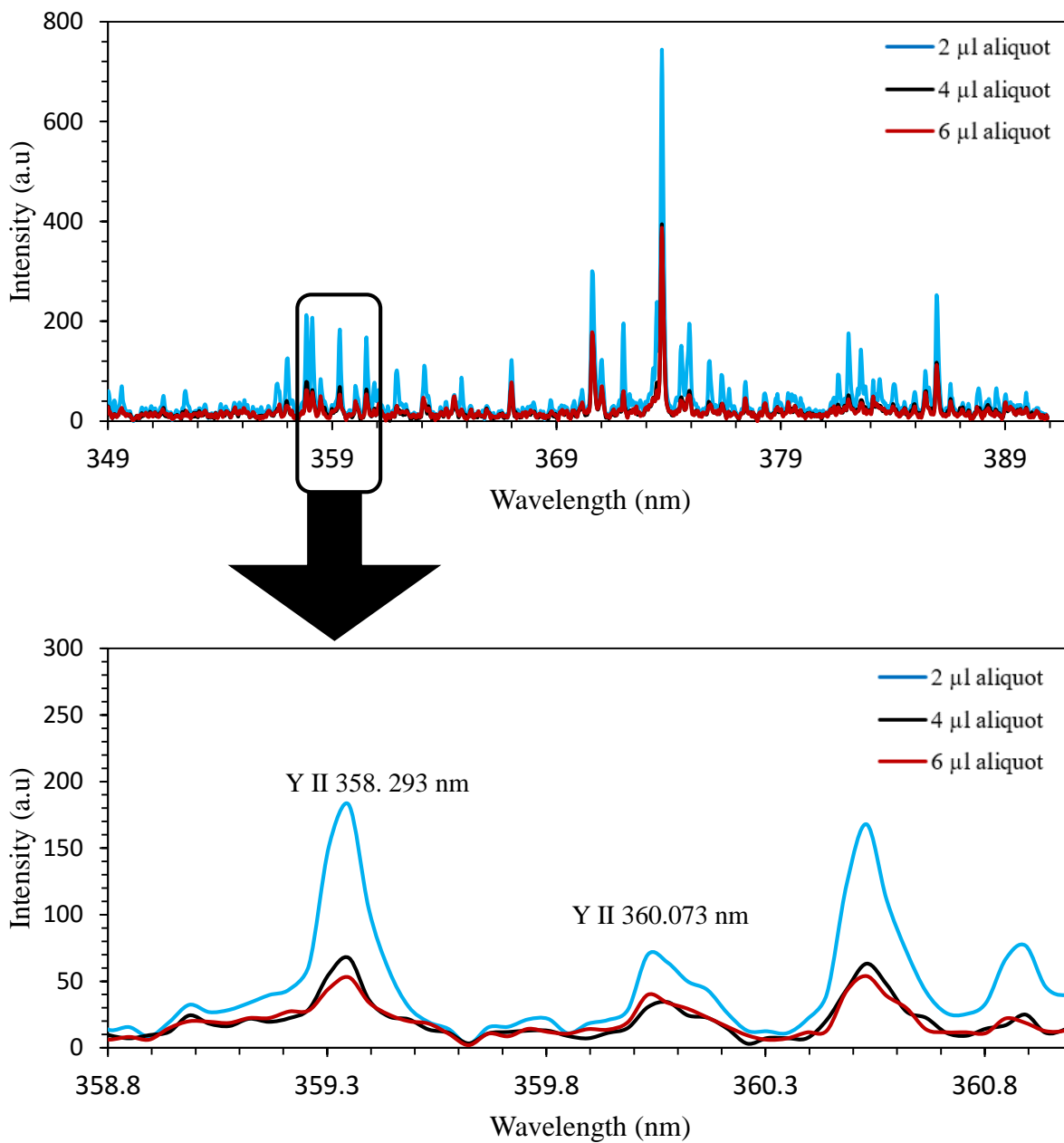


**Figure 5.4.3:** Spectral line intensity variation with the volume of drop deposition coating for the same sample.



**Figure 5.4.3** shows that the smaller the microliter aliquots, the higher the spectral line intensity acquired. This enhancement can be attributed to two factors. First, an evaporating liquid droplet containing particles suspended in it forms a ring called ‘Coffee Ring’ which is due to the induced capillary motion that depends on the rate of evaporation of the liquid to the motion of the particles (Shen *et al.*, 2010). The smaller the volume of the liquid aliquot, the smaller the radius of the dry coating. The particles cluster closer together hence interaction with laser energy is more direct and stronger compared to when the particles are far apart. Secondly, this signal enhancement can be attributed to the nature and type of substrate used. A good substrate for drop coating deposition should have a negligible solvent affinity, high optical reflectance and minimum optical absorbance (Zhang *et al.*, 2003). Perspex wafers are designed to meet these characteristics. Indeed, perspex substrate produced the better signal enhancement compared to glass. Hence, this study shows that perspex is suitable for trace elemental analysis (similar to those potentially encountered in a nuclear forensic scene) in LIBS.

The signal to noise ratio (SNR) or the signal to background ratio (SBR) of a methodology are the fundamental parameters used in evaluating the sensitivity of any analytical technique. In evaluating SNR, the point corresponding to the central wavelength of the chosen peak/the maximum point of the emission peak was chosen to represent the area under the curve for such a peak (Prochazka *et al.*, 2015). It is worth noting that, each sample was analyzed by averaging 50 spectra acquired randomly from the sample in order to attain more statistically significant results. The background was acquired by selecting regions close to the emission line that did not show any sign of elemental peak emission. Hence the mean of the selected regions represented the background. The noise that is associated with the background was computed by determining the

standard deviation from the background average value of the average spectra (Sládková *et al.*, 2017). The computed SNR for Rb II 779.985 nm is presented in **Table 5.1**.

**Table 5.1:** SNR and SNB for Rb II 779.985 nm line corresponding to 9 ppm of Rb in simulate liquid solution for varying volume of drop coat on Perspex

Parameter	The volume of the drop coat ( $\mu\text{l}$ )		
	2 $\mu\text{l}$	4 $\mu\text{l}$	6 $\mu\text{l}$
Standard deviation of background (Counts)	4.318	2.984	2.524
Average background (Counts)	18.188	11.521	11.325
Intensity (Counts)	250.000	116.100	111.700
Signal to noise ratio (SNR)	57.895	38.905	44.261
Signal to background ratio (SBR)	13.746	10.077	9.863

For the same fission products composition, the average spectra for pellet and fused glass were plotted on the same scale to find out the spectral response. The resulting graph is in **Figure 5.4.4**.

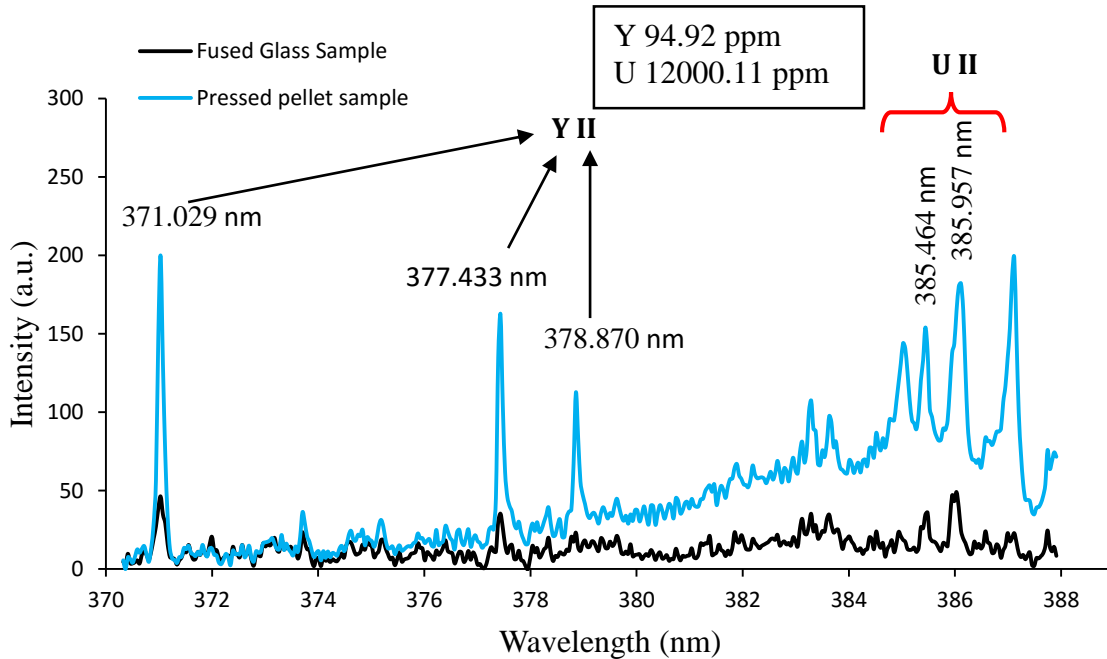


**Figure 5.4.4:** Comparison between spectra acquired from fused glass and pellet samples.

The Y, Zr and U lines are conspicuous in the two spectra. The pellet sample provides enhanced peaks compared to the fused glass form of the same sample. This is attributed to the spectral interference and fluorescence that affect the overall peak response in the glass. Also where small elemental concentrations are involved, analysis via fused glass becomes difficult. However, the peaks obtained from the glass form are stable peaks resting on the base with minimal background influence compared to pellet form. The background continuum on the pellet sample is primarily due to bremsstrahlung and recombination radiations within the plasma (Liu *et al.*, 2018). In a similar study, using the glass matrix, it was found out that glass provided a more stable physical matrix that limits inconsistencies encountered during absorption of the laser energy (Pease, 2013). In addition, the fused glass form provides an ideal environment that reduces detector saturation on prominent peaks as a result of dilution of the sample.

A further contrast between the three forms of the same sample (pellet form, fused glass, and liquid aliquots) is in **Figure 5.4.5** below.

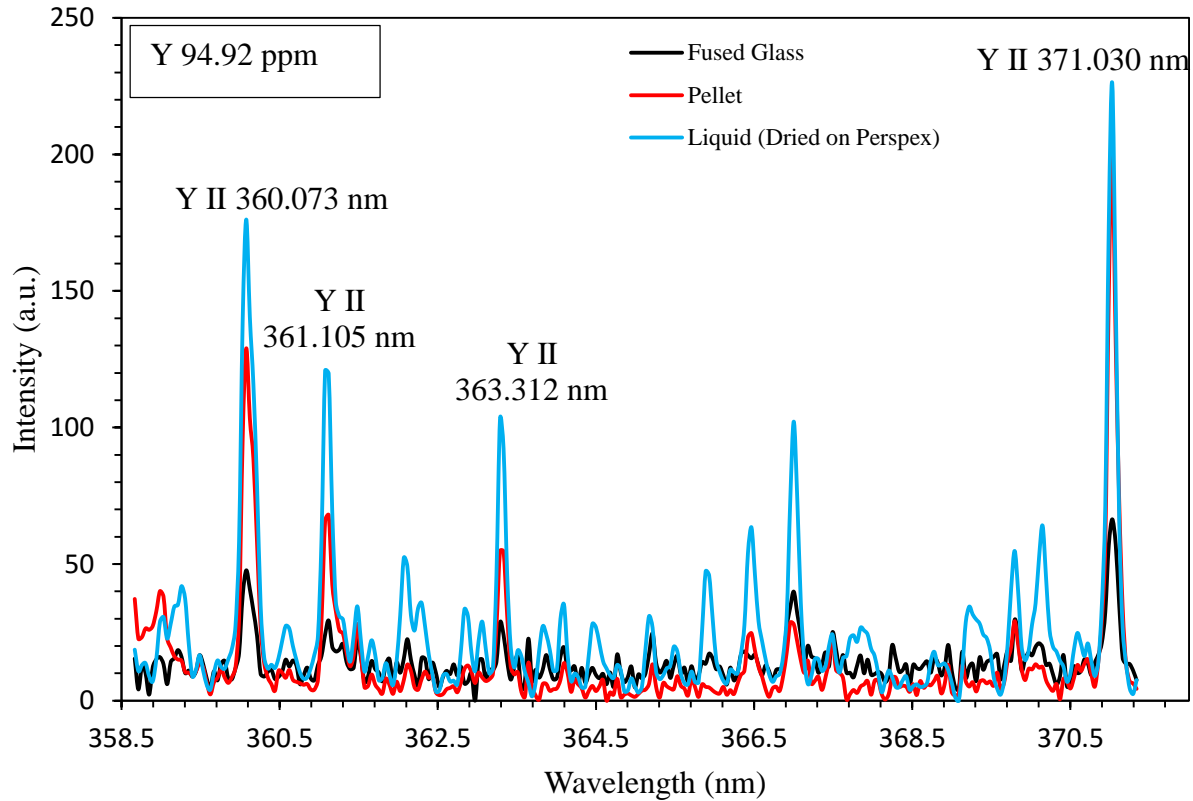


**Figure 5.4.5:** Comparison of spectra acquired from fused glass, pressed powders and aliquot deposition coatings.

Notably, the drop deposition coating on perspex wafer produced enhanced peaks (a factor of 1.82) compared to glass and a factor of 1.97 for pellet sample form. The inherent ability of the perspex wafer surface to enhance spectral lines compared to glass and silicon substrates can be attributed to the structure of the surface. The surface is highly polished such that the individual particles forming the surface behave like a near nano-structured surface hence behaving in a similar manner like nano-enhanced LIBS (De Giacomo *et al.*, 2014; Ye *et al.*, 2002). The

incorporation of nanoparticles on the sample surface aids in the breakdown of the threshold of the material thus enhancing the electric field localized around the nanoparticles. As such, there is an efficient coupling of the laser energy with the surface so that, much of the laser energy goes into excitation. This near nanostructuring provides sufficient points of plasma ignition that offers efficient ablation (De Giacomo *et al.*, 2014). Therefore the electron density of the resulting plasma becomes high resulting in higher optical photon emission which is translated into the observed enhanced peaks.

### **5.5 Univariate Calibration of FP in Simulate HLW**

The optimized conditions were set and fifty spectra were randomly acquired on the sample surface of each sample. The spectra were accumulated and averaged to get a representative spectrum for each of the samples. Notably, this was done in order to account for inhomogeneity in the samples.

Trace detection and quantification of any element requires the knowledge of the LoD. Three blanks of each form of the sample were prepared. Detection limits for the three forms of the sample (fused glass, pellet form and liquid deposition) were evaluated and compared. In evaluating the LoD, the peak area for a chosen number of samples was evaluated in Origin Pro 9.1 by performing non-linear curve fitting adopting the Gaussian function and Levenberg Marquart iteration algorithm.

The fitted area was then taken as a rather uniform representation of the intensity of each of the peaks. Samples with different concentrations were chosen and the area under the peak for two selected emission lines was calculated. The sensitivity was extracted from the slope of the linear function with the highest  $R^2$  value. Some of the graphical plots are as shown in **Figure 5.5.1**, **Figure 5.5.2** and **Figure 5.5.3**

It was noted that fused glass samples exhibited the highest LoD whereas the liquid samples offered lower detection limits. According to Liu *et al.* (2015), analysis of elements on glass samples is often accompanied by spectral interference which results in submersion of the spectral emissions in the background signals. Therefore, detection of such trace elements following a univariate approach is difficult and thus the LoD is high. The pellet samples gave lower detection limits compared to glass because of the presence of a more physical matrix that facilitates detection of the emission lines. The liquid deposits on perspex wafers provided the lowest detection limits because of reduced matrix interferences and the fact that the perspex surface was highly polished to a level where the surface behaves like a nano-structured surface hence improved sensitivity of spectral emissions (De Giacomo *et al.*, 2014; Ye *et al.*, 2002). Techniques that offer low detection limit are desirable in NF as trace concentrations of elements (FP) are involved from which useful NF signatures should be extracted.

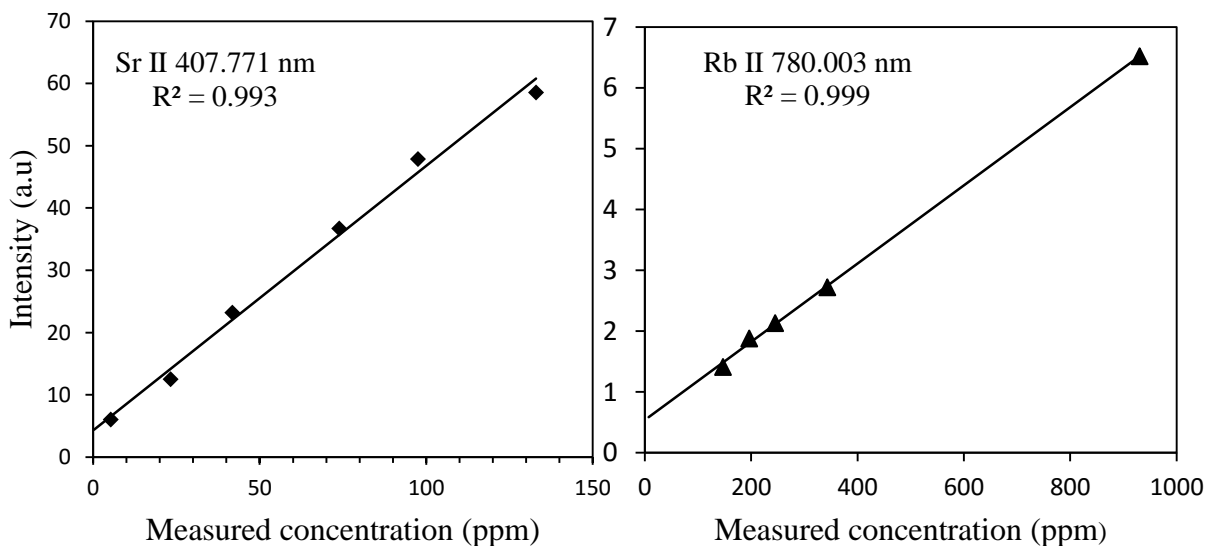


**Figure 5.5.1:** Selected univariate graphs for fission products acquired from fused glass samples

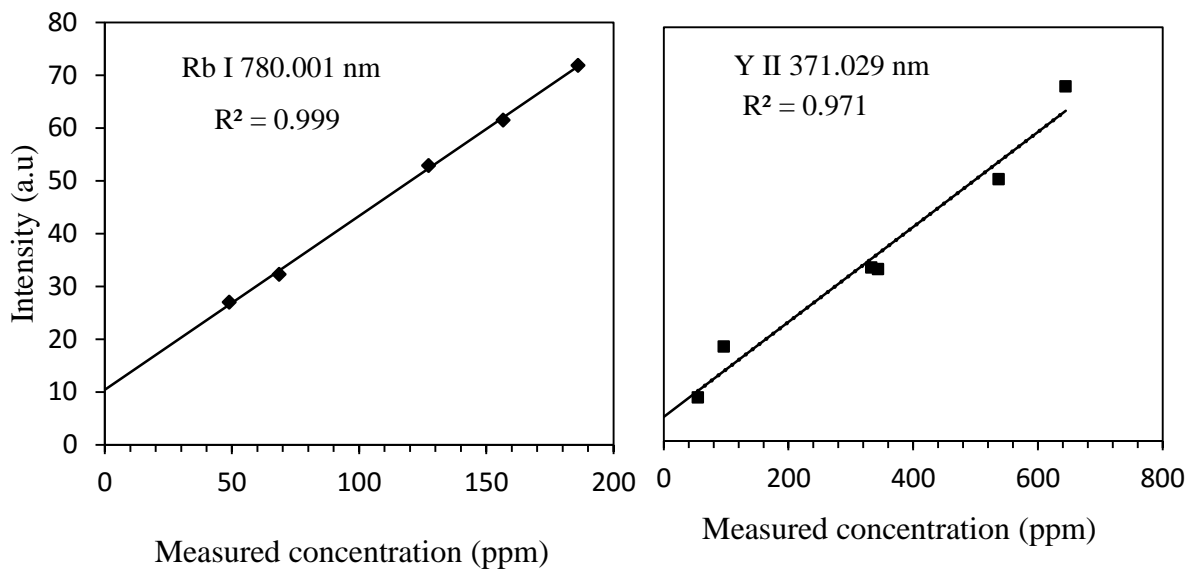


**Figure 5.5.2:** Selected univariate regression plots for fission products in spectra acquired from pellet (powders) samples.

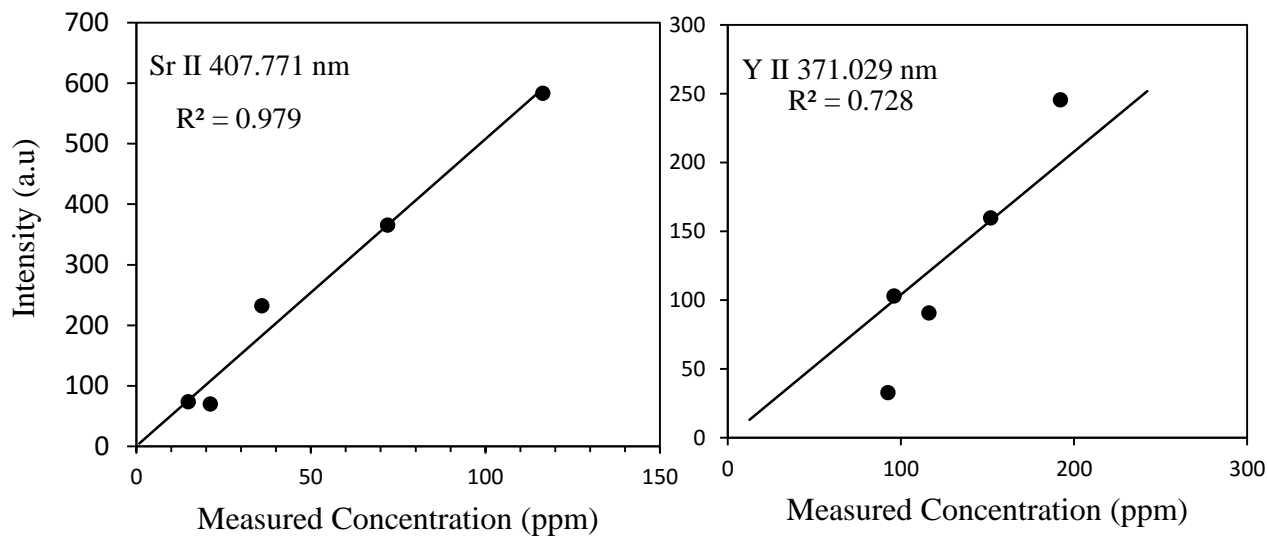


**Figure 5.5.3:** Selected univariate calibration graphs for fission products in spectra acquired from the liquid sample.

Following the  $3\sigma$  criterion in equation (4.3), **Table 5.2** shows some of the detection limits that were evaluated for the three forms of the sample discussed herein and compared with a few other reported literature.

**Table 5.2:** Limit of detection for Rb, Sr, Zr and Y elements in fused glass, pellet, and DCD-LIBS samples

<b>Target Element (Peak)</b>	<b>LoD for fused glass samples (ppm)</b>	<b>LoD pellet sample (ppm)</b>	<b>LoD for DCD (ppm)</b>	<b>LoD reported [Matrix, <math>\lambda</math>, Ref]</b>
<b>Rubidium (780.011 nm)</b>	181.6	25.5	6.0	1, [starch, 780.023 nm, Cremers and Radziemski, 2013]
<b>Strontium (407.771 nm)</b>	175.0	18.8	6.5	19 [SrCl <sub>2</sub> & Al <sub>2</sub> O <sub>3</sub> mixture, 460.73 nm, Fichet <i>et al.</i> , 1999] 130, [UO <sub>2</sub> pellet, 407.77 nm, Bhatt <i>et al.</i> , 2015]
<b>Zirconium (360.119 nm)</b>	199.1	67.7	54.6	290, [glass, 360.119 nm, Kurniawan <i>et al.</i> , 1995] 190, [air, 360.119 nm, Kurniawan <i>et al.</i> , 1995]
<b>Yttrium (371.029 nm)</b>	129.1	70.1	7.2	2, [NaCl, 371.03 nm, Cremers <i>et al.</i> , 2006]

Zirconium does not react directly with nitric acid, however, its dissolution is increased in the presence of hydrofluoric acid (HF) (Prajapati *et al.*, 2014; Wall and Whitener, 1959). The detection limit for Zr in DCD is relatively high compared to other FP investigated, primarily due to the poor dissolution of ZrO<sub>2</sub> in nitric acid. The dissolution rate of ZrO<sub>2</sub> depends only on the changes in HF. Moreover, a significant quantity of ZrO<sub>2</sub> can only dissolve when 13M nitric acid



is used. In this thesis 3M nitric acid was used as this is the concentration of nitric acid used during nuclear wastes reprocessing (Benedict *et al.*, 1982) ; Audero *et al.*, 1995).

## **5.6 Multivariate Modelling for Quantitative Analysis of the FP in HLW**

In this section multivariate modeling involving ANN, PCA and SVM are discussed. One of the limitations of multi-linear univariate calibration or even calibration free LIBS is that both methods suffer from high detection limits. This is true especially when trace quantities of the element of interest are involved. The use of multivariate data processing, therefore, enables reduction of high dimension complex data to a form that is easy to extract essential information from the spectral data and make viable inferences. In addition, ideally, it is difficult to achieve a linear relationship between the emitted intensities of the spectral lines and concentration. Such linear relationships work well for high concentrations and fail for very low concentrations. ANN was used to achieve multivariate calibration as discussed in subsection 5.6.1. PCA and SVM were utilized in multivariate pattern recognition and sample discrimination based on the spiked FP as discussed in section 5.7.1 section 5.7.2 respectively.

### **5.6.1 ANN Model for Quantitative Analysis of FP in HLW**

In this work, neural networks (NN) was chosen as a multivariate modeling technique owing to advantages that have been published over time (Cilimkovic, 2015; Beale *et al.*, 2010; Jain *et al.*, 1996). These advantages include the ability of NN to learn from examples especially from input-output relationships and ability to model non-linear relationships between data (Naguib and Sherbet, 2001).

Utilization of the entire spectrum requires large computer memory in order to achieve ANN modeling. Because of this limitation, there is a need for data compression procedures through spectral feature selection, which reduces redundancy in the data and achieves a more robust

calibration model. Therefore, the emission lines of the target elements which were spectrally isolated and free of interference were selected. The selected spectral regions were set in MATLAB 7.8.0 (R2009a) as the input to the ANN network. The corresponding known concentrations were administered as targets in the network. Prior to running the network, the input matrix was normalized by means of the inbuilt *mapstd* function which transforms the inputs to possess a zero mean and unity standard deviation. This is done in order to bring both high and low valued data to participate equally in the chemometric modeling.

Optimization for the best performing parameters of the ANN network was done. This included a variation of the number of neurons, the learning rate of the model, the number of layers of the network and even the transfer function. The number of layers was varied with other variables held constant such that the number of layers that produced the highest accuracy in prediction of samples not shown to the network was selected. The best layer was set constant and the number of neurons was varied. The process was repeated until the architecture that offered the highest  $R^2$  was chosen.

The outcome is as illustrated in **Table 5.3**, **Table 5.4** and **Table 5.5** . It was found that a two-layer network with three neurons and *tansig* transfer function resulted into the rapid convergence of the network. In addition, highest  $R^2$  and the lowest MSE values for training, test and validation were achieved under these conditions. As such, these parameters were adopted and utilized for subsequent modeling.

**Table 5.3:** Model prediction ability with a variation of ANN layers for *newff* algorithm

Network Layers	Number of neurons	Transfer function	Learning rate	R <sup>2</sup>
2	2	tansig	0.0001	<b>0.9844</b>
3	2	tansig	0.0001	0.9624
4	2	tansig	0.0001	0.9795
5	2	tansig	0.0001	0.9380
6	2	tansig	0.0001	0.9633

**Table 5.4:** Model prediction ability with a variation of the number of neurons for *newff* algorithm

Network Layers	Number of neurons	Transfer function	Learning rate	R <sup>2</sup>
2	2	tansig	0.0001	0.7272
2	3	tansig	0.0001	<b>0.9555</b>
2	4	tansig	0.0001	0.9227
2	5	tansig	0.0001	0.8556
2	6	tansig	0.0001	0.8462

**Table 5.5:** Prediction ability of the model with varied learning rate for *newff* algorithm

Network Layers	Number of neurons	Transfer function	Learning rate	R <sup>2</sup>
2	3	tansig	0.0001	0.9426
2	3	tansig	0.001	<b>0.9790</b>
2	3	tansig	0.01	0.8821
2	3	tansig	0.1	0.8312

These optimized parameters were obtained through feature selection of Y lines with feed forward back propagation algorithm with Levenberg-Marquit (LM) optimization function. The output of the layers was calculated from the net input by means of the *tansig* transfer function. The number of neurons was set to be 3 with a learning rate of 0.001. The associated code is given in Appendix 2.

Two ANN algorithms were compared for the best performing architecture. Quantitative models developed using the networks were then compared to infer a model that is best suited for such data consisting of selective LIBS spectral regions set around the peaks of trace elements mimicking fission products in fused glass (a representative of fission elements in vitrified glass) and similar elements in liquid form (trace fission products in simulate liquid nuclear waste). Hence, the cascade correlation algorithm and the common feed forward back propagation were employed and compared.

A comparison between cascade correlation algorithm (*newcf*) and feed forward back propagation algorithm (*newff*) for the fused glass samples data reveals the following ANN regression plots (**Figure 5.6.1** and **Figure 5.6.2**) for synthetic samples that were not shown to the network. The same samples were maintained for the two architectures.

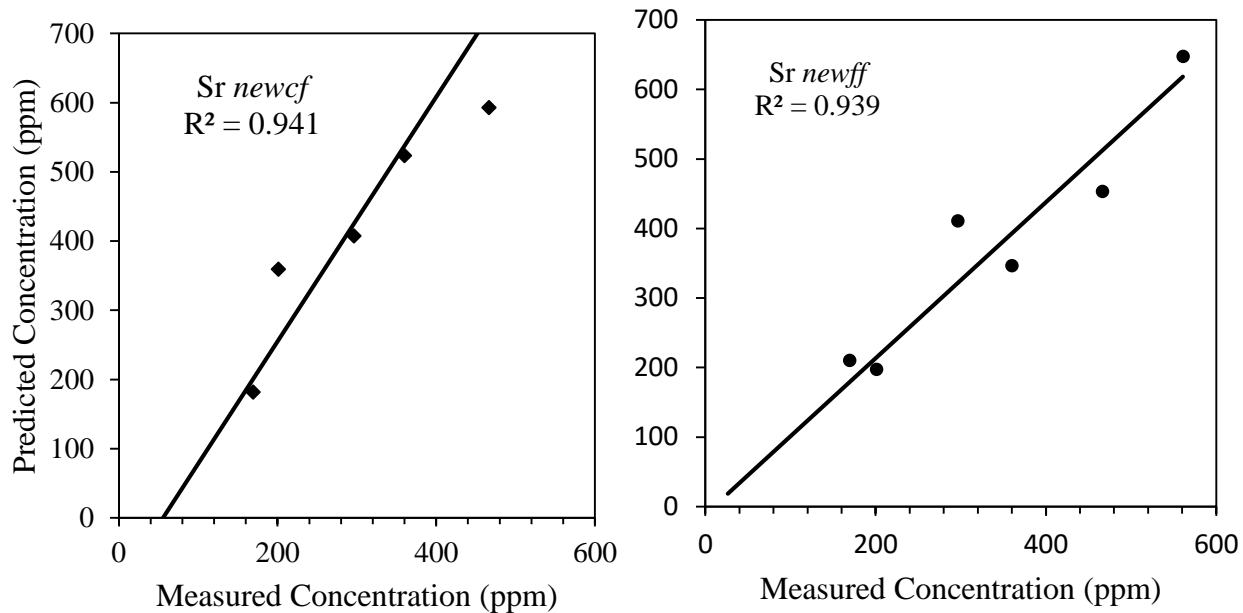


**Figure 5.6.1:** ANN multivariate regression plots for Sr utilizing newcf and newff algorithms respectively using fused glass samples data.

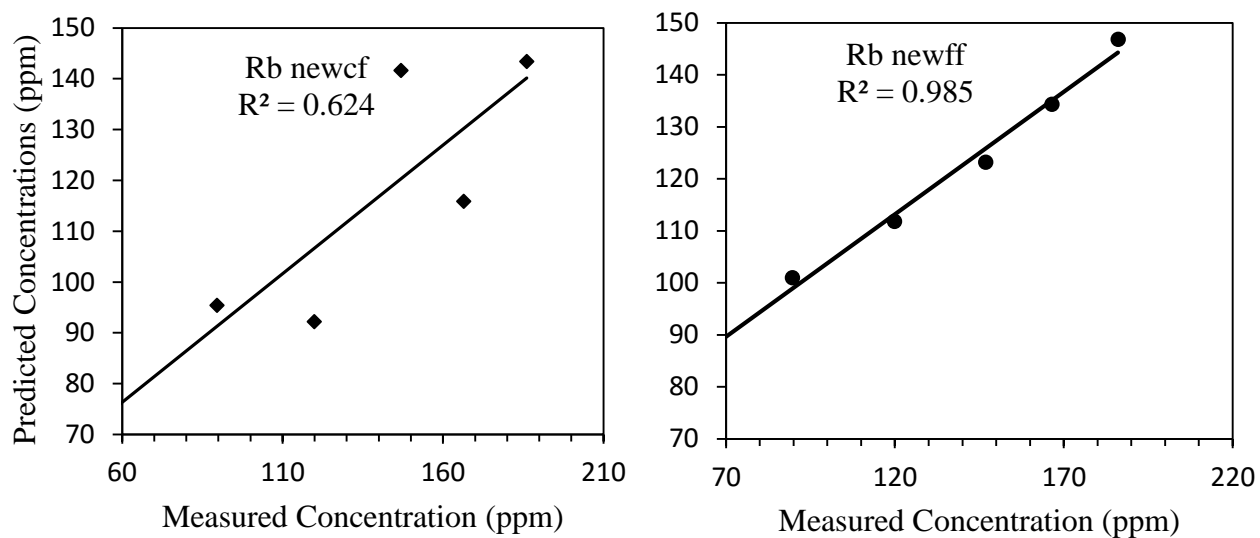


**Figure 5.6.2:** ANN multivariate regression plots for Rb comparing newcf and newff algorithm (newff) for the fused glass samples data.

Cascade-correlation architecture leads to a higher coefficient of correlation between the predicted concentration and the measured concentrations. However, investigation of the individual predictions to that of the original concentrations reveals that the cascade correlation algorithm leads to a higher margin of error compared to the feed forward back propagation algorithm. Therefore when all other factors are held constant newff algorithm provides more reliable predictions.

The relative error of prediction (REP) for each of the algorithm was evaluated based on the procedure reported by (Dingari *et al.*, 2012b). Thus;

$$\text{REP}(\%) = \frac{100}{N} \sum_i^N \left| \frac{\hat{C}_i - C_i}{C_i} \right| \quad (5.1)$$

Where N is the total number of spectra in the dataset,  $\hat{C}_i$  is the measured concentration and  $C_i$  is the concentration predicted by the model. Therefore the REP is considered as one of the figures of merit in multivariate analysis as it shows the accuracy and precision of the model. This figure of analytical merit was computed for all of the models developed as shown in **Table 5.6**. The lower the REP the more accurate the model.

**Table 5.6:** Relative Error of Prediction (REP) for the feed forward back propagation (*newff*) and cascade correlation (*newcf*) models developed utilizing feature selected fused glass data

<b>Multivariate Regression Plots (Fused glass feature selection)</b>	<b>Relative Error of Prediction (%)</b>	
	<i>newff</i>	<i>newcf</i>
<b>Strontium</b>	12.35	36.38
<b>Rubidium</b>	9.61	15.18
<b>Zirconium</b>	7.30	17.51
<b>Yttrium</b>	3.78	13.23

Since the feed forward back propagation algorithm worked best for these samples, it was adopted as the preferred algorithm and was used to develop the remaining models for the solid and liquid forms of each of the simulated samples. Other researchers e.g. Cilimkovic (2015), Skorpil and Stastny, (2006) have also identified the feed-forward algorithm to be rapid and has the ability to converge more easily compared to the cascade correlation algorithm. Utilizing this *newff* algorithm the ANN regression plots in subsections 5.6.1.1, subsection 5.6.1.2 and subsection 5.6.1.3 were developed.

### **5.6.1.1 Fused Glass Samples**

**Figure 5.6.3** shows selected ANN regression plots for quantification of FP in fused glass utilizing ANN. For samples that had been set aside for model validation, the coefficient of correlation for the developed models was above 0.98 as shown on the graphs.

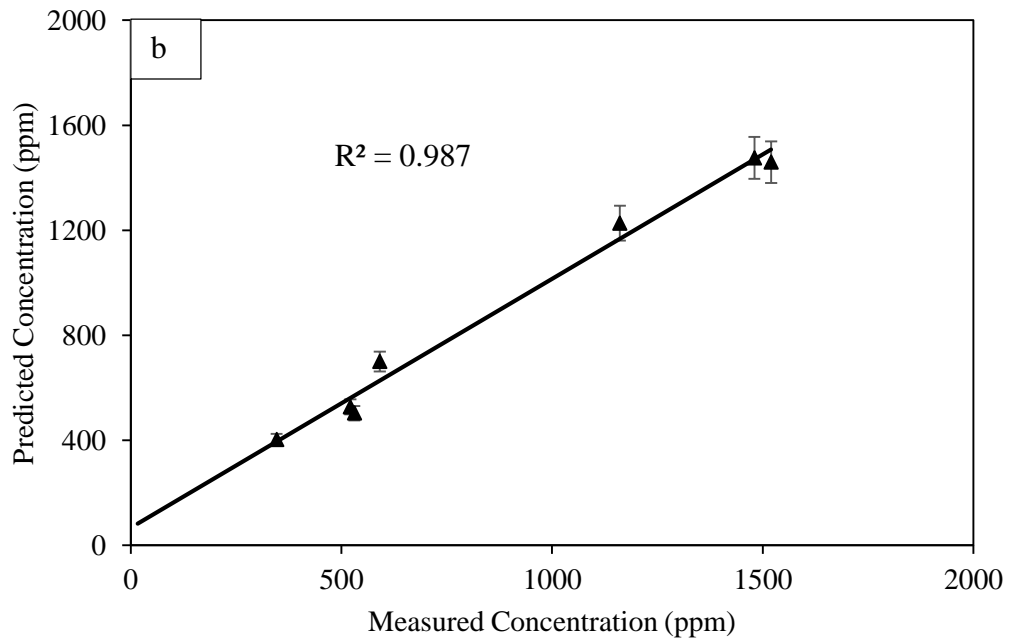
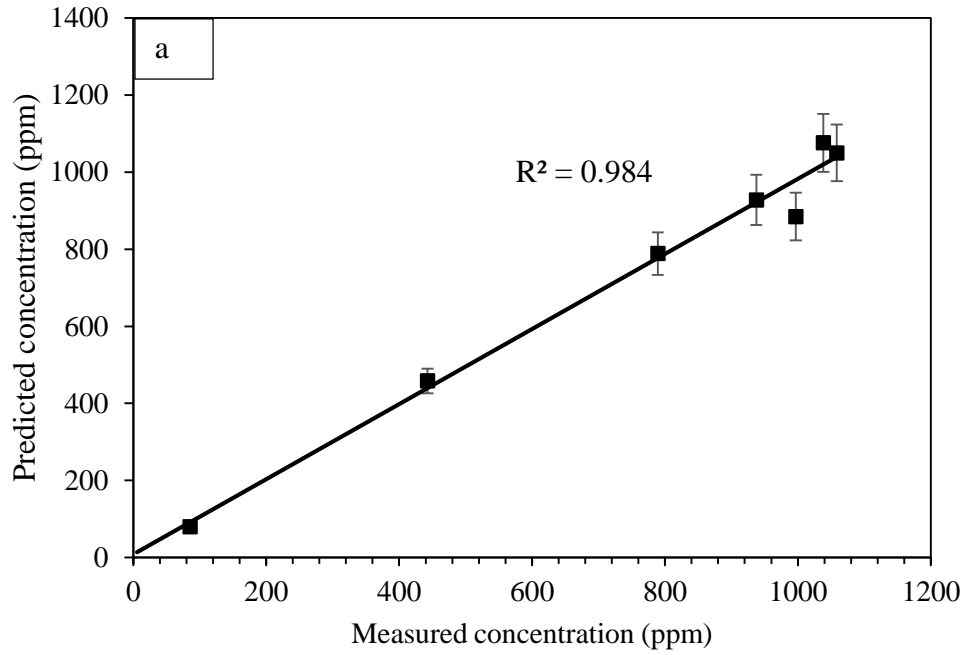


**Figure 5.6.3:** ANN multivariate regression plots for a) Y and b) Zr in fused glass.



### 5.6.1.2 ANN Regression Plots for Pellet Samples (Pressed Simulate Nuclear Powders)

Selected ANN regression plots for Y, Sr, and Rb are given in Figure 5.6.5. The sample (†) in **Figure 5.6.5** (c) corresponding to 19 ppm Rb during model training predicted the same value regardless of the training iterations. This could be associated with the LoD of Rb which is 25.25 following the univariate approach. Hence, the concentration of the sample lies below the computed detection limit (<LoD). If the samples are omitted from the calibration curve a high precision calibration curve is obtained. Hence, via multivariate modeling, the values can be mapped to fit in the calibration curve together with samples of higher concentrations.

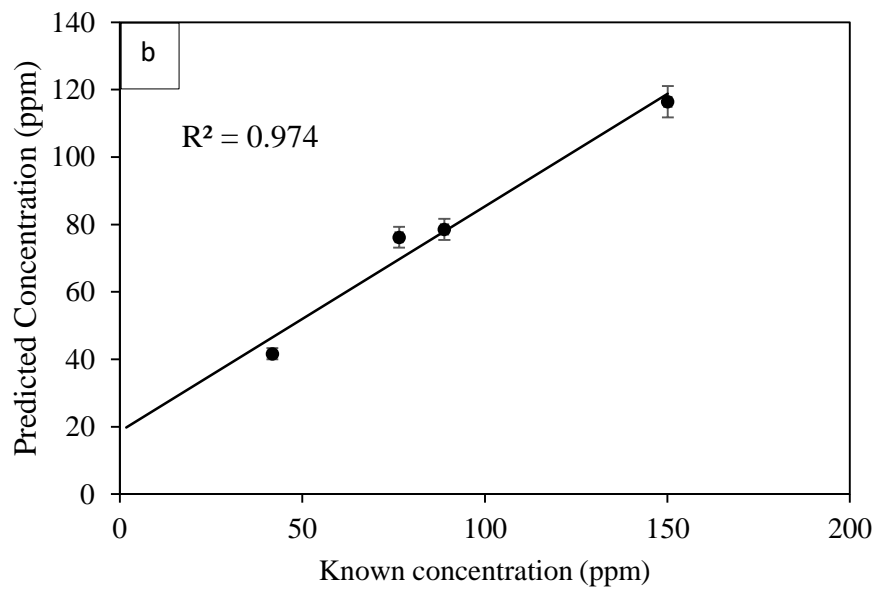
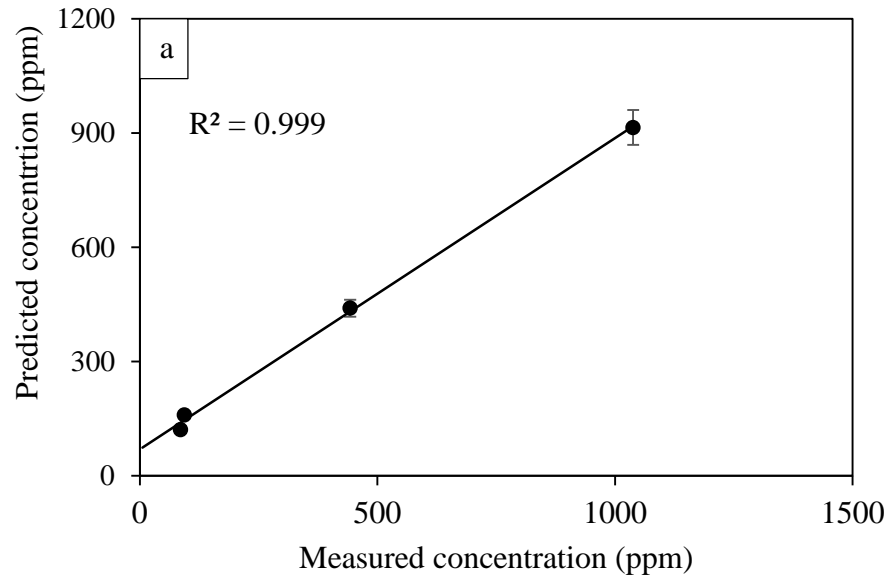


**Figure 5.6.4:** ANN regression plots for (a) Y, (b) Sr using data acquired from pellet samples

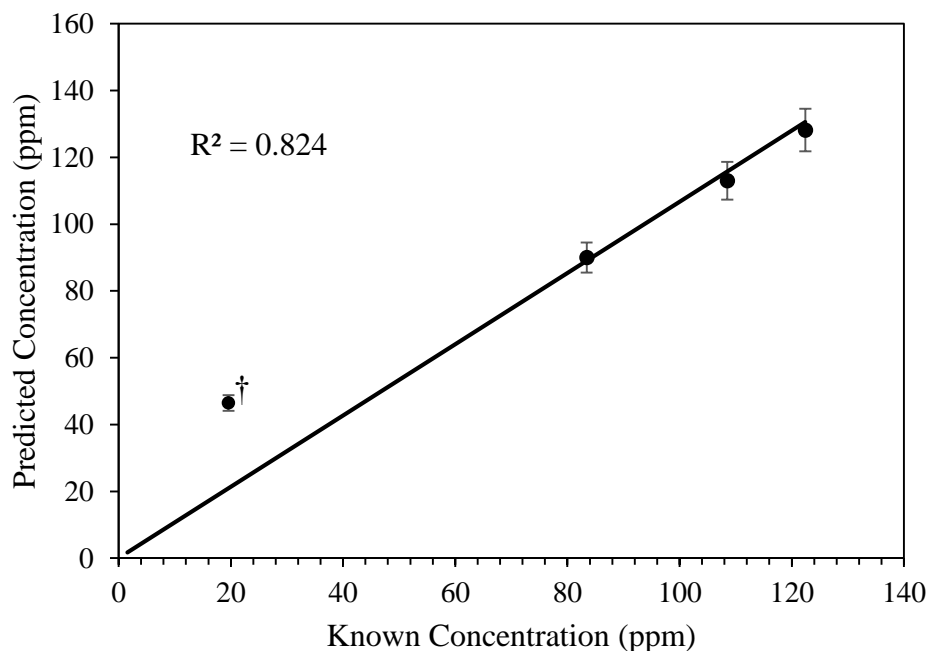


**Figure 5.6.5:** ANN regression plot for Rb using data acquired from pellet samples.

### 5.6.1.3 Drop Coating Deposition LIBS (DCD-LIBS)

The modeling procedure was also extended to the same samples but prepared as liquid deposits on perspex substrate. The accuracy and prediction ability of the model are presented in Table 5.7. However, it is important to appreciate the potential of LIBS in analyzing tiny volumes. Small aliquots of only  $2 \mu\text{l}$  deposited on a suitable substrate can furnish important nuclear forensic signatures especially in nuclear accidents/detonation events. Presented in **Figure 5.6.6** and **Figure 5.6.7** are representative curves acquired using the ANN models developed.

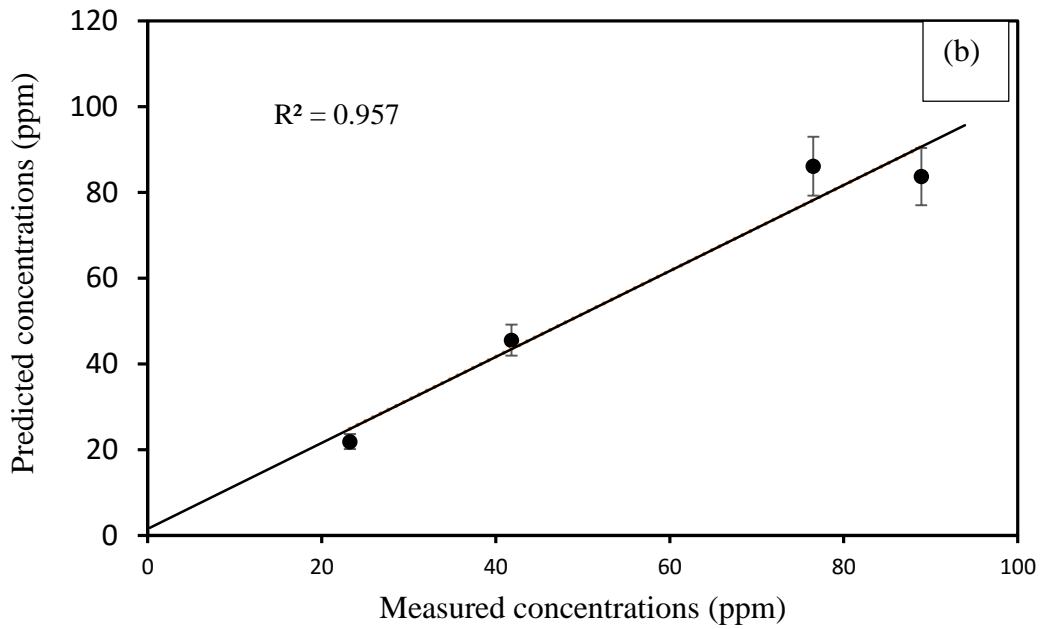
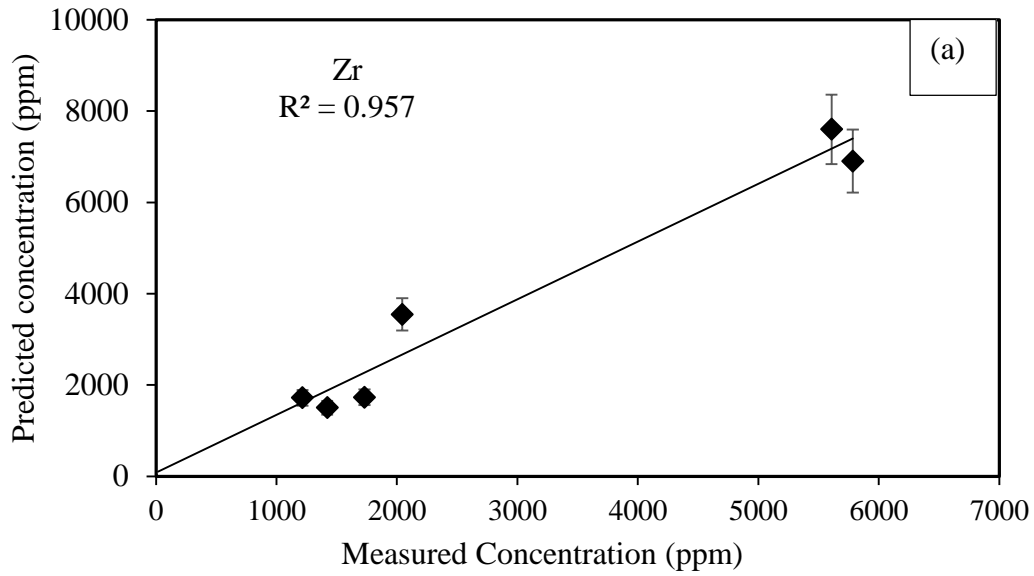


**Figure 5.6.6:** ANN regression plots for (a) Zr and (b) Sr for 2  $\mu$ l simulate HLNW liquid deposited on perspex substrate.

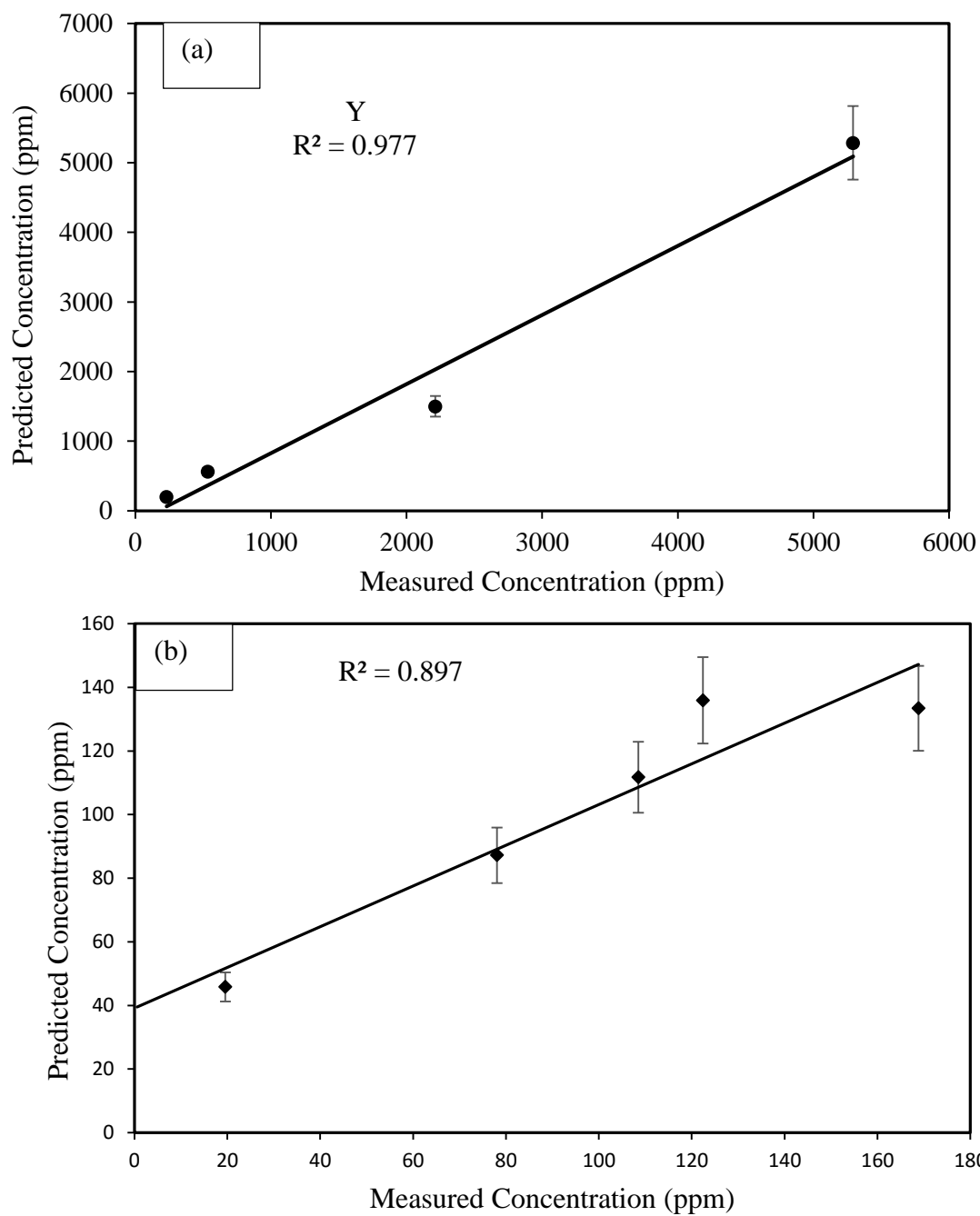


**Figure 5.6.7:** ANN regression plots for (a) Y and (b) Rb for 2  $\mu$ l simulate HLNW liquid deposited on perspex substrate.

The ability of the developed multivariate calibration models to predict synthetic samples which were hidden from the network is given by the explained variance value and the REP whose values for each model in fused glass, pellet, and liquid forms are as shown in **Table 5.7**.

**Table 5.7:** Model performance based on the explained variance ( $R^2$ ), the Relative Error of Prediction (REP) and univariate LoD for fused glass, pelletized and liquid sample forms of the same analyte

Element	Fused glass			Pelletized Form			Dry Liquid micro drop Form		
	$R^2$	REP (%)	LoD	$R^2$	REP (%)	LoD	$R^2$	REP (%)	LoD
<b>Sr</b>	0.939	12.350	175.0	0.974	8.730	18.8	0.957	1.470	6.5
<b>Rb</b>	0.985	9.610	181.0	0.991	5.560	25.5	0.897	11.680	6.0
<b>Y</b>	0.984	3.780	129.1	0.999	31.060	70.1	0.977	12.350	7.2
<b>Zr</b>	0.987	7.300	199.1	0.750	15.020	67.7	0.957	4.180	54.6

### 5.6.2 ANN Models Validation Results for Nuclear Pellets and HLLW Simulates

Prediction ability of the DCD ANN models was further achieved with the use of synthetic ICP standard solution prepared in a similar way as the simulated samples. The percentage deviation from certified value is < 10 % as shown in **Table 5.8**. The prediction ability of the pressed powder pellet models was also done using river clay PTXRFIAEA09 SRM whose findings are in **Table 5.9**. The concentrations of selected FP (Sr, Y, and Zr) were found to have < 12 % deviation from the certified values.

**Table 5.8 : HLLW Model validation results using certified standards.**

<b>Name of the Standard</b>	<b>Certified Standard Concentration (ppm)</b>	<b>Average Predicted (TriPLICATE) (ppm)</b>	<b>Deviation from the certified value (%)</b>
Strontium ICP standard, CertiPUR <sup>®</sup> MERCK Darmstadt Germany	100	91.34 ± 2.34	8.66
Zirconium Atomic Absorption Standard Solution, SIGMA Chemical Company, USA	500	542.14 ± 5.51	8.43
Yttrium ICP standard, CertiPUR <sup>®</sup> MERCK, Darmstadt Germany	100	93.61 ± 4.14	6.39

**Table 5.9: Simulate nuclear pellet validation results using River Clay PTXRFIAEA09**

<b>Element</b>	<b>Certified Concentration (ppm)</b>	<b>Model Predicted (TriPLICATE) Concentration (ppm)</b>	<b>Percentage error (%)</b>
<b>Rb</b>	105.57 ± 5.77	115.06 ± 3.16	9.0
<b>Sr</b>	101.9 ± 3.03	89.59 ± 5.32	12.1
<b>Y</b>	27.89 ± 2.15	24.63 ± 4.26	11.7
<b>Zr</b>	317.91 ± 14.2	296.27 ± 15.21	6.8

## **5.7 Hypothetical Nuclear Forensic Scenario and Approach to Attribution**

In nuclear forensics, materials suspected to be of nuclear or radioactive origin are probed in pursuit of evidence to inform attribution. Some occurrences that may require the application of nuclear forensic include; detonation events involving such materials, spillage of nuclear wastes while moving to repository sites, radioactive dispersal devices (RDD) by malicious groups, etc. Such NF situations require a specific methodology for analysis and drawing inferences as tiny samples are involved.

This work attempts to develop the methodology for analysis of such NF situations. If a dirty bomb is blown off there is a need to determine its composition via (FP composition) and link it to the most likely origin of such material. One potential analytical plan would be to cordon the crime scene, collect fragments of the exploded device or even debris (e.g glass debris) for direct LIBS analysis. In addition, if the particles are allowed to rest on surfaces (say plant leaves) and dew allowed to form, the liquid aliquots can be sampled and analyzed via dry coat on a suitable substrate.

Such trace micro-analytical capability offers a nuclear forensic methodology useful in attributing the material to its source or even analyzing materials from radiological crime scenes. As such, qualitative and quantitative elemental composition can be achieved via LIBS and the developed ANN models discussed here.

### **5.7.1 Principal Component Analysis of Simulate HLNW Samples**

As mentioned earlier, in a typical nuclear scenario, for example, detonated nuclear device/radiological crime scene, the contents of the device involved get mixed in a manner that is difficult to separate in order to reveal the identity of the exploded device. If data from such

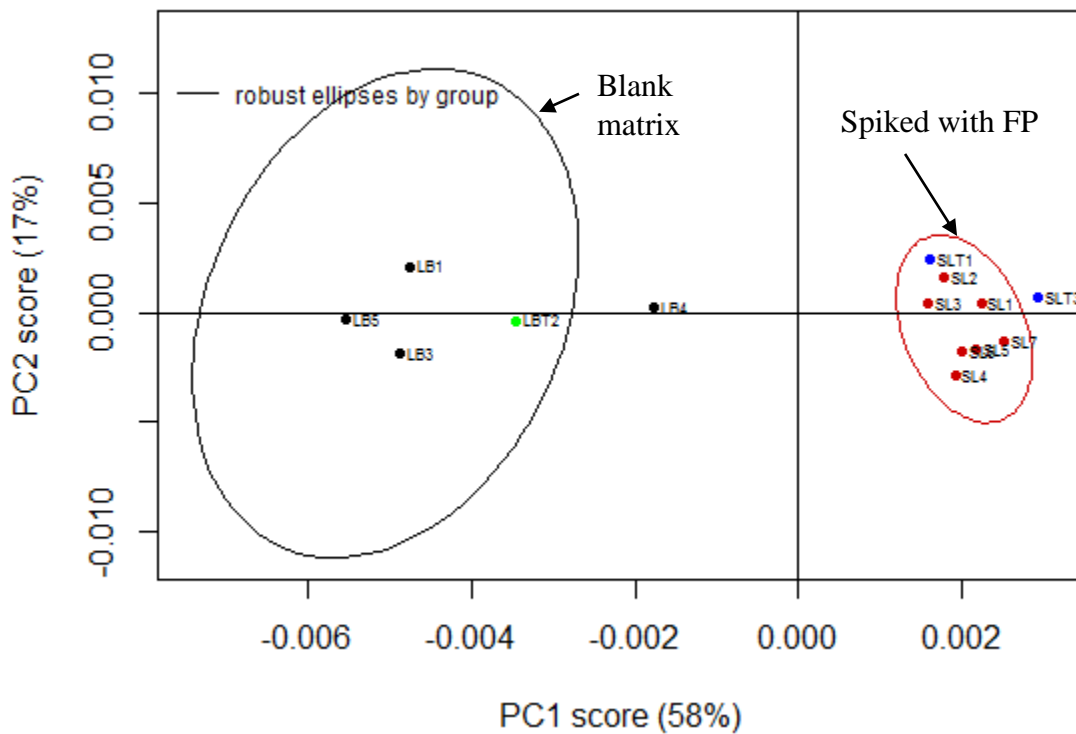


samples is acquired then pattern recognition can be explored to reveal trends (e.g relationship between samples collected, the FP present, etc.)

In this work, HLNW liquid samples containing known trace amounts of selected FP were utilized together with the reference blank liquid matrix. Three samples were set aside for method validation. A PCA was done on the samples to realize the behavior of the two groups. Their spectra data acquired through LIBS was used as input to PCA in **R** (Version 1.0.143 – © 2009-2016 RStudio, Inc) through ‘Chemospec’ chemometric statistical packages (Hanson, 2014). The corresponding code is given in Appendix 4. The data was pretreated via normalization and baseline restoration.

**Figure 5.7.1** (PC-2 against PC-1) and **Figure 5.7.3** (PC-3 against PC-1) show the scores plot for the two sets of data. The liquid samples spiked with trace quantities of FP cluster together (SL group). The reference liquid blank samples also grouped together (LB group). The loadings plot illustrates that the peaks from the spiked elements are responsible for the positive PC-1 clustering as shown in **Figure 5.7.2** and **Figure 5.7.3**. Two samples spiked with FP (SLT1 and SLT3) were introduced to the model and they grouped together with the spiked liquid samples while blank validation sample (LBT2) clustered with the blank liquid samples. This is important in nuclear forensic analysis since samples suspected to be of nuclear origin can be identified and discriminated against those that do not contain FP. The 3D plot in **Figure 5.7.4** shows that the distinct clusters with PC1 carrying most of the information about the samples. The samples SL5 and SLT3 group closely together as shown in **Figure 5.7.4**. This is most likely because the samples had the same uranium concentrations (sample 3 and 5 in appendix 1). Notably, spectra of tiny liquid aliquots (2 µl) collected from a nuclear scene and deposited on a suitable substrate can be compared with reference spectral database and furnish nuclear forensic information to

inform attribution. Similar, approaches have been attempted by Banas *et al.* (2010) in which PCA together with a spectral library was utilized to simulate post-blast residues. However as this research involved explosive materials of non-nuclear origin, this work has exploited the potential utility of the approach especially in cases involving nuclear materials such as RDD. As such, PCA offers the ability to visualize such data since such events are characterized by low concentrations of the target elements (FP).



**Key:**

- LB – Blank liquid samples
- SL – Spiked Liquid sample (spiked with trace FP)
- LBT – Blank liquid test sample
- SLT- Spiked liquid Test sample (spiked with trace FP)

**Figure 5.7.1:** PCA Scores plot for simulate high level liquid nuclear wastes. The samples SL and SLT contain FP spiked in trace quantitative levels while LB and LBT are reference blank samples matrix samples.

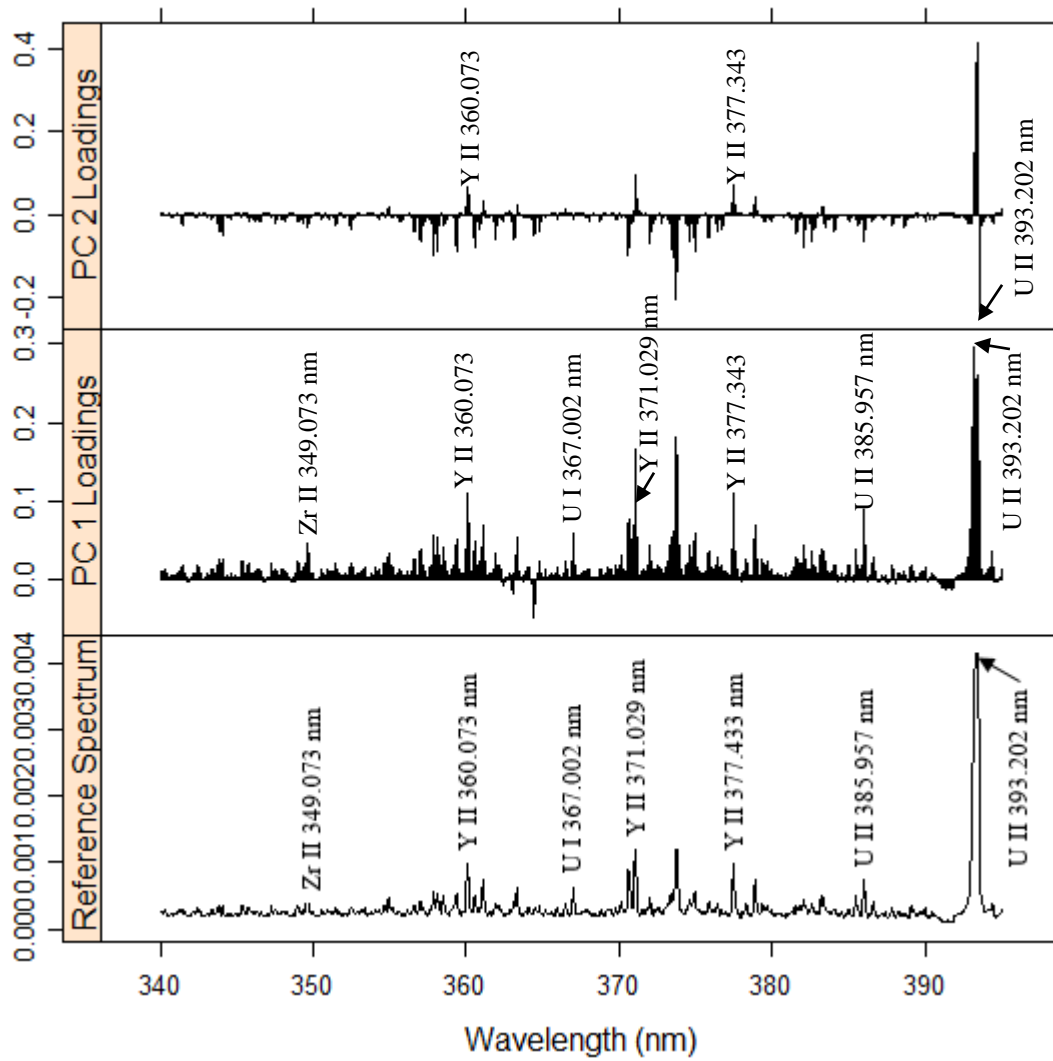
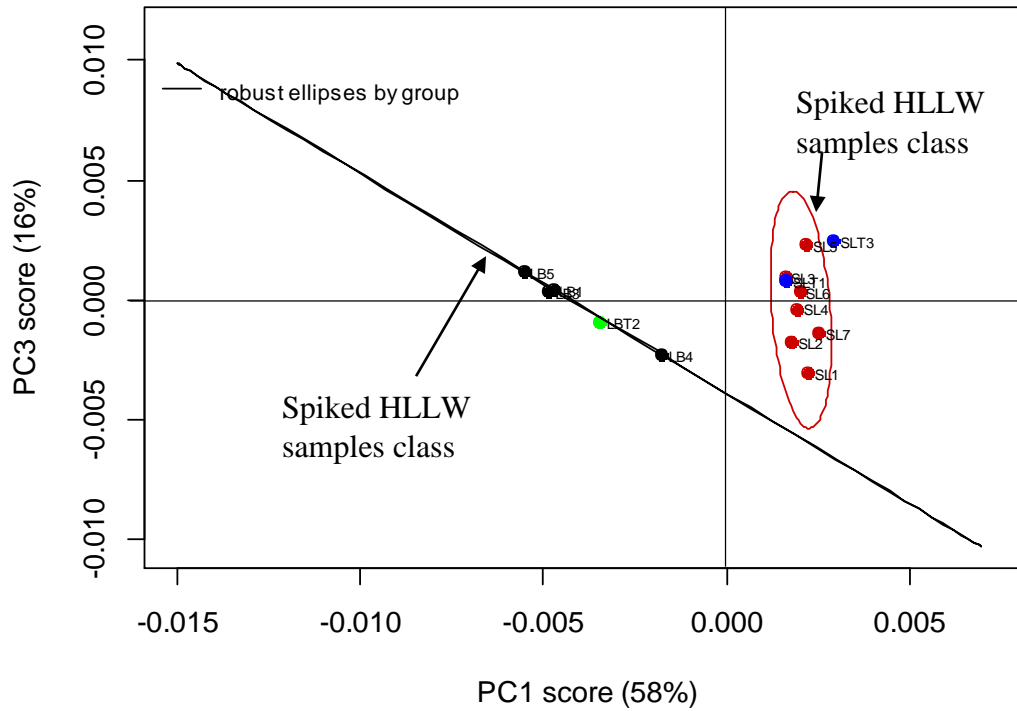
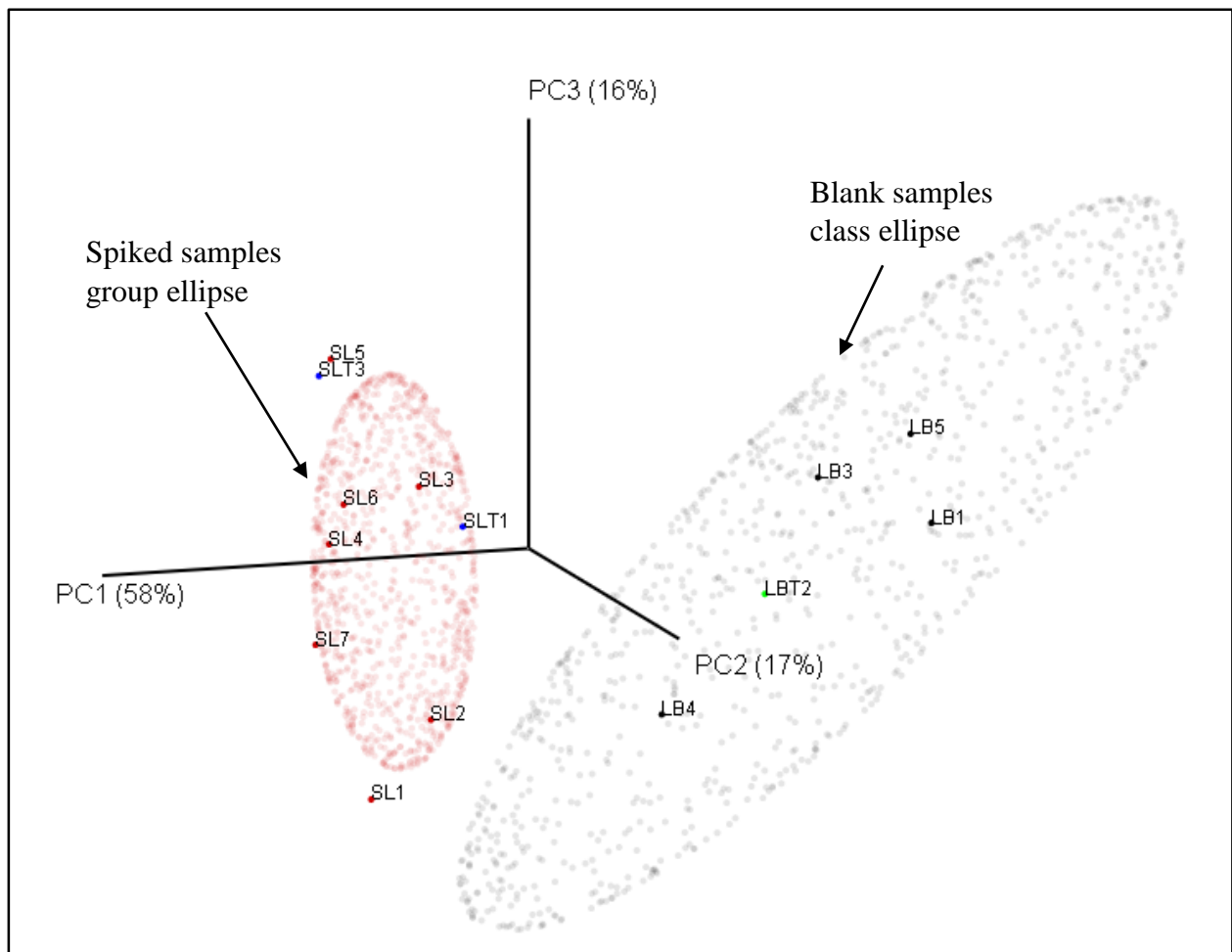


Figure 5.7.2: PCA loadings plots for simulate high-level nuclear waste liquid samples



**Figure 5.7.3:** PC1 and PC3 scores plot for simulate high level liquid nuclear wastes.SL and SLT contain FP spiked at (0-1000 ppm) levels while LB and LBT are reference samples.



**Figure 5.7.4:** 3D PCA scores plot for simulate HLLW. The samples SL and SLT contain FP spiked within 0-1000 ppm levels while LB and LBT are blank samples.

### 5.7.2 Support Vector Machine (SVM) Classification of Simulate Nuclear Wastes

The goal of NF is to achieve attribution of intercepted NRM and/or characterizing materials acquired from nuclear scenes (e.g. detonation events). Such attribution depends largely on quantitative and qualitative data that has been discussed in this thesis. Supervised machine learning using e.g SVM has the potential to reveal any hidden properties of the data such as selected FP distribution in different samples acquired from a nuclear scene. Coexistence of FP

and U in typical concentrations they occur can reveal the stage of the material in the NFC (Sekimoto and Miyashita, 2006). Equally, detection of zirconium in such materials can give clues about the nature of the sample as this element is utilized as cladding for nuclear fuel. In any case, even the lowest detection of FP at a radiological/nuclear crime scene depicted as a nuclear terrorism act requires utmost attention and analytical methodologies to deter such occurrences (Alkış, 2017). In this sub-section, SVM was used to visualize decision boundaries between individual FP for a material that has been classified as HLLW by means of the PCA approach as discussed in section 5.7.1.

#### 5.7.2.1 Choice of Optimized SVM Parameters

Among the parameters that affect the output of an SVM classifier, the kernel type, the gamma ( $\gamma$ ) and the cost (C) were optimized. The factor C controls the degree of violation of the margin (Cisewski *et al.*, 2012a, Huang and Wang, 2006). A decreasing value of C widens the margin to accommodate more support vectors and vice versa (James *et al.*, 2013). For radial basis kernels (RBK) functions,  $\gamma$  is utilized as a measure of similarity between two given points. A range of these parameters were used to tune the SVM classifier through 10 cross validation to attain the optimal parameter combination. The choice of Kernel type also affects the classification accuracy. **Figure 5.7.5** shows a linear kernel (LK) function and RBK function using the same data set containing selected Zr and Rb peaks. RBK function provided the most flexible separating hyperplanes and was found to be the most appropriate for the HLW LIBS data.

For independent samples data hidden from the model, the confusion matrix in **Table 5.10** shows that all Zr bearing samples were correctly classified as belonging to Zr class whereas for Rb class one sample was confused with Zr samples thus giving an overall correct grouping accuracy of 92.85 %.

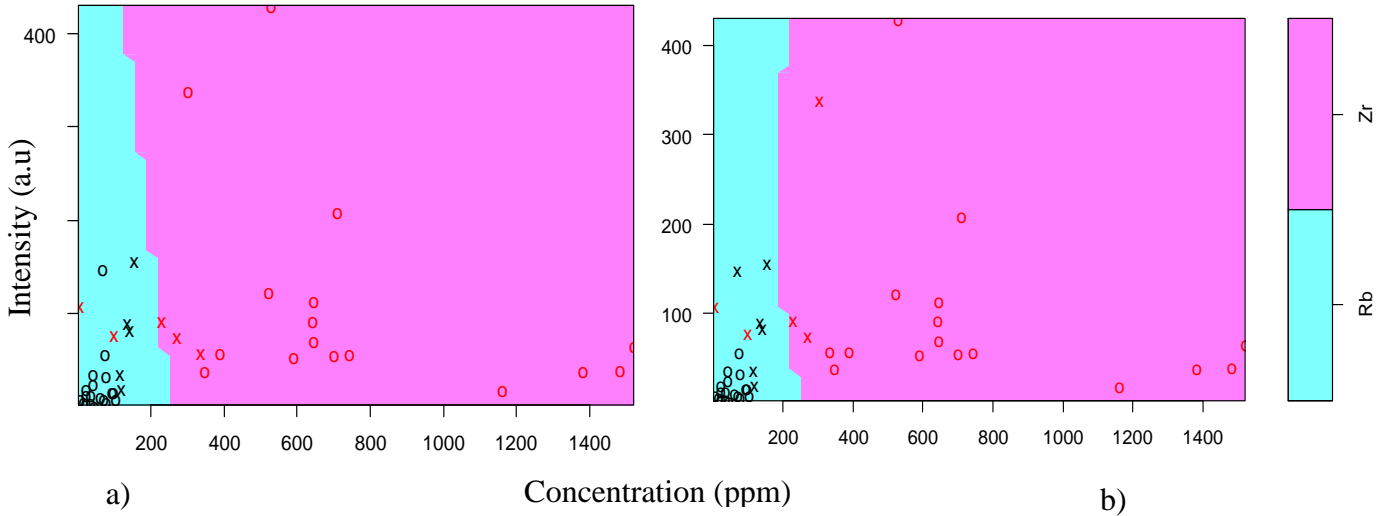


**Figure 5.7.5:** SVM plots utilizing selected zirconium and rubidium lines in fused glass with; a) linear kernel, b) RBK function.

**Table 5.10:** Confusion matrix of test data set ( $C = 1000$ ,  $\gamma = 1$ , *RBK*, 10 fold cross validation)

Clustering ability		Predicted	
		Rb	Zr
Actual Class	Rb	6	1
	Zr	0	7
Classification accuracy (%)		92.85	

### 5.7.2.2 SVM utilizing Fused Nuclear Glass Simulate Samples

Selected spectral regions corresponding to the peaks of FP were utilized as inputs to the SVM classification model. This matrix consists of data that had been randomly selected and hidden from the model. The fission products (Sr and Rb) and U SVM classified samples as given in Figure 5.7.6. The corresponding confusion matrix is given in Table 5.11. The overall grouping/clustering accuracy was 82.35 %. As a result, out of 17 samples, 3 were misclassified.

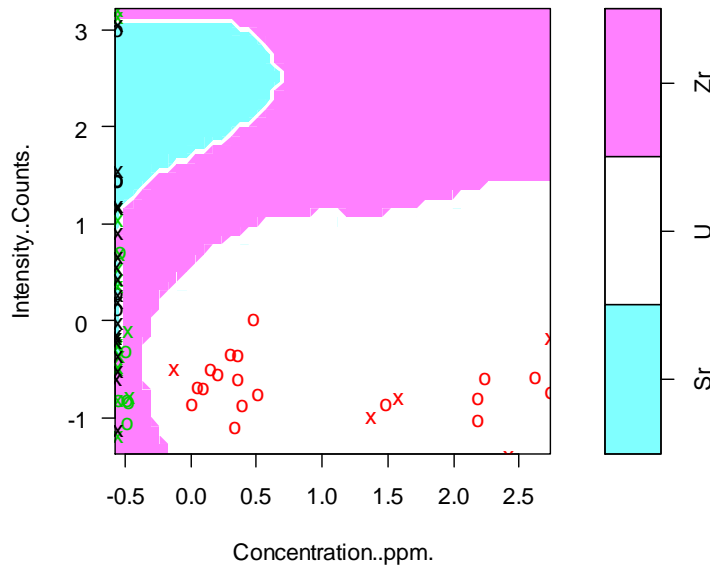


**Figure 5.7.6:** SVM plot of the feature selected fused glass samples training dataset ( $C = 1000$ ,  $\gamma = 1$ , *RBK*).



**Table 5.11:** Confusion matrix of validation test data set at ( $C = 1000$ ,  $\gamma = 1$ , RBK )

		Predicted		
		Sr	U	Zr
Actual Class	Sr	5	0	2
	U	0	6	0
	Zr	1	0	3
Classification accuracy (%)		82.35		

Zr and Y support vector classifier for HLNW in powdered samples (pressed into pellets) was also performed. **Figure 5.7.7** shows a linear model developed that clusters samples as to whether they contain Zr or Y. The tuned model ( $C = 100$ ,  $\gamma = 0.001$  and RBK function) was utilized in the classification (**Figure 5.7.7**). All the 14 samples that were reserved for testing the model were correctly classified as shown in the confusion matrix in **Table 5.12**.

A similar approach was followed to develop a classification model for distinguishing samples containing U from those containing Zr. As U and Zr always occur in high level nuclear wastes usually in high concentrations (Audero *et al.*, 1995), their detection in a nuclear scene could infer a device of nuclear origin. A test set validation set was input to the model to realize the ability of the SVM model to discriminate such samples based on selected regions/features of U and Zr as shown in **Table 5.13**. Results of the model indicated a 100% accuracy in distinguishing 7 samples containing Zr and 7 samples containing U. **Figure 5.7.8** gives the output acquired from the model.

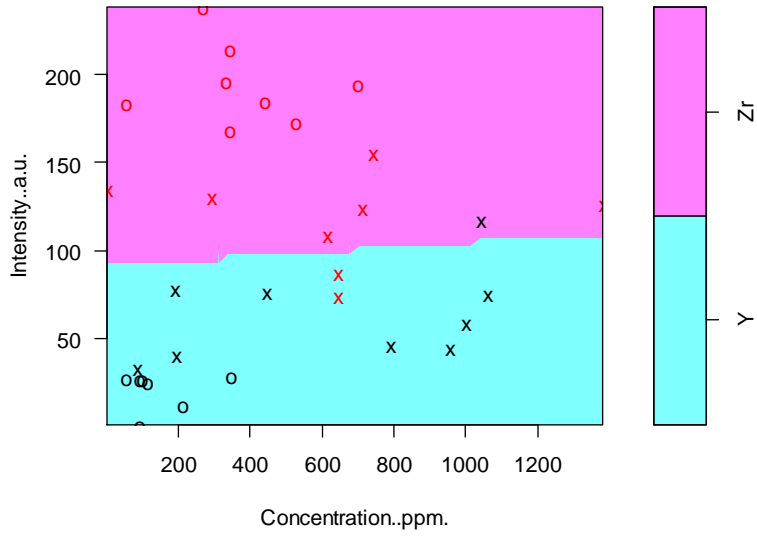


**Figure 5.7.7:** Y-Zr SVM classification plot for Pellet samples ( $C = 1000, \gamma = 0.001, RBK$ ).

**Table 5.12:** Confusion matrix for Y-Zr SVM classifier utilizing data from pellet samples at 10 fold cross validation ( $C = 1000, \gamma = 0.001, RBK$ )

Clustering ability		Predicted	
		Y	Zr
Actual Class	Y	7	0
	Zr	0	7
Classification accuracy (%)		100	

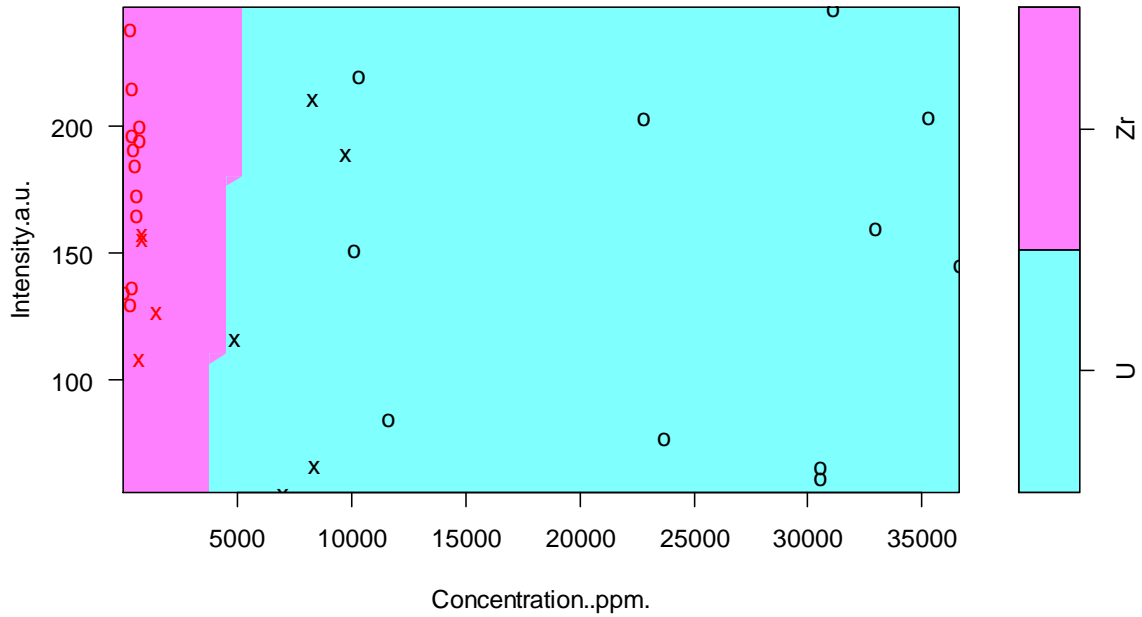


**Figure 5.7.8:** SVM plot for for U-Zr SVM classifier utilizing data from pellet samples ( $C = 1000$ ,  $\gamma = 0.001$  and RBK).

**Table 5.13:** Confusion matrix for U-Zr SVM classifier utilizing data from pellet samples ( $C = 1000$ ,  $\gamma = 0.001$  and RBK)

Clustering ability		Predicted	
		U	Zr
Actual Class	U	7	0
	Zr	0	7
Classification accuracy (%)		100	

Multiclass SVM classifier was done by considering selected FP and subjecting them to the algorithm. SVM is a binary classification methodology. However, multi-class classification was done by considering one class against all other classes as reported by (Franc and Hlavác, 2002).

An input matrix comprising of 115 samples (23 samples per FP) with different concentrations and their peak information was prepared. Of these, 80 randomly selected samples were utilized in training and tuning the model. The resulting tuned model ( $C = 1000$  and  $\gamma = 0.1$ ) was validated with a set of data with 35 samples randomly selected and hidden from the data set. Consistent with the sections above, in this work a typical simulate high level nuclear waste using the SVM classifier containing all the selected FPs is as shown in the **Figure 5.7.9**. The corresponding confusion matrix is as shown in **Table 5.14**. The actual U, Sr and Rb samples were correctly predicted and classified into their respective groups. Out of 9 samples containing Y, 5 were correctly identified as Y, however, 4 of the samples were confused to belong to Zr and Sr groups respectively. Finally, 4 out of 5 samples containing Zr were classified correctly and one sample was grouped together with Sr samples.

Discrimination against FPs is followed to narrow down into one fission product class against all FP classes to isolate samples that are suspected to be of non-nuclear origin. As characterization of nuclear wastes is necessary before waste disposal, Thus these support vector classifiers are discussed in this work to offer a supplementary capability not only to check on the process control for nuclear waste treatment but also to support regulatory compliance for a safe nuclear regime (IAEA, 2007). As such, this method can be extended to all FPs in HLW and aid in nuclear waste material characterization. Wastes from reprocessing of spent fuel are characterized as being contaminated with FPs and other trans-uranium nuclides.

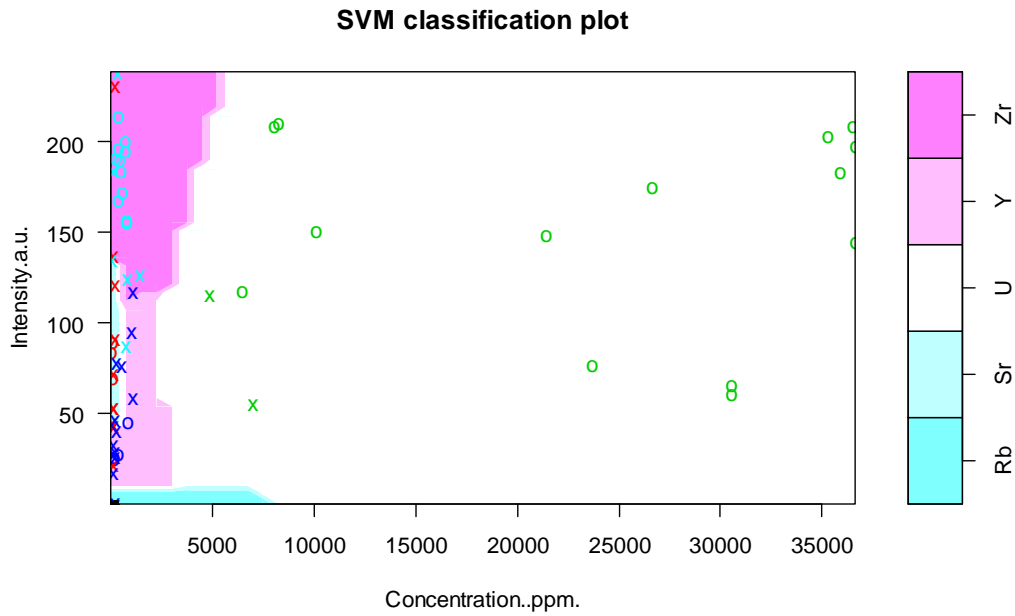


**Figure 5.7.9:** SVM clustering of FP utilizing simulated HLNW powders pressed into pellets with the best model ( $C = 1000$ ,  $\gamma = 0.1$  and RBK).

**Table 5.14:** Ability of SVM model to cluster independent test pellet data at ( $C = 1000$ ,  $\gamma = 0.1$  and RBK)

Clustering ability		Predicted				
		Rb	Sr	U	Y	Zr
Actual Class	<b>Rb</b>	9	0	0	0	0
	<b>Sr</b>	0	5	0	0	0
	<b>U</b>	0	0	7	0	0
	<b>Y</b>	0	2	0	5	2
	<b>Zr</b>	0	1	0	0	4
Classification accuracy		85.71 %				

In conclusion, it was demonstrated that SVM reveals acceptable sample discrimination in terms of the fission products at trace concentrations. The use of SVM classifications in NF is limited. However, SVM with LIBS data has been applied in automatic classification of proteins abundant in blood plasma and potential biomarkers for ovarian cancer with an accuracy of over 99.24 % (Vance *et al.*, 2010). Also, Dingari *et al.* (2012a) demonstrated the application of SVM with LIBS data acquired from pharmaceutical samples. An improved classification accuracy of over 10% was achieved while using SVM as contrasted with to PLS and SIMCA. In another study, SVM was utilized in the classification of powders suspected to belong to either *Bacillus* spores class of nonbiological confusant substances (Cisewski *et al.*, 2012). As SVM has produced excellent results in sample discrimination in other applications, the methodology developed in this work illustrates that SVM, when combined with LIBS, can be useful in NF.

### **5.7.3 Chemometric LIBS Methodology**

In this thesis, a chemometric LIBS methodology for rapid, minimally invasive detection, and quantitative analysis of nuclear fission products in simulate high-level nuclear wastes have been developed. In nuclear crime scene situation such as (detonations involving ‘dirty bombs’), nuclear security analytics requires rapid, minimally invasive and remote techniques are desirable. The role of NF analysis is to achieve attribution and offer sufficient evidence useful in bringing the perpetrators into Law Enforcement.

An analytical strategy for such situations can follow the chemometric LIBS methodology developed in this thesis as illustrated in **Figure 5.7.10**. Glass debris, dust particles and fluids recovered from nuclear crime scenes etc., are sampled for either laboratory analysis. This methodology can be integrated into a software-user interface of a portable LIBS system for *in*

*situ* quantification and classification of FPs that coexist with uranium in nuclear scenes. Detection of FP in typical concentrations they occur in NRM can distinguish material of nuclear origin from those that are not using the qualitative model employing PCA and SVM. Further discrimination of sampled materials that contain one fission product in relation to other fission products is achieved by the SVM classifier useful in nuclear material classification based on FPs. The combined chemometric LIBS methodology for characterizing high-level wastes is presented in **Figure 5.7.10**.

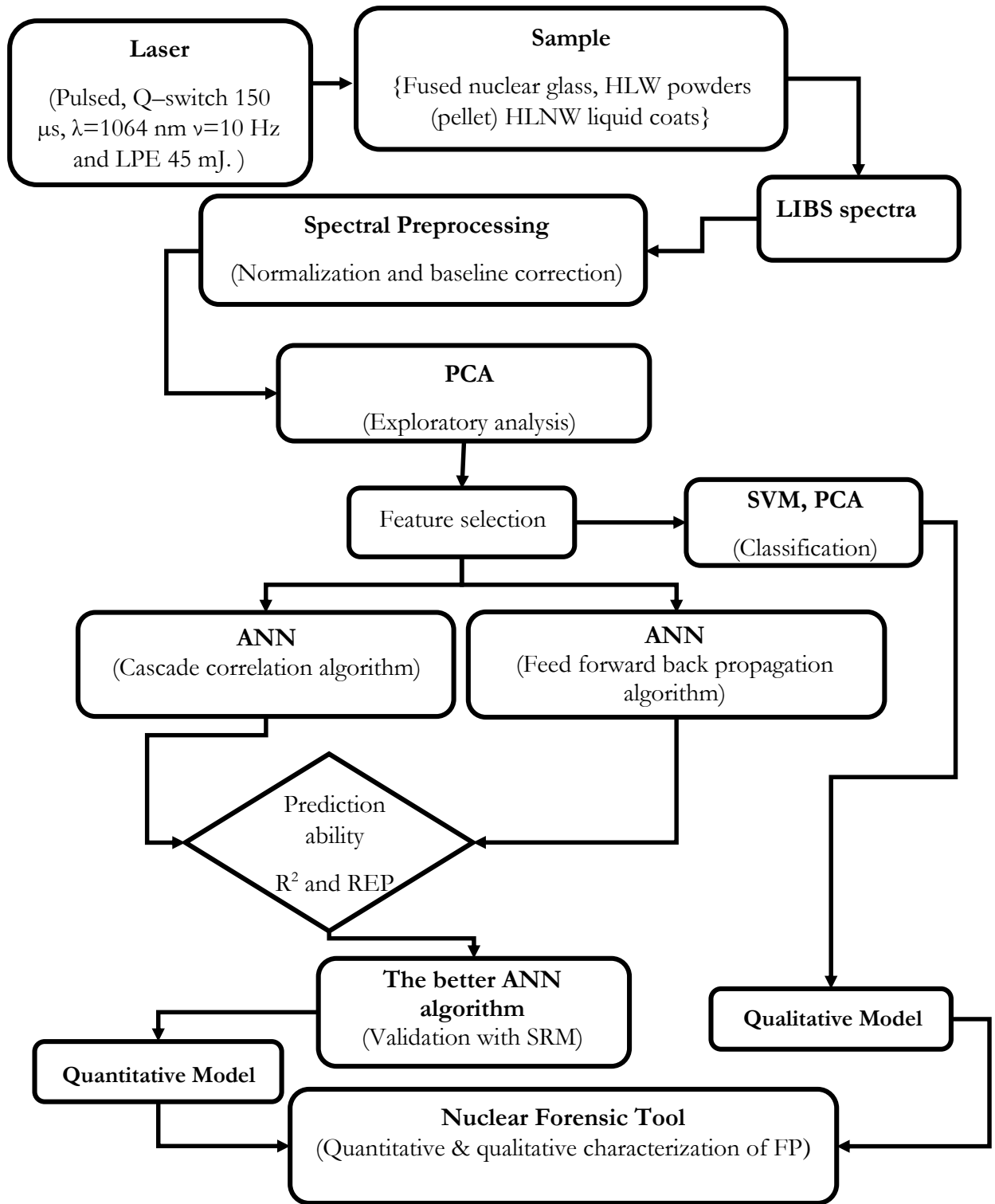


Figure 5.7.10: Chemometric-LIBS nuclear forensic tool for analysis of FP in HLNW.



## CHAPTER VI

### CONCLUSION, RECOMMENDATIONS AND PROSPECTS

#### 6.1 Summary and Conclusions

This research was undertaken to realize multivariate modeling oriented towards developing a rapid LIBS technique for detecting and quantifying nuclear fission products (Rb, Sr, Y, and Zr) in high level nuclear waste and applying the NF information to infer attribution. Models for qualitative and quantitative prediction of fission products in high-level nuclear waste for vitrified, powder and liquid forms respectively, were developed. PCA was utilized for exploratory data analysis for outlier detection prior to quantitative modeling in addition to pattern recognition applicable to NF. Two ANN algorithms (cascade correlation (CC) and feed forward back propagation (FFBP) were explored. The FFBP algorithm offered the lowest REP and high  $R^2$ . Overall, > 95% model accuracy were achieved with < 10% REP. Using the HLLW models Sr was found to be  $91.34 \pm 2.34$  ppm, a deviation of 8.66 % from the certified value. For Zr, it was  $542.14 \pm 5.51$  ppm, a deviation of 8.43 % from certified value and Y,  $93.61 \pm 4.14$  ppm constituting a deviation of 6.39 % from the certified value. For ANN models developed using pellet samples, validation results using PTXRFIAEA09 SRM, Rb was found to be  $115.06 \pm 3.16$  ppm with 9.0 % deviation from the certified value, for Sr, it was  $89.59 \pm 5.52$  ppm, with a deviation of 12.1 % from the certified value. For Y, it was found to be  $24.63 \pm 4.26$  ppm with a deviation of 11.7% from the certified value. Finally, Zr was found to be  $296.27 \pm 15.21$  ppm a deviation of 6.8 % from the certified value.

Detection limits (for the spiked elements in various sample types) were computed with fused glass (LoD  $\leq$  200 ppm), pressed powders pellets (LoD  $\leq$  71 ppm) and HLNW

liquids ( $\text{LoD} \leq 8 \text{ ppm}$ ). The HLW liquid analytes offered the lowest LoD and highest spectral response attributed to good laser-matter interaction influenced by the choice of substrate.

The ability to analyze tiny ( $2\mu\text{l}$ ) volumes liquid samples using LIBS coupled with chemometrics was found to be a useful methodology in nuclear forensics investigations and attribution. The reduced sample sizes depict the actual situation encountered in a typical nuclear forensics situation. In case of a detonated nuclear device where materials get mixed in inseparable forms, the suspended particulate matter of the constituents of the device always settle on surfaces for example plant leaves around the scene. If dew drops are allowed to form, then the particles can dissolve or get suspended within the dew drop. Sampling of such liquids can furnish trace composition NF signatures that can be analyzed to infer nuclear forensics and attribution.

Accurately tuned SVM models were developed with the ability to characterize samples based on the composition of the FP. Notably,  $> 85 \%$  prediction accuracy was realized. These models are contextually conveyed to infer nuclear forensic attribution. Thus, materials containing the fission products group together in distinct groups and those materials of a common nuclear origin can easily be identified using PCA. Their particular concentrations infer the locus of the material in the nuclear fuel cycle.

Coupling chemometric techniques (ANN, PCA, and SVM) with LIBS eliminates the limitations commonly encountered in classical analysis techniques. This work forms a very crucial component of nuclear forensics as the models developed together with NF library can be integrated into a suitable software-user interface with a portable LIBS system to analyze and characterize materials suspected to be from the back end of the nuclear fuel cycle.

## 6.2 Recommendations and Prospects

The decay of  $^{235}\text{U}$  in the nuclear reactor is accompanied by over 300 fission products and minor actinides. The methodology developed in this work using a few chosen fission products representatives can be extended to all the fission products that accompany the decay of  $^{235}\text{U}$  in the reactor. A comprehensive LIBS spectral library consisting of these elements can be developed and adopted as a reference framework in achieving nuclear forensics as well as responding to nuclear crimes in our country.

The major challenge encountered in this work was that of acquiring matrix matching standards for method validation. The author proposes a method whereby, the simulation of nuclear wastes utilizing known (ISO standards samples) other than laboratory salts to especially develop the models and then utilize the developed models to characterize unknown (samples). The utility of ISO standard can yield more robust models.

Finally, terrorism involving nuclear materials is likely to become sophisticated especially with the continuous global nuclear renaissance. As such refined counteract approaches to such terrorism are desirable. Data fusion is one of the probable techniques (Castanedo, 2013 , Fatima *et al.*, 2017 , Moros *et al.*, 2010). Three or more analytical techniques (e.g. LIBS, laser Raman, etc.) can be set to operate under the same combined sensing platform to acquire data for simulated HLNW. Through parametric fusion, the identity of suspected nuclear material can be developed to be a unique signature for HLNW. This approach has potential robustness as instead of relying on a single technique, combined techniques can provide more knowledge hence assist in developing nuclear forensic signatures in support of nuclear security.

## REFERENCES

- Ali, A. K. and Raouf, D. N. (2011). Preparation of Silver Nanoparticles by Pulsed Laser Ablation in Liquid Medium. *Eng. Technol. J.* **29**, 3058–3066.
- Alkış, M. A. (2017). Threat of Nuclear Terrorism: Towards an Effective Nuclear Security Regime. Master's Thesis, Hacettepe University Graduate School of Social Sciences.
- Andrade-Garda, J. M., Carlosena-Zubieta, A., Gómez-Carracedo, M. P., and Gestal-Pose, M. (2009). Multivariate Regression using Artificial Neural Networks. In "Basic Chemometric Techniques in Atomic Spectroscopy," pp244–283.
- Angeyo, H. K. (2018). Developing Kenya's Educational Capacity in Nuclear Security Through Nuclear Forensics Research. *Int. J. Nucl. Secur.* **4**, No 1, Article 2.
- Angeyo, H. K. (2013). A Conceptual Framework Towards Developing Chemometrics and Machine Learning Assisted Spectrometries for Rapid Nuclear Forensic Analysis. In "Nuclear Security Conference, Enhancing Global Efforts." IAEA, Vienna, Austria.
- Audero, M. A., Bevilacqua, A. M., Bernasconi, N. B. de, Russo, D. O., and Sterba, M. E. (1995). Immobilization of simulated high-level waste in sintered glasses. *J. Nucl. Mater.* **223**, 151–156.
- Baisden, P. A. and Choppin, G. R. (2007). Nuclear waste management and the nuclear fuel cycle. *Radiochem. Nucl. Chem.*, 1–63.
- Banas, K., Banas, A., Moser, H. O., Bahou, M., Li, W., Yang, P., Cholewa, M., and Lim, S. K. (2010). Multivariate analysis techniques in the forensics investigation of the postblast residues by means of fourier transform-infrared spectroscopy. *Anal. Chem.* **82**, 3038–3044.
- Barbini, R., Colao, F., Fantoni, R., Lazic, V., Palucci, A., Capitelli, F., and Van der Steen, H. J. L. (2000). Laser induced breakdown spectroscopy for semi-quantitative elemental analysis in soils and marine sediments. In "Proceedings of EARSeL-SIG-Workshop LIDAR," Vol. 1, pp122–129.
- Beale, M. H., Hagan, M. T., and Demuth, H. B. (2010). Neural network toolbox 7. *User's Guide MathWorks*.
- Bell, M. J. (1973). ORIGEN: the ORNL isotope generation and depletion code. Oak Ridge National Lab.
- Benedict, M., Levi, H., and Pigford, T. (1982). Nuclear chemical engineering. *Nucl. Sci. Eng.* **82**, 476.
- Bevilacqua, A. M., Bernasconi, N. B. M. de, and Sterba, M. E. (1987). Desarrollo de la Formulación y Preparación de Residuos Simulados de Alta Actividad Tipo PHWR. In

- “Proc. Annual Meeting Argentine Association of Nuclear Technology.” Bariloche, Argentina.
- Bhatt, B., Angeyo, H. K., and Dehayem-Kamadjeu, A. (2018). LIBS Development Methodology for Forensic Nuclear Materials Analysis. *Anal. Methods* **10**, 791–798.
- Bhatt, B., Angeyo, H. K., and Dehayem-Massop, A. (2015). Nuclear Forensic Analysis via Chemometric Laser Induced Breakdown Spectroscopy. In “8th Euro-Mediterranean Symposium on Laser-Induced Breakdown Spectroscopy.” Linz, Austria.
- Bleise, A., Danesi, P. R., and Burkart, W. (2003). Properties, use and health effects of depleted uranium (DU): a general overview. *J. Environ. Radioact.* **64**, 93–112.
- Bodansky, D. (2007). Nuclear energy: principles, practices and prospects (Second Edition), pp 171-192. Springer-Verlag, New York LLC.
- Castanedo, F. (2013). A Review of Data Fusion Techniques. In “The Scientific World Journal.”
- Choi, I., Chan, G. C.-Y., Mao, X., Perry, D. L., and Russo, R. E. (2013). Line selection and parameter optimization for trace analysis of uranium in glass matrices by laser-induced breakdown spectroscopy (LIBS). *Appl. Spectrosc.* **67**, 1275–1284.
- Cilimkovic, M. (2015). Neural networks and back propagation algorithm. *Inst. Technol. Blanchardstown Blanchardstown Road North Dublin* **15**.
- Cisewski, J., Snyder, E., Hannig, J., and Oudejans, L. (2012a). Support vector machine classification of suspect powders using laser-induced breakdown spectroscopy (LIBS) spectral data. *J. Chemom.* **26**, 143–149.
- Cisewski, J., Snyder, E., Hannig, J., and Oudejans, L. (2012b). Support vector machine classification of suspect powders using laser-induced breakdown spectroscopy (LIBS) spectral data. *J. Chemom.* **26**, 143–149.
- Cremers, D. A. and Radziemski, L. J. (2013). Handbook of Laser-Induced Breakdown Spectroscopy. John Wiley & Sons.
- Cremers, D. A., Yueh, F.-Y., Singh, J. P., and Zhang, H. (2006). Laser-Induced Breakdown Spectroscopy, Elemental Analysis. Wiley Online Library.
- De Giacomo, A., Gaudiuso, R., Koral, C., Dell’Aglia, M., and De Pascale, O. (2014). Nanoparticle enhanced laser induced breakdown spectroscopy: effect of nanoparticles deposited on sample surface on laser ablation and plasma emission. *Spectrochim. Acta Part B At. Spectrosc.* **98**, 19–27.
- De Lucia, F. C., Gottfried, J. L., Munson, C. A., Miziolek, A. W., and others (2008). Multivariate analysis of standoff laser-induced breakdown spectroscopy spectra for classification of explosive-containing residues. *Appl. Opt.* **47**, G112–G121.

- Decker, D. K. and Allison, G. T. (2011). “Before the First Bomb Goes Off: Developing Nuclear Attribution Standards and Policies.” Harvard Kennedy School, Belfer Center for Science and International Affairs.
- Dey, P. K. and Bansal, N. K. (2006). Spent fuel reprocessing: a vital link in Indian nuclear power program. *Nucl. Eng. Des.* **236**, 723–729.
- D’haeseleer, W. D. (1998). The future of energy and the energy of the future. *Atw Int. Z. Für Kernenerg.* **43**, 507–511.
- Dingari, N. C., Barman, I., Myakalwar, A. K., Tewari, S. P., and Kumar Gundawar, M. (2012a). Incorporation of support vector machines in the LIBS toolbox for sensitive and robust classification amidst unexpected sample and system variability. *Anal. Chem.* **84**, 2686–2694.
- Dingari, N. C., Horowitz, G. L., Kang, J. W., Dasari, R. R., and Barman, I. (2012b). Raman spectroscopy provides a powerful diagnostic tool for accurate determination of albumin glycation. *PLoS One* **7**, e32406.
- Donald, I. W., Metcalfe, B. L., and Taylor, R. J. (1997). The immobilization of high level radioactive wastes using ceramics and glasses. *J. Mater. Sci.* **32**, 5851–5887.
- Doucet, F. R., Faustino, P. J., Sabsabi, M., and Lyon, R. C. (2008). Quantitative molecular analysis with molecular bands emission using laser-induced breakdown spectroscopy and chemometrics. *J. Anal. At. Spectrom.* **23**, 694–701.
- Doucet, F. R., Lithgow, G., Kosierb, R., Bouchard, P., and Sabsabi, M. (2011). Determination of isotope ratios using laser-induced breakdown spectroscopy in ambient air at atmospheric pressure for nuclear forensics. *J. Anal. At. Spectrom.* **26**, 536–541.
- Duchêne, S., Detalle, V., Bruder, R., and Sirven, J. B. (2010). Chemometrics and laser induced breakdown spectroscopy (LIBS) analyses for identification of wall paintings pigments. *Curr. Anal. Chem.* **6**, 60–65.
- Eby, N., Hermes, R., Charnley, N., and Smoliga, J. A. (2010). Trinitite—the atomic rock. *Geol. Today* **26**, 180–185.
- Erdem, A., Çilingiroğlu, A., Giakoumaki, A., Castanys, M., Kartsonaki, E., Fotakis, C., and Anglos, D. (2008). Characterization of Iron age pottery from eastern Turkey by laser-induced breakdown spectroscopy (LIBS). *J. Archaeol. Sci.* **35**, 2486–2494.
- Fahlman, S. E. and Lebiere, C. (1990). The cascade-correlation learning architecture, In: *Advances in Neural Information Processing Systems*. Vol. 2. Morgan-Kaufman, Los Altos.
- Fatima, H., Satpathy, S., Mahapatra, S., Dash, G. N., and Pradhan, S. K. (2017). Data fusion visualization application for network forensic investigation - a case study. In “2017 2nd International Conference on Anti-Cyber Crimes (ICACC),” pp252–256.

- Fausett, L. (1994). Fundamentals of neural networks: architectures, algorithms, and applications. pp. 10-15, Prentice-Hall, Inc.
- Fichet, P., Mauchien, P., and Moulin, C. (1999). Determination of Impurities in Uranium and Plutonium Dioxides by Laser-Induced Breakdown Spectroscopy. *Appl. Spectrosc.* **53**, 1111–1117.
- Filik, J. and Stone, N. (2007). Drop coating deposition Raman spectroscopy of protein mixtures. *Analyst* **132**, 544–550.
- Franc, V. and Hlavác, V. (2002). Multi-class support vector machine. In “Pattern Recognition, 2002. Proceedings. 16th International Conference on,” Vol. 2, pp236–239. IEEE.
- Gaona, I., Serrano, J., Moros, J., and Laserna, J. J. (2014). Evaluation of laser-induced breakdown spectroscopy analysis potential for addressing radiological threats from a distance. *Spectrochim. Acta Part B At. Spectrosc.* **96**, 12–20.
- Gottfried, J. L., De Lucia Jr, F. C., Munson, C. A., and Miziolek, A. W. (2009). Laser-induced breakdown spectroscopy for detection of explosives residues: a review of recent advances, challenges, and future prospects. *Anal. Bioanal. Chem.* **395**, 283–300.
- Grenthe, I., Drożdżynski, J., Fujino, T., Buck, E. C., Albrecht-Schmitt, T. E., and Wolf, S. F. (2008). Uranium. In “The chemistry of the actinide and transactinide elements,” pp253–698. Springer.
- Hanson, B. A. (2014). ChemoSpec: an R Package for the Chemometric Analysis of Spectroscopic Data. *Package Version*, 2–0.
- Henderson, H. (2014). “Nuclear Power: A Reference Handbook: A Reference Handbook.” ABC-CLIO.
- Hibbert, D. B., Minkinen, P., Faber, N. M., and Wise, B. M. (2009). IUPAC project: A glossary of concepts and terms in chemometrics. *Anal. Chim. Acta* **642**, 3–5.
- Ho, D. M. L., Jones, A. E., Goulermas, J. Y., Turner, P., Varga, Z., Fongaro, L., Fanghänel, T., and Mayer, K. (2015). Raman spectroscopy of uranium compounds and the use of multivariate analysis for visualization and classification. *Forensic Sci. Int.* **251**, 61–68.
- Huang, C.-L. and Wang, C.-J. (2006). A GA-based feature selection and parameters optimization for support vector machines. *Expert Syst. Appl.* **31**, 231–240.
- Hussain, T. and Gondal, M. A. (2013). Laser induced breakdown spectroscopy (LIBS) as a rapid tool for material analysis. *J. Phys. Conf. Ser.* **439**, 12050.
- IAEA (2017). Incidents and Trafficking Database (ITDB) Incidents of nuclear and other radioactive material out of regulatory control IAEA Fact Sheet.

- IAEA (2014). “Worldwide Open Proficiency Test for X Ray Fluorescence Laboratories PTXRFIAEA09: Determination of Major, Minor and Trace Elements in a River Clay.” INTERNATIONAL ATOMIC ENERGY AGENCY, Vienna.
- IAEA (2007). “Strategy and Methodology for Radioactive Waste Characterization.” International Atomic Energy Agency, pp. 1-178, Vienna, Austria.
- Jain, A. K., Mao, J., and Mohiuddin, K. M. (1996). Artificial neural networks: A tutorial. *IEEE Comput.* **29**, 31–44.
- James, G., Witten, D., Hastie, T., and Tibshirani, R. (2013). “An introduction to statistical learning with applications in R,” pp. 337-410, Springer, New York, USA.
- Jones, A. E., Turner, P., Zimmerman, C., and Goulermas, J. Y. (2014). Classification of spent reactor fuel for nuclear forensics. *Anal. Chem.* **86**, 5399–5405.
- Judge, E. J., Barefield, J. E., Berg, J. M., Clegg, S. M., Havrilla, G. J., Montoya, V. M., Le, L. A., and Lopez, L. N. (2013). Laser-induced breakdown spectroscopy measurements of uranium and thorium powders and uranium ore. *Spectrochim. Acta Part B At. Spectrosc.* **83**, 28–36.
- Jung, E. C., Lee, D. H., Yun, J.-I., Kim, J. G., Yeon, J. W., and Song, K. (2011). Quantitative determination of uranium and europium in glass matrix by laser-induced breakdown spectroscopy. *Spectrochim. Acta Part B At. Spectrosc.* **66**, 761–764.
- Kappel, S., Boulyga, S. F., and Prohaska, T. (2012). Direct uranium isotope ratio analysis of single micrometer-sized glass particles. *J. Environ. Radioact.* **113**, 8–15.
- Kasem, M. A. and Harith, M. A. (2015). Laser-Induced Breakdown Spectroscopy in Africa. *In* “Journal of Chemistry.”
- Kim, Y.-S., Han, B.-Y., Shin, H. S., Kim, H. D., Jung, E. C., Jung, J. H., and Na, S. H. (2012). Determination of uranium concentration in an ore sample using laser-induced breakdown spectroscopy. *Spectrochim. Acta Part B At. Spectrosc.* **74**, 190–193.
- Kočíšová, E. and Procházka, M. (2011). Drop-coating deposition Raman spectroscopy of liposomes. *J. Raman Spectrosc.* **42**, 1606–1610.
- Kristo, M. J. (2012). Nuclear forensics. *In* “Handbook of Radioactivity Analysis (Third Edition),” pp1281–1304. Elsevier, California, USA.
- Kurniawan, H., Nakajima, S., Batubara, J. E., Marpaung, M., Okamoto, M., and Kagawa, K. (1995). Laser-Induced Shock Wave Plasma in Glass and its Application to Elemental Analysis. *Appl. Spectrosc.* **49**, 1067–1072.
- Labbé, N., Swamidoss, I. M., André, N., Martin, M. Z., Young, T. M., and Rials, T. G. (2008). Extraction of information from laser-induced breakdown spectroscopy spectral data by multivariate analysis. *Appl. Opt.* **47**, G158–G165.



- L'Annunziata, M. F. (2012). "Handbook of radioactivity analysis." pp. 704-706, Academic Press, Oceanside, California, USA.
- Laville, S., Sabsabi, M., and Doucet, F. R. (2007). Multi-elemental analysis of solidified mineral melt samples by laser-induced breakdown spectroscopy coupled with a linear multivariate calibration. *Spectrochim. Acta Part B At. Spectrosc.* **62**, 1557–1566.
- Leggitt, J., Inn, K., Goldberg, S., Essex, R., LaMont, S., and Chase, S. (2009). Nuclear forensics—metrological basis for legal defensibility. *J. Radioanal. Nucl. Chem.* **282**, 997–1001.
- LIBS 2500 PLUS Operational Manual (2008). Laser Induced Breakdown Spectroscopy: Installation Manual. Ocean Optics. Inc.
- Liu, J., Zhang, R., Li, X., Chen, J., Liu, J., Qiu, J., Gao, X., Cui, J., and Heshig, B. (2018). Continuous background correction using effective points selected in third-order minima segments in low-cost laser-induced breakdown spectroscopy without intensified CCD. *Opt. Express* **26**, 16171–16186.
- Liu, L., Li, S., Huang, X., Lu, Y., Chen, K., Pik, R., Jiang, L., Silvain, J. F., and Lu, Y. F. (2015). Detection of trace-level uranium and samarium in glasses by combined laser-induced breakdown spectroscopy and plasma-induced fluorescence spectroscopy. *J. Anal. At. Spectrom.* **30**, 1128–1132.
- Long, G. L. and Winefordner, J. D. (1983). Limit of detection. A closer look at the IUPAC definition. *Anal. Chem.* **55**, 712A–724A.
- Loudyi, H., Rifai, K., Laville, S., Vidal, F., Chaker, M., and Sabsabi, M. (2009). Improving laser-induced breakdown spectroscopy (LIBS) performance for iron and lead determination in aqueous solutions with laser-induced fluorescence (LIF). *J. Anal. At. Spectrom.* **24**, 1421–1428.
- Mao, X., Bol'shakov, A. A., Perry, D. L., Sorkhabi, O., and Russo, R. E. (2011). Laser ablation molecular isotopic spectrometry: parameter influence on boron isotope measurements. *Spectrochim. Acta Part B At. Spectrosc.* **66**, 604–609.
- Martin, M. Z., Allman, S., Brice, D. J., Martin, R. C., and Andre, N. O. (2012). Exploring laser-induced breakdown spectroscopy for nuclear materials analysis and in-situ applications. *Spectrochim. Acta Part B At. Spectrosc.* **74**, 177–183.
- May, M., Abedin-Zadeh, R., Barr, D., Carnesale, A., Coyle, P. E., Davis, J., Dorland, W., Dunlop, W., Fetter, S., and Glaser, A. (2008). Nuclear forensics: role, state of the art, and program needs. *Am. Assoc. Adv. Sci. Am. Phys. Soc. Wash. DC*.
- Mayer, K., Wallenius, M., and Varga, Z. (2012). Nuclear forensic science: correlating measurable material parameters to the history of nuclear material. *Chem. Rev.* **113**, 884–900.

- McIntyre, H. C. (1975). Natural-uranium heavy-water reactors. *Sci. Am.* **233**, 17–27.
- Molgaard, J. J., Auxier II, J. D., Giminaro, A. V., Oldham, C. J., Cook, M. T., Young, S. A., and Hall, H. L. (2015). Development of synthetic nuclear melt glass for forensic analysis. *J. Radioanal. Nucl. Chem.* **304**, 1293–1301.
- Moody, K. J., Grant, P. M., and Hutcheon, I. D. (2014). “Nuclear forensic analysis.” CRC Press.
- Moros, J., Lorenzo, J. A., Lucena, P., Miguel Tobaría, L., and Laserna, J. J. (2010). Simultaneous Raman Spectroscopy–Laser-Induced Breakdown Spectroscopy for Instant Standoff Analysis of Explosives Using a Mobile Integrated Sensor Platform. *Anal. Chem.* **82**, 1389–1400.
- Mukhono, P. (2012). Chemometrics-assisted laser induced breakdown spectroscopy of high background radiation area (HBRA) geothermal field matrices. Thesis, University of Nairobi.
- Murray, R. and Holbert, K. E. (2014). Nuclear energy: an introduction to the concepts, systems, and applications of nuclear processes: Seventh Edition, pp. 369-374, Elsevier Inc.
- Musazzi, S. and Perini, U. (2014). “Laser-induced breakdown spectroscopy.” pp.3-413, Springer-Verlag Berlin Heidelberg.
- Myakalwar, A. K., Sreedhar, S., Barman, I., Dingari, N. C., Rao, S. V., Kiran, P. P., Tewari, S. P., and Kumar, G. M. (2011). Laser-induced breakdown spectroscopy-based investigation and classification of pharmaceutical tablets using multivariate chemometric analysis. *Talanta* **87**, 53–59.
- Naguib, R. N. and Sherbet, G. V. (2001). “Artificial neural networks in cancer diagnosis, prognosis, and patient management.” pp. 2-31 CRC press, Washington D.C.
- Nash, K. L., Lumetta, G. J., Clark, S. B., and Friese, J. (2006). Significance of the nuclear fuel cycle in the 21st century, pp. 3-20, ACS Publications.
- Noll, R. (2012). Laser-induced breakdown spectroscopy, pp.7-420, Springer-Verlag Berlin Heidelberg.
- Pease, P. (2013). Fused glass sample preparation for quantitative laser-induced breakdown spectroscopy of geologic materials. *Spectrochim. Acta Part B At. Spectrosc.* **83**, 37–49.
- Pontes, M. J. C., Cortez, J., Galvão, R. K. H., Pasquini, C., Araújo, M. C. U., Coelho, R. M., Chiba, M. K., Abreu, M. F. de, and Madari, B. E. (2009). Classification of Brazilian soils by using LIBS and variable selection in the wavelet domain. *Anal. Chim. Acta* **642**, 12–18.
- Prajapati, R. R., Srinivasan, T. G., Chandramouli, V., and Bhagwat, S. S. (2014). Dissolution kinetics of zirconium dioxide in nitric acid. *Desalination Water Treat.* **52**, 490–497.

- Prochazka, D., Bilík, M., Prochazková, P., Klus, J., Pořízka, P., Novotný, J., Novotný, K., Ticová, B., Bradáč, A., Semela, M., and others (2015). Detection of tire tread particles using laser-induced breakdown spectroscopy. *Spectrochim. Acta Part B At. Spectrosc.* **108**, 1–7.
- R. Bhatt, C. R., Alfarraj, B., Ayyalasomayajula, K. K., Ghany, C., Yueh, F. Y., and Singh, J. P. (2015). Study of atomic and molecular emission spectra of Sr by laser induced breakdown spectroscopy (LIBS). *Appl. Opt.* **54**, 10264–10271.
- Ralchenko, Y., Fuhr, J. R., Martin, W. C., Podobedova, L., Reader, J., Sansonetti, J. E., and Wiese, W. L. (2006). NIST atomic spectra database. <http://physics.nist.gov/asd3>.
- Rinke-kneapler, C. N. and Sigman, M. E. (2014). Applications of Laser Spectroscopy in Forensic Science, pp.461-495, Woodhead publishing, University of Florida, USA.
- Robel, M., Kristo, M. J., and Heller, M. A. (2009). Nuclear forensic inferences using iterative multidimensional statistics, Institute of Nuclear Materials Management Lawrence, 50<sup>th</sup> Annual Meeting, 16<sup>th</sup> July 2009, Tucson, AZ, USA.
- Rousseau, R. M. (2001). Concept of the influence coefficient. *Rigaku J* **18**, 8–14.
- Russo, R. E., Bol'shakov, A. A., Mao, X., McKay, C. P., Perry, D. L., and Sorkhabi, O. (2011). Laser Ablation Molecular Isotopic Spectrometry. *Spectrochim. Acta Part B At. Spectrosc.* **66**, 99–104.
- Russo, R. E., Mao, X. L., Liu, H. C., Yoo, J. H., and Mao, S. S. (1999). Time-resolved plasma diagnostics and mass removal during single-pulse laser ablation. *Appl. Phys. A* **69**, S887–S894.
- Şahin, S., Yapıcı, H., and Bayrak, M. (1999). Spent mixed oxide fuel rejuvenation in fusion breeders. *Fusion Eng. Des.* **47**, 9–23.
- Sailor, W. C., Bodansky, D., Braun, C., Fetter, S., and Zwaan, B. van der (2000). A nuclear solution to climate change? *Science* **288**, 1177–1178.
- Salas-Gonzalez, D., Górriz, J. M., Ramírez, J., López, M., Alvarez, I., Segovia, F., Chaves, R., and Puntonet, C. G. (2010). Computer-aided diagnosis of Alzheimer's disease using support vector machines and classification trees. *Phys. Med. Biol.* **55**, 2807–2817.
- Sally, V. K. (2014). “Goyal's IIT Foundation Course Physics : For Class-10,” pp. 318, Goyal Brothers Prakashan.
- Schetinin, V. (2003). A learning algorithm for evolving cascade neural networks. *Neural Process. Lett.* **17**, 21–31.
- Sekimoto, H. and Miyashita, S. (2006). Startup of “Candle” burnup in fast reactor from enriched uranium core. *Energy Convers. Manag.* **47**, 2772–2780.

- Shalev-Shwartz, S. and Ben-David, S. (2014). Understanding machine learning: From theory to algorithms, pp. 21-22, Cambridge University Press.
- Shen, X., Ho, C.-M., and Wong, T.-S. (2010). Minimal size of coffee ring structure. *J. Phys. Chem. B* **114**, 5269–5274.
- Sirven, J.-B., Bousquet, B., Canioni, L., and Sarger, L. (2006). Laser-induced breakdown spectroscopy of composite samples: comparison of advanced chemometrics methods. *Anal. Chem.* **78**, 1462–1469.
- Sirven, J.-B., Pailloux, A., M'Baye, Y., Coulon, N., Alpettaz, T., and Gosse, S. (2009). Towards the determination of the geographical origin of yellow cake samples by laser-induced breakdown spectroscopy and chemometrics. *J. Anal. At. Spectrom.* **24**, 451–459.
- Skorpil, V. and Stastny, J. (2006). Back-Propagation and K-Means Algorithms Comparison. In “2006 8th international Conference on Signal Processing,” Vol. 3.
- Sládková, L., Prochazka, D., Pořízka, P., Škarková, P., Remešová, M., Hrdlička, A., Novotný, K., Čelko, L., and Kaiser, J. (2017). Improvement of the Laser-Induced Breakdown Spectroscopy method sensitivity by the usage of combination of Ag-nanoparticles and vacuum conditions. *Spectrochim. Acta Part B At. Spectrosc.* **127**, 48–55.
- Stacey, W. M. (2018). Nuclear Reactor Physics, pp 157-164, John Wiley & Sons, USA
- Stavropoulos, P., Palagas, C., Angelopoulos, G. N., Papamantellos, D. N., and Couris, S. (2004). Calibration measurements in laser-induced breakdown spectroscopy using nanosecond and picosecond lasers. *Spectrochim. Acta Part B At. Spectrosc.* **59**, 1885–1892.
- Takeuchi, K. and Collier, N. (2005). Bio-medical entity extraction using support vector machines. *Artif. Intell. Med.* **33**, 125–137.
- Tripathi, M., Eseller, K., Yueh, F.-Y., and Singh, J. (2009). Multivariate calibration of spectra obtained by Laser Induced Breakdown Spectroscopy of plutonium oxide surrogate residues. *Spectrochim. Acta Part B At. Spectrosc.* **64**, 1212–1218.
- Van Grieken, R. and Markowicz, A. (2001). Handbook of X-ray Spectrometry, pp. 179-181, CRC Press, USA.
- Vance, T., Reljin, N., Lazarevic, A., Pokrajac, D., Kecman, V., Melikechi, N., Marcano, A., Markushin, Y., and McDaniel, S. (2010). Classification of LIBS protein spectra using support vector machines and adaptive local hyperplanes. In “Neural Networks (IJCNN), The 2010 International Joint Conference on,” pp1–7. IEEE.
- Varmuza, K. and Filzmoser, P. (2016). “Introduction to multivariate statistical analysis in chemometrics.” Chapter 5, CRC press, New York.
- Wall, E. V. and Whitener, E. M. (1959). Concentrated nitric and dilute hydrofluoric acid mixtures in dissolution of zirconium metal. *Ind. Eng. Chem.* **51**, 51–54.

- Watanabe, M. (2015). Sample preparation for X-ray fluorescence analysis IV. Fusion bead method—part 1 basic principles. *Engl. Version*, 12.
- Williams, R. D., Hing, S. N., Greer, B. T., Whiteford, C. C., Wei, J. S., Natrajan, R., Kelsey, A., Rogers, S., Campbell, C., Pritchard-Jones, K., and others (2004). Prognostic classification of relapsing favorable histology Wilms tumor using cDNA microarray expression profiling and support vector machines. *Genes. Chromosomes Cancer* **41**, 65–79.
- Wilson, P. D. (1996). “The nuclear fuel cycle : from ore to wastes,” pp. 5-55, Oxford University Press, New York
- Xue, C. X., Zhang, R. S., Liu, H. X., Yao, X. J., Liu, M. C., Hu, Z. D., and Fan, B. T. (2004). QSAR models for the prediction of binding affinities to human serum albumin using the heuristic method and a support vector machine. *J. Chem. Inf. Comput. Sci.* **44**, 1693–1700.
- Xuegang, L., Jin, C., Yanchao, Z., and Jianchen, W. (2012). Precipitation of zirconium and molybdenum in simulated high-level liquid waste concentration and denitration process. *Procedia Chem.* **7**, 575–580.
- Yamada, Y., Kohno, H., and Murata, M. (1995). A low dilution fusion method for major and trace element analysis of geological samples. *X-Sen Bunseki No Shinpo* **26**, 33–44.
- Yang, N., Eash, N. S., Lee, J., Martin, M. Z., Zhang, Y.-S., Walker, F. R., and Yang, J. E. (2010). Multivariate analysis of laser-induced breakdown spectroscopy spectra of soil samples. *Soil Sci.* **175**, 447–452.
- Yapıcı, H. (2003). Study on transmutation of minor actinides discharged from high burn-up PWR-MOX spent fuel in the force-free helical reactor. *Ann. Nucl. Energy* **30**, 413–436.
- Ye, J. Y., Balogh, L., and Norris, T. B. (2002). Enhancement of laser-induced optical breakdown using metal/dendrimer nanocomposites. *Appl. Phys. Lett.* **80**, 1713–1715.
- Zhang, D., Xie, Y., Mrozek, M. F., Ortiz, C., Davisson, V. J., and Ben-Amotz, D. (2003). Raman detection of proteomic analytes. *Anal. Chem.* **75**, 5703–5709.

## APPENDICES

### Appendix 1: Target Concentrations Spiking Scheme

**Table A 1:** The target concentrations of fission products spiking scheme

	Target Concentrations (ppm)					
<b>Target FP</b>	<b>Sr</b>	<b>Rb</b>	<b>Te</b>	<b>Zr</b>	<b>Y</b>	<b>U</b>
<b>Sample 1 (S1)</b>	35.99	58.76	51.03	54.79	37.97	26585.47
<b>Sample 2 (S2)</b>	76.21	29.38	178.62	96.69	92.56	35832.00
<b>Sample 3 (S3)</b>	14.82	156.69	51.03	644.63	151.89	36619.52
<b>Sample 4 (S4)</b>	116.44	186.07	178.62	268.59	73.57	22770.09
<b>Sample 5 (S5)</b>	101.62	68.55	153.10	698.34	112.73	36619.52
<b>Sample 6 (S6)</b>	97.38	176.27	89.31	333.06	96.12	31093.33
<b>Sample 7 (S7)</b>	71.98	127.31	63.79	386.78	116.29	21412.30
<b>Sample 8 (S8)</b>	112.20	48.96	76.55	537.19	192.23	35261.73
<b>Sample 9 (S9)</b>	40.22	146.89	127.58	343.80	53.40	36456.59
<b>Sample 10 (S10)</b>	44.46	166.48	76.55	343.80	100.86	32939.92
<b>Sample 11 (S11)</b>	67.74	146.89	76.55	300.83	219.52	30509.48
<b>Sample 12 (S12)</b>	95.27	186.07	178.62	709.09	212.40	30482.32
<b>Sample 13 (S13)</b>	74.10	186.07	25.52	3.22	346.49	23625.50
<b>Sample 14 (S14)</b>	21.17	39.17	47.92	612.39	955.22	10057.17
<b>Sample 15 (S15)</b>	69.86	58.76	63.90	290.08	789.09	6418.05
<b>Sample 16 (S16)</b>	59.28	58.76	95.84	741.32	996.75	4797.96
<b>Sample 17 (S17)</b>	33.87	127.31	191.69	440.49	937.42	10283.83
<b>Sample 18 (S18)</b>	35.99	127.31	159.74	741.32	1058.45	9642.38
<b>Sample 19 (S19)</b>	21.17	9.79	95.84	225.62	1038.28	8195.12
<b>Sample 20 (S20)</b>	88.91	19.59	95.84	526.44	442.60	8010.09
<b>Sample 21 (S21)</b>	41.81	122.41	297.60	643.23	85.44	11550.41
<b>Sample 22 (S22)</b>	150.12	83.44	254.94	642.15	93.74	8262.48
<b>Sample 23 (S23)</b>	76.51	108.51	61.82	1380.36	191.04	6897.66
<b>Sample 24 (S24)</b>	23.22	78.05	44.73	1520.03	106.79	9211.45
<b>Sample 25 (S25)</b>	93.30	82.65	150.47	530.74	72.38	8622.65
<b>Sample 26 (S26)</b>	5.27	62.77	70.45	1480.38	94.93	12000.11
<b>Sample 27 (S27)</b>	138.47	168.83	265.01	346.06	46.28	10224.42
<b>Sample 28 (S28)</b>	133.01	173.24	18.69	1160.97	18.99	10645.17
<b>Sample 29 (S29)</b>	97.55	89.61	170.76	591.01	48.81	7824.29
<b>Sample 30 (S30)</b>	73.93	119.87	231.30	520.96	65.26	7374.28

## Appendix 2: Artificial Neural Network Algorithm

Load data

% The input data is put in folder I, the target data in folder T, the sample data in folder S and the expected target concentrations in folder O

% normalize the inputs and target matrices

```
[In, Is] = mapstd (I);
```

```
[Tn, Ts] = mapstd (T);
```

```
Ss = mapstd (S);
```

% The function mapstd normalizes the inputs and targets so that they will have zero mean and unity standard deviation. Here, I is the input data, T is the target data and S is the sample input data. These normalized data is stored in folders Is and Ts and they contain zero mean and unity standard deviation of the original targets

% Create a feed forward network with 2 hidden neurons and 3 output neurons and set TRAINLM (Levenberg-Marquardt function). In case of cascade correlation algorithm newff was replaced with newcf

```
net = newff(In,Tn,[2],3,{'tansig'});
```

% Divide the input data such that 60% of the data is used for training, 25% of the data is used for testing and 15% of the data is used for validation

```
net.divideparam.trainratio = 0.60;
```

```
net.divideparam.testratio = 0.25;
```

```
net.divideparam.valratio = 0.15;
```

% set the target maximum number of iterations

```
net.trainParam.epochs = 50;
```

% set the learning rate of the algorithm

```
net.trainParam.lr = 0.001;
```

% set the number of epochs between displays

```
net.trainParam.show = 20;
```

% set the training MSE error target

```
net.trainParam.goal = 0.00001;
```

% Train the network

```
net = train(net,In,Tn);  
% Perform a simulation of the network and store the results in a folder M  
M = sim(net,Sn);  
% transform the results stored in M back to their original form stored in the folder Ts. Here, the  
results predicted are of zero mean and unity standard deviation in accordance with the mpstd  
function applied earlier hence they must be transformed back to their original form.  
P = mapstd('reverse',M,Ts);  
% Determine the correlation coefficient for the predicted and actual concentrations  
R=corrcoef(P,O);
```



### Appendix 3: Support Vector Machine Algorithm (Binary Clustering) in R

```
# Load library containing support vector machine algorithm and tools
library(e1071)
# Read data from a file and store it in R as LIBSData
LIBSData <- read.csv("Data.csv", sep = ",")
#View the imported data in R Studio
LIBSData
#Get the summary of the data five number summary (minimum, first
quartile, median upper quartile, and maximum value) the mean and the
samples of each FP
summary(LIBSData)
#Provides the nature of the dataset in this case 'data frame'
class(LIBSData)
# point plot (scatter plots) of the LIBSData to visualize the data
plot(LIBSData[,1], LIBSData[,2], type = "p")
# point plot with column 3 containing FP as the color code
plot(LIBSData[,1], LIBSData[,2], type = "p", col = LIBSData[,3])
# Create an indexing protocol for the total samples fed to the
network.
s<-sample(n,k)
# For example, if n = 30 then select randomly a set of k = 24 samples
for model training
s<-sample(30,24)
#Based on the index chosen above, divide the data into two classes for
model training
LIBSData_train <- LIBSData[s,1:3]
# Assign the remaining data as testing data based on the remaining
randomly indexed choices
LIBSData_test <- LIBSData[-s,1:3]
#Visualize the Test data and the training data sets
LIBSData_test
LIBSData_train
```

```

#Perform a support vector machine classification based on the FP
species column with LIBSData_train data at a cost of 10 utilizing a
linear, or radial or polynomial kernel by changing the kernel type.
svmfit <-svm(FP~.,data=LIBSData_train, kernel="radial", cost=10,
gamma=1)
#print the resulting model
print(svmfit)
#graphically visualize the clustered training data and the
corresponding hyperplanes of the model.
plot(svmfit,LIBSData_train[,1:3])
#For selected cost and gamma values, fine tune the model to realize
the best parameter combination.
tuned <- tune(svm, FP~., data = LIBSData_train, kernel = "linear",
ranges= list(cost = c(0.01,0.1, 1, 10,100,1000)))
# Display the tuned model and the errors associated
summary(tuned)
# Store the best model in BestModel
BestModel<-tuned$best.model
plot(Bestmodel,LIBSData_train[,1:3])
#predict the test data
Predicted <- predict(Bestmodel, LIBSData_test[,1:3],type="class")
#Visualize the predicted data
plot(Predicted)
#Display in table format (confusion matrix) for easier view
table(predict,LIBSData_test[,3])
#Determine the accuracy in prediction
mean(Predicted== LIBSData_test[,3])

```

## Appendix 4: Principal Component Analysis Code in R

```
library(ChemoSpec)
library(devtools)
library(utils)
library(knitr)
library(R.utils)
files2SpectraObject(gr.crit = c("SL", "LB"), gr.cols = c("red3", "gray0"),
                    freq.unit = "Wavelength (nm)", int.unit = "peak intensity (a.u)", descrip = "Simulate
Liquid Nuclear Wastes",
                    out.file = "pcasim", sep=",")
#A new file called pcasim.RData is created which can be accessed as follows
LPCA <- loadObject("pcasim.RData")
#Making the data available
data(TPCA)
sumSpectra(TPCA)
# Create a title of the plot
myt <- expression(bolditalic(liquid~nuclear~wastes ~Sectra))
plotSpectra(LPCA, main = myt,
            which = c(1, 2, 7),
            yrange = c(0, 1500), offset = 100, lab.pos = 341)
#zoom into specific region of the spectra
plotSpectra(LPCA, main = myt,
            which = c(1, 2, 7, 27,30,37,60, 63), xlim = c(420, 425),
            yrange = c(0, 3000), offset = 100, lab.pos = 382)
library(baseline)
#baseline restoration on spectra
BLPCA <- baselineSpectra(LPCA, int = FALSE, method = "rfbaseline", retC = TRUE)
```

```

# To remove a sample from the spectra say
noLB1 <- removeSample(TPCA, rem.sam = c("LB1", "FSL0"))

#Normalize baseline subtracted spectra
NormPCA <- normSpectra(BLPCA)

#Remove frequencies that do not contain regions of interest
RNormPCA <- removeFreq(NormPCA, rem.freq = NormPCA$freq > 400 & NormPCA$freq <
982)

RRRNormPCA <- removeFreq(RNormPCA, rem.freq = RNormPCA$freq > 198 &
RNormPCA$freq < 340)

#principal component analysis
class <- c_pcaSpectra(RRRNormPCA, choice = "noscale")
plotScores(RRRNormPCA, main = myt, class,
           pcs = c(1,2), ellipse = "rob", tol = 1.0, leg.loc = "topright")

#Possible PCA outliers based on Orthogonaal distance
diagnostics <- pcaDiag(RRRNormPCA, class, pcs = 2, plot = "OD")

#possible PCA Outliers based on Score Distance
diagnostics <- pcaDiag(RRNormPCA, class, pcs = 2, plot = "SD")


#Remove outliers from the data
ORRNormPCA <- removeSample(RRRNormPCA, rem.sam = c("LB4","SL2","SL1","SL7"))

#principal component analysis
class <- c_pcaSpectra(ORRNormPCA, choice = "noscale")
plotScores(ORRNormPCA, main = myt, class,
           pcs = c(1,2), ellipse = "rob", tol = 1.0, leg.loc = "top")

#Plot Scree plot
plotScree(class, main = myt)
plotScree2(class, main = myt)
out <- cv_pcaSpectra(NormPCA, pcs = 5, choice = "noscale")

```

## Appendix 5: ICP standard Solutions Validation Certificates



### Certificate of Analysis Certipur® Reference Material

---

#### Yttrium ICP Standard 1000 mg/l Y CertiPUR®

**1.70368.0100** Lot No: HC631658

This Certificate of Analysis is based on the data from the Merck Calibration Laboratory for ICP-OES, according to DIN EN ISO / IEC 17025.  
Accredited by the DKD (Deutscher Kalibrierdienst), the accreditation body at PTB (Physikalisch-Technische Bundesanstalt).

**DAR Reg.-No.:** DKD-K-14302  
**Ref. Calibration Certificate:** 160/DKD-K-14302/07-01

**Composition:** Yttrium nitrate in nitric acid Suprapur® 2-3%

**Assay:** 986 mg/kg **Analysis:** ICP-OES  
1000 mg/l (calculated)

**Measurement Uncertainty:** ± 3 mg/kg (± 0.3%)  
This value represents the expanded uncertainty (U) for a coverage probability of 95%. Refer to page 2 for further details.

**Traceability:** This ICP Standard has been measured applying high precision ICP-OES in comparison to the corresponding NIST SRM® 3167a, lot 790412

**Trace impurities µg/ml:**

Ag <0.02	Cr <0.02	In <0.02	Ni <0.02	Sb <0.02	Tl <0.02
Al <0.05	Cu <0.02	Ir <0.02	Os <0.20	Sc <0.02	Tm <0.02
As <0.20	Dy <0.02	K <0.20	P <0.20	Se <0.20	U <0.02
Au <0.02	Er <0.02	La <0.02	Pb <0.05	Si <0.20	V <0.02
B <0.05	Eu <0.02	Li <0.02	Pd <0.02	Sm <0.02	W <0.05
Ba <0.02	Fe <0.05	Lu <0.02	Pr <0.02	Sn <0.02	Y *
Be <0.02	Ga <0.02	Mg <0.02	Pt <0.02	Sr <0.02	Yb <0.02
Bi <0.20	Gd <0.05	Mn <0.02	Rb <0.02	Ta <0.05	Zn <0.02
Ca <0.05	Ge <0.02	Mo <0.02	Re <0.02	Tb <0.02	Zr <0.02
Cd <0.02	Hf <0.02	Na <0.10	Rh <0.02	Te <0.20	
Ce <0.02	Hg <0.02	Nb <0.05	Ru <0.02	Th <0.02	
Co <0.02	Ho <0.02	Nd <0.02	S <0.20	Ti <0.05	

**Date of release:** 23. January 2007  
**Minimum shelf life:** 31. January 2010

  
**Wolfgang Gemand**  
 (responsible laboratory manager quality control)





Certificate of Analysis  
Certipur® Reference Material

**Strontium ICP Standard 1000 mg/l Sr CertiPUR®**

1.70354.0100

Lot No: HC694788

This Certificate of Analysis is based on the data from the Merck Calibration Laboratory for ICP-OES, according to DIN EN ISO / IEC 17025. Accredited by the DKD (Deutscher Kalibrierdienst), the accreditation body at PTB (Physikalisch-Technische Bundesanstalt).

DAR Reg.-No.: DKD-K-14302  
Ref. Calibration Certificate: 108/DKD-K-14302/06-04

Composition: Strontium nitrate in nitric acid Suprapur® 2-3%

Assay: 983 mg/kg  
997 mg/l (calculated) Analysis: ICP-OES

Measurement: ± 4 mg/kg (± 0.4%)  
Uncertainty: This value represents the expanded uncertainty (U) for a coverage probability of 95%. Refer to page 2 for further details.

Traceability: This ICP Standard has been measured applying high precision ICP-OES in comparison to the corresponding NIST SRM® 3153a, lot 990906

Trace impurities µg/ml:

Ag <0,02	Cr <0,02	In <0,02	Ni <0,02	Sb <0,02	Tl <0,02
Al <0,05	Cu <0,02	Ir <0,02	Os <0,20	Sc <0,02	Tm <0,02
As <0,20	Dy <0,02	K <0,20	P <0,20	Se <0,20	U <0,02
Au <0,02	Er <0,02	La <0,02	Pb <0,05	Si <0,20	V <0,02
B <0,05	Eu <0,02	Li <0,02	Pd <0,02	Sm <0,02	W <0,05
Ba <0,02	Fe <0,05	Lu <0,02	Pr <0,02	Sn <0,02	Y <0,02
Be <0,02	Ga <0,02	Mg <0,02	Pt <0,02	Sr *	Yb <0,02
Bi <0,20	Gd <0,02	Mn <0,02	Rb <0,02	Ta <0,05	Zn <0,02
Ca <0,05	Ge <0,02	Mo <0,02	Re <0,02	Tb <0,02	Zr <0,02
Cd <0,02	Hf <0,02	Na <0,10	Rh <0,05	Te <0,20	
Ce <0,02	Hg <0,02	Nb <0,05	Ru <0,02	Th <0,02	
Co <0,02	Ho <0,02	Nd <0,02	S <0,20	Ti <0,05	

Date of release: 25. April 2006

Wolfgang Gernand  
responsible (laboratory manager quality control)

